THE GEOLOGY OF THE GOLD BUTTE BREAKAWAY ZONE AND THE MECHANICAL EVOLUTION OF NORMAL FAULT SYSTEMS

Thesis by

Robert J. Brady

In Partial Fulfillment of the Requirements

for the Degree of

Doctor of Philosophy

California Institute of Technology

Pasadena, California

1998

(Submitted May 14, 1998)

Acknowledgments

The completion of this thesis is the result not just of my own work, but of the help and support of many people. I'm happy to be able to give them some acknowledgment here, and I apologize to anyone who may be forgotten.

When I was trying to choose which institute to attend for my Ph. D. program, I was given the advice, by Dr. P. Simony, that the caliber of the other graduate students would be at least as important as that of the faculty members, because the students are the ones with whom I would spend the most time and discuss the most science. This has turned out to be true, and I would like to thank Mark Abolins, Mihai Ducea, Nathan Niemi, Jim Spotila, Slawek Tulaczyk, and Elizabeth Warner-Holt for the useful discussions that occurred during our many bull sessions. Special thanks go to Slawek and Nathan for helping me puzzle my way through problems with mechanics and math. Of course, the non-academic activities with these and other students at Caltech, while perhaps less common, have been every bit as important. For occasionally dragging me out of Pasadena and into the mountains to regain some sensible perspective on life, I must thank Jeff Hashimoto and John Holt.

Many of the faculty and staff at Caltech have contributed to my research. Martha House, Peter Reiners, and Ken Farley helped by contributing data and useful comments. Andrew Meigs, Joann Stock and Dr. L. Silver were always willing to talk about my research and offer helpful questions and comments. Special thanks goes to my advisor, Brian Wernicke, for providing a combination of the necessary resources and a relatively unrestricted environment in which to do my research. I also owe thanks to Tony Soeller for his help in the Caltech Spatial Interpretation Lab, and to Cherylinn Rangel, for saving me from bureaucracy and day to day problems.

My field work benefited greatly from the help of my two field assistants, Glenn Spinelli and Matt Herrin, as well as from interesting discussions with Keith Howard, Sue Beard, Joan Fryxell, and Jim Faulds. Steve Rowland led me on a short trip through the Paleozoic stratigraphy of Frenchman Mountain, which led to great improvements in my mapping.

The people to whom I owe the greatest thanks are my parents, John and Patricia Brady, and my wife Janice Rae. My parents taught me the value of education and the importance of questioning and curiosity, and they have always supported me. Janice has put up with my many months of absence due to field work and other research related trips, and has remained supportive through it all. Perhaps most importantly, she has made the past few years more fun, and has kept me from becoming too absorbed in my work

Abstract

The Gold Butte breakaway zone is the easternmost and oldest of the major Tertiary normal fault systems in the central Basin and Range province of the southwestern U.S. The normal faults of the breakaway zone crop out across the South Virgin Mountains (SVM), and define a narrow boundary zone between the Colorado Plateau and the highly extended central Basin and Range Province. Geochronologic data, including $^{40}Ar/^{39}Ar$ muscovite ages, (U-Th)/He apatite ages, and (U-Th)/Pb monazite ages, suggest that extension within the breakaway zone occurred rapidly at ~15 Ma, consistent with earlier work (Fitzgerald, 1991). Approximately 400 km^2 of the SVM was mapped at a scale of 1:12 000. This mapping shows that extension initiated on a set of steeply west dipping normal faults. Later faults soled into the earlier faults rather than cutting them, requiring motion to continue on both fault sets, with the earlier faults remaining active to dips of less than 30°. Total extension across the SVM is at least ~21 km. The latest deformation to affect the region was isostatic uplift of the footwall to the Lakeside Mine Fault Zone, with resultant formation of a basement dome and associated folding and late stage faulting adjacent to the dome. Seismic reflection data suggest that the crustal thickness of the region is 30 to 35 kilometers. When combined with the high average elevation of the denuded basement block, this suggests that extension of the upper crust has been compensated by emplacement of fluid mid to lower crust. The lower crust and Moho are seismically transparent, so the lower crust is probably not made up of basaltic intrusions; rather, it has probably flowed in from surrounding areas. A mechanical model has been developed which considers the behavior of an elastic upper crust isostatically compensated by flow in the lower crust. This model shows that gradual isostatic upwarping of the thinning region should generate compressional flexural stresses near the base of the elastic upper crust. These stresses may shut down the active faults and force new normal faults to root outside of the extended region.

Table of Contents

List of Tables

List of Figures

List of Oversized Plates

(In Separate Box)

Chapter 1

Introduction

Prior to the early 1970's, continental extension in the Basin and Range Province of the southwestern U.S. and elsewhere was thought to occur on steeply dipping block faults, with the total extension generally being relatively minor (Gilbert, 1875; Davis, 1925; Stewart, 1971; Thompson and Burke, 1974). However, over the last three decades, field studies in the Basin and Range Province have resulted in a significant advance in our understanding of how continental extension occurs. These studies showed that extension within the continent was, in places, extreme and that extension was often accommodated on shallowly dipping faults (Anderson, 1971; Armstrong, 1972; Davis, 1973; Wright and Troxel, 1973; Coney, 1974; Proffett, 1977; Wernicke, 1981; Miller et al., 1983).

While the existence of highly extended regions affected by shallowly dipping normal faults has become fairly widely accepted, a satisfactory explanation of their kinematic and dynamic evolution is still being sought. In particular, many workers have been attempting to explain how shallowly dipping normal faults may have formed (Buck, 1988; Spencer and Chase, 1989; Yin, 1989; Axen, 1992; Forsyth, 1992; Wills and Buck, 1997), since they are theoretically not favorably oriented for active slip (Anderson, 1942; Sibson, 1985; Nur et al., 1986; Agnon and Reches, 1995). In addition to this fundamental mechanical problem, there has been considerable discussion regarding the cause of the high elevation of many highly extended regions and the domainal character of extension within the Basin and Range Province (c.f. Spencer, 1984; Block and Royden, 1990; Wernicke, 1992). All of this recent interest in the evolution of highly extended continental terrains has resulted in a much more sophisticated understanding of normal fault systems and the mechanical properties of earth materials during extension, but it has yet to produce a widely accepted model which explains all, or even most, aspects of continental extensional fault systems.

This dissertation describes the results of my work, with contributions from several others, which has been aimed at better understanding the kinematic and dynamic evolution of large-offset continental normal fault systems. In addition to the introduction and summary chapters, there are three main chapters. These three chapters were all written as independent journal articles, therefore each includes independent abstracts, reference sections, et cetera.

Chapter two is entitled: "The kinematic evolution of a large offset continental normal fault system, South Virgin Mountains, Nevada." It includes the main results of ten months of detailed geologic mapping in the South Virgin Mountains of southeasternmost Nevada and a small area in northwestern Arizona. This effort resulted in the production of a 1:12 000 scale geologic map which covers about 400 km^2 of extensionally deformed Paleozoic to Early Mesozoic strata and overlying Tertiary rocks in the South Virgin Mountains. This mapping was complemented by several geochronologic analyses of crystalline rocks which constrain the timing of unroofing and the thermal evolution of the region. The region was selected for detailed study because it includes the well exposed normal faults which make up the Gold Butte breakaway zone, the extensional fault system which occurs at the boundary between the essentially unextended Colorado Plateau and the highly extended central Basin and Range Province. The mapped strata are adjacent to the Gold Butte crystalline block, which was extensionally unroofed at about 15 Ma (Fitzgerald et al., 1991; Fryxell et al., 1992). Since the region has been highly extended, includes a compact stratigraphic section and datable exposures of crystalline rock, and almost certainly had a pre-extensional geometry similar to the little deformed Colorado Plateau, it provided an exceptional opportunity to unravel the detailed kinematic history of a large offset normal fault system.

Chapter three, "Crustal structure of the Basin and Range to Colorado Plateau transition in the Lake Mead region from BARGE seismic reflection data," presents results of the Basin and Range Geoscientific Experiment (BARGE). This experiment involved the acquisition of over 120 km of marine style deep seismic reflection data on the waters of Lake Mead, Nevada and Arizona, as well as acquisition of large offset refraction data. Only the reflection data are discussed in chapter three. The seismic reflection profiles extend from western Lake Mead, across and around the South Virgin Mountains, and nearly onto the Colorado Plateau. The results therefore offer an opportunity to examine how the deep crust and Moho have behaved in this region, which reaches from well within the extended domain out to the abrupt transition into unextended upper crust. In particular, the BARGE data set provides an opportunity to observe the roles of deep crustal flow, magmatism, and possibly shearing along the Moho and to see how these processes may change with position in an extensional system.

Chapter four, "The effects of isostatically driven lower crustal flow on normal fault longevity and orientation," presents a mechanical model which attempts to explain some of the first order features of the Gold Butte breakaway zone and other large offset continental normal fault systems. The model offers an explanation for why some normal fault systems shut down after accommodating a large amount of offset, and predicts how much slip should be accommodated on a particular normal fault system if the elastic upper crustal thickness, fault dip, slip rate, and lower crustal viscosity are known . It also offers a partial explanation for why large domains of the Basin and Range are affected by a series of shallowly dipping normal faults which dominantly dip in one direction and are active sequentially in a downdip direction. The model considers the evolution of fiber stresses within an extending region of the continental crust. The crust is assumed to be relatively simple, with an elastic upper crust and a fluid lower crust (c.f. Byerlee, 1978; Brace and Kohlstedt, 1980). Extension of the upper crust is isostatically compensated by flow of the lower crust, resulting in upwarping of the elastic upper crust across the extending region. This upwarping, in turn, generates fiber stresses within the elastic upper crust. These fiber stresses combine with the regional stress field to determine which areas of the upper crust are going to fail extensionally and experience active normal faulting.

Chapter 2

Evolution of a large-offset continental normal fault system, South Virgin Mountains, Nevada

Robert Brady, Brian Wernicke

Division of Geological and Planetary Sciences, California Institute of Technology, Pasadena, California 91125

Joan Fryxell

Department of Geological Sciences, California State University, San Bernardino, California

Mark Martin

Department of Earth, Atmospheric, and Planetary Sciences, Massachusetts Institute of Technology, Cambridge, Massachusetts

Daniel Lux

Department of Geological Sciences, University of Maine, Orono, Maine

(This chapter was re-formatted from a manuscript in preparation, for submission to the *Geological Society of America Bulletin*)

Abstract. The Gold Butte breakaway zone is a normal fault system that defines a sharp boundary between the unextended Colorado Plateau to the east and highly extended crust of the central Basin and Range Province to the west. These extensional faults developed in flat lying rocks in the foreland of the Cordilleran fold and thrust system. These originally flat lying rocks can be broken into over thirty mappable units in approximately three kilometers of stratigraphic section. The system of normal faults

which makes up the breakaway zone is well exposed in three dimensions in the rugged and virtually unvegetated South Virgin Mountains of southeastern Nevada and northwestern Arizona. The exceptional three dimensional exposure, compact stratigraphy, and well defined pre-faulting configuration of the rocks permitted a detailed reconstruction of the kinematic evolution of this large-offset normal fault system. A data set consisting of over 300 km^2 of new detailed geologic mapping and thermochronologic data was collected from the South Virgin Mountains. Reconstruction of cross-sections shows that the Gold Butte breakaway zone accommodated more than 15 kilometers of roughly east-west directed Miocene extension. Extension within the area was initially accommodated on a set of moderately to steeply dipping listric normal faults. As these faults slipped and were rotated to shallower dips, later steeply to moderately dipping faults initiated and soled into the earlier structures. Some of the earlier faults must have remained active to dips of less than 20°. Rotation due to isostatically driven upflexing of the extensionally thinned region is superimposed on rotation due to active slip and domino style rotation of the fault blocks. Total horizontal axis rotations have been great enough to rotate originally vertical to steeply west dipping faults into essentially horizontal present day orientations. This evolution of a large offset continental normal fault system is inconsistent with the widely accepted view that many near-horizontal normal faults, developed within the shallow continental crust, were rotated to their present orientations within the hanging walls of later, cross-cutting normal faults. However, re-examination of other areas suggests that the evolutionary sequence seen in the South Virgin Mountains may, in fact, be widely applicable.

2.1 Introduction

Several decades of geologic mapping in the Basin and Range Province have shown that shallowly dipping extensional fault surfaces are relatively common (e.g. Longwell, 1945; Anderson, 1971; Proffett, 1977; Miller et al., 1983; Wernicke et al., 1985; John and Foster, 1993), but theoretical fault mechanics suggests that such shallowly dipping normal faults should not be able to slip (c.f. Anderson, 1942; Sibson, 1985; Nur et al., 1986; Agnon and Reches, 1995). A number of models explain shallowly dipping structures in a manner which is consistent with mechanical theory by invoking rotation of normal faults to lower dips after they have ceased to slip (e.g. Proffett, 1977; Miller et al., 1983; Buck, 1988). For example, in the Snake Range, the Lemitar Mountains, and the Yerington district, shallowly dipping faults have been interpreted as being the result of multiple generations of cross-cutting, steeply dipping normal faults, with older faults being rotated to shallow dips above younger faults (Proffett, 1977; Chamberlin, 1982, 1983; Miller et al., 1983, respectively) (Figure 1a). Shallowly dipping normal faults have also been explained as originally steeply dipping faults which have been rotated to shallower dips after being abandoned above an upflexing footwall (Buck, 1988) (Figure 1b).

However, many shallowly dipping normal faults can not be explained by either of these mechanisms. Some of these faults probably initiated at very low dips (e.g. Wernicke et al., 1985; John and Foster, 1993), and many others may have started as initially more steeply dipping structures that remained active as they rotated to relatively low dips. The rotation of these faults is probably due to a combination of domino-style rotation and isostatically driven footwall flexure (Figure 1c). If this explanation is correct, many occurrences of shallowly dipping normal faults might be best interpreted this

Figure 1. Schematic cross-sections of the upper crust showing three models of normal fault evolution, all of which result in both shallowly and more steeply dipping normal faults. Incipient faults are shown as dashed lines, active faults as heavy black lines, inactive faults as thinner black lines. a) Multiple generations of dominos; only moderately to steeply dipping faults are active, shallowly dipping faults have been rotated above younger cross-cutting faults (c.f. Proffett, 1977; Miller et al., 1983). b) Rolling hinge model; initially steeply dipping faults are flexurally rotated above an uplifting footwall, becoming inactive at low dips. New, steep faults break through the intact hanging wall as old faults become inactive and are abandoned on the uplifted footwall (Buck, 1988). c) Synchronous slip model; after some slip and rotation of initially steep faults, younger steep faults break and sole into the rotated older faults. All faults remain active and rotate domino-style, as well as rotating as a result of isostatic uplift of the thinning region.

II - 5

a)

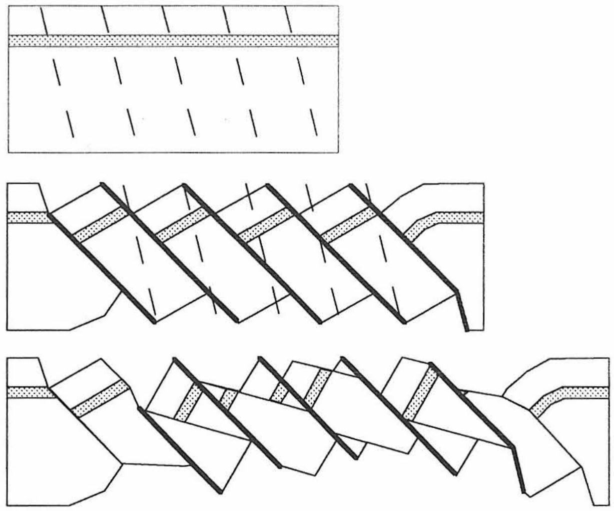

b)

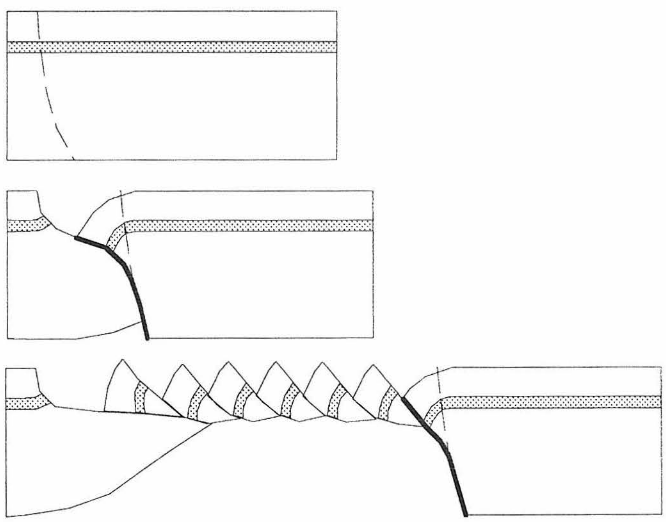

c)

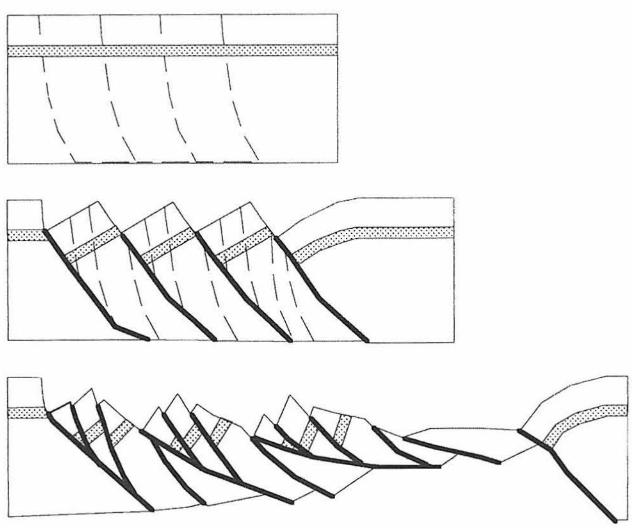

way, since rotation by younger structures would not be necessary in order to achieve low dips.

Detailed geologic studies were conducted in the Gold Butte breakaway zone in the South Virgin Mountains of southeastern Nevada and northwestern Arizona (Figure 2), a region which is well suited for testing the existing kinematic models of continental normal fault systems. The breakaway zone defines a sharp transition from stable, essentially unextended crust of the Colorado Plateau to strongly extended crust of the Basin and Range (stretching factor $\beta \approx 3.5$; Wernicke et al., 1988)). The Plateau, consisting of high-grade Proterozoic basement nonconformably overlain by a thin (~ 2 km) Paleozoic cover, forms a "headwall" from which steeply east-tilted normal fault blocks, bounded by both steep and shallow normal faults, including both basement and cover, were derived.

The mapped area comprises a series of eight moderately to strongly tilted fault blocks deformed by multiple generations of normal faults in Middle Miocene time (Figure 3). These major fault blocks are bounded by normal faults with a kilometer or more of normal throw, and internally disrupted by numerous smaller offset normal faults. The four structurally lowest blocks, including (from lowest to highest) the Wheeler Ridge, Iceberg Ridge, Indian Hills, and Connoly Wash blocks are located astride the eastern end of Lake Mead, Nevada (Figure 3). The fifth block in the stack is the Azure Ridge block, which is interpreted to be structurally continuous with the Gold Butte crystalline block. The next three blocks, which include Tramp Ridge, Lime Ridge, and the Maynard Spring block, lie north of, and structurally above, the Gold Butte crystalline block. The Gold Butte crystalline block is a roughly 15 kilometer wide basement dome, unroofed by one of the extensional faults of the Gold Butte breakaway zone (Fryxell et al., 1992).

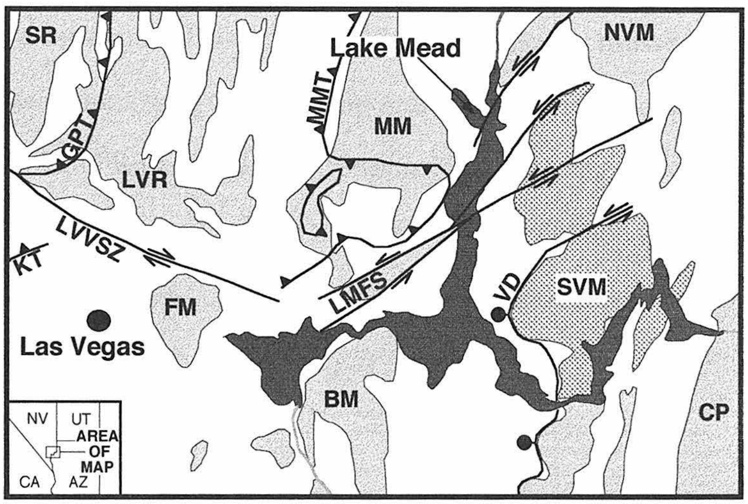

Figure 2. Location map, showing the South Virgin Mountains (stippled) and surrounding area, as well as major structural features. Light grey indicates the location of mountainous terrane. BM - Black Mountains, CP - Colorado Plateau, FM - Frenchman Mountain, GPT - Gass Peak Thrust, KT - Keystone Thrust, LMFS - Lake Mead Fault System, LVR - Las Vegas Range, LVVSZ - Las Vegas Valley Shear Zone, MM - Muddy Mountains, MMT - Muddy Mountains Thrust, NVM - North Virgin Mountains, SR - Sheep Range, SVM - South Virgin Mountains, VD - Virgin Detachment.

Most of the faults which make up the breakaway zone are exposed where they cut through the compact Paleozoic to Tertiary stratigraphy of the South Virgin Mountains. This stratigraphic section includes over thirty mappable units in about three kilometers of section. The rocks of the South Virgin Mountains were not deformed by earlier compressional events, as evidenced by the lack of compressional structures within the region, and the very gentle sub-Tertiary unconformity across the whole of the South Virgin Mountains and Beaver Dam Mountains (Wernicke and Axen, 1988). The faulted sections exposed in the South Virgin Mountains must restore to a configuration which is continuous with the flat-lying sediments of the Colorado Plateau. Since the faults of the Gold Butte breakaway zone are well exposed, have accommodated large magnitude extension, and may be restored to a well defined structural datum, the area provides an exceptional opportunity to study the kinematic evolution of a continental normal fault system.

2.2 Geologic Setting

During Late Jurassic and Cretaceous time, the Lake Mead area was part of the foreland to the thin-skinned Sevier thrust belt (Burchfiel et al., 1974) which developed within the sedimentary rocks of the Paleozoic miogeocline. The easternmost thrusts seem to have been localized along the hinge zone of the miogeocline, which trends roughly NE-SW, and runs just to the west of Lake Mead. Accordingly, the easternmost thrust sheet at the latitude of Lake Mead is exposed close by to the west, in the Muddy Mountains (Longwell, 1949; Longwell et al., 1965; Bohannon, 1983) (Figure 1). South of Lake Mead, the thrust belt changes to a NW-SE trend, and thrusting involves Precambrian crystalline basement rocks (Burchfiel and Davis, 1975).

Following Cretaceous thrusting, the Lake Mead region seems to have been tectonically stable until Neogene time, although Late Cretaceous arc magmatism and Paleocene volcanism affected areas approximately 100 km to the south of Lake Mead. In addition, Paleozoic and Mesozoic strata were removed from a basement high which formed immediately to the south of Lake Mead. The exact age and extent of this basement high remains unclear, due in part to an incomplete understanding of the age and pre-extensional configuration of the sub-Tertiary unconformity. However, the presence of Eocene or older deposits filling northeastward-draining paleocanyons, which cut into the southwestern part of the Colorado Plateau, shows that the basement high had formed by Eocene time (Young, 1966, 1979).

The present day physiographic features of the eastern Lake Mead area are primarily the result of Miocene extensional processes. During Miocene time, extension initiated at the edge of what is now the Colorado Plateau, accommodated on the faults of the Gold Butte breakaway zone. The breakaway zone created a sharp transition from stable, essentially unextended crust of the Colorado Plateau to highly extended crust of the central Basin and Range Province (stretching factor $\beta \approx 3.5$; Wernicke et al., 1988)). The faults of the Gold Butte breakaway zone strongly control the topography of, and are well exposed in, the South Virgin Mountains. The South Virgin Mountains include east tilted fault blocks which contain Proterozoic basement overlain by Paleozoic to Tertiary strata (Figure 3).

The timing of extension on the Gold Butte breakaway is constrained by fission track ages from across the crystalline block. Fitzgerald et al. (1991) discovered apatite fission track ages of approximately 15 Ma across most of the northern Gold Butte crystalline complex, which was interpreted as an extensional unroofing age. Further low temperature thermochronology was attempted by Wolf (1997) using U-Th/He in

Figure 3. Simplified geologic map of the South Virgin Mountains, Nevada and Arizona. The eight major fault blocks, listed in ascending structural order, are: the Wheeler Ridge Block, the Iceberg Ridge Block, the Indian Hills Block, the Connoly Wash Block, the Azure Ridge Block, the Tramp Ridge Block, the Lime Ridge Block, and the Maynard Spring Block. Each of these is bounded by a normal fault with a kilometer or more of throw.

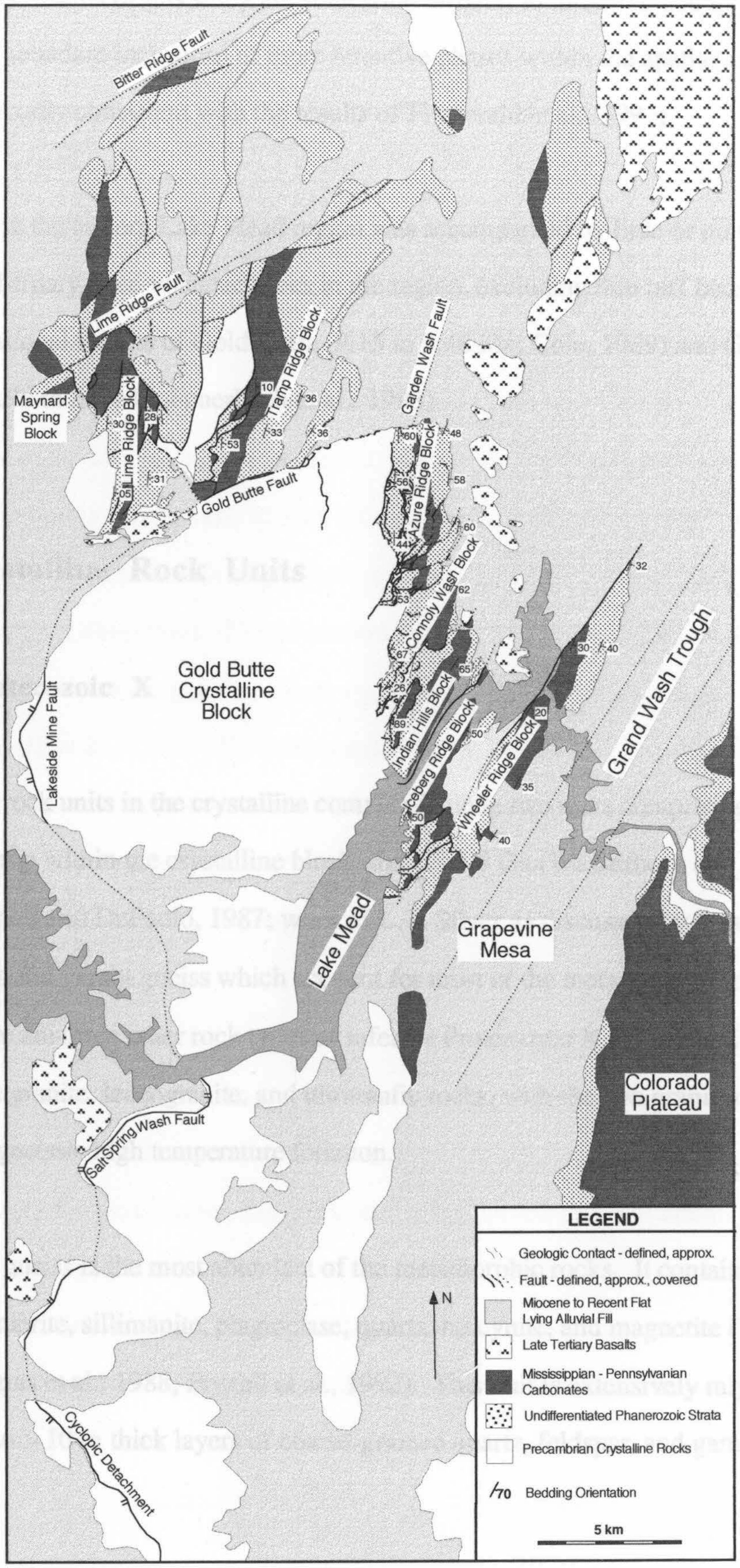
Bitter Ridge Fault
Lime Ridge Fault
Tramp Ridge Block
Garden Wash Fault
Maynard Spring Block
Lime Ridge Block
Gold Butte Fault
Azure Ridge Block
Connoly Wash Block
Gold Butte Crystalline Block
Lakeside Mine Fault
Indian Hills Block
Iceberg Ridge Block
Wheeler Ridge Block
Grand Wash Trough
Lake Mead
Grapevine Mesa
Colorado Plateau
Salt Spring Wash Fault
Cyclopic Detachment
N
LEGEND
Geologic Contact - defined, approx.
Fault - defined, approx., covered
Miocene to Recent Flat Lying Alluvial Fill
Late Tertiary Basalts
Mississippian - Pennsylvanian Carbonates
Undifferentiated Phanerozoic Strata
Precambrian Crystalline Rocks
70 Bedding Orientation
5 km

apatite. The results of this study are somewhat difficult to interpret, due to problems caused by abundant inclusions of more retentive phases within the apatite crystals, but they are broadly consistent with the results of Fitzgerald et al. (1991).

Extension in the eastern Lake Mead region was accompanied by little or no magmatism. The only Tertiary aged volcanic rocks in the region, excluding thin tuff beds, are the post-extensional basalts of Gold Butte (9.15 to 9.46 Ma; Cole, 1989) and Grand Wash Trough (3.99 to 6.9 Ma; Feuerbach et al., 1993).

2.3 Crystalline Rock Units

2.3.1 Proterozoic X

The oldest rock units in the crystalline complex include two units comprising about half of the outcrop within the crystalline block; the 1.7-1.8 Ga (Wasserburg and Lanphere, 1965; Bennett and DePaolo, 1987; work of L.T. Silver as discussed by Stewart, 1980) orthogneiss and garnet gneiss which account for most of the metamorphic country rock. There are three other rock types of inferred Proterozoic X age, including the hornblende granite, leucogranite, and ultramafic rocks, with the two granites locally exhibiting gneissic high temperature foliation.

The garnet gneiss is the most abundant of the metamorphic rocks. It contains garnet, biotite, cordierite, sillimanite, plagioclase, quartz, hercynite, and magnetite (Volborth, 1962; Thomas et al., 1988; Fryxell et al., 1992). This unit is extensively migmatitic, with 1 cm to > 10 m thick layers of coarse-grained quartz, feldspar, and garnet; the remainder of the unit is gneissic and has a well-developed foliation with no lineation (Fryxell et al., 1992).

2.3.2 Proterozoic Y

The Gold Butte Granite (1.45 ±0.25 Ga; Silver et al., 1977) is a large pluton of rapakivi granite that forms about 30% of the basement outcrop (Volborth, 1962; Fryxell et al., 1992). This granite shows a distinctive texture of large (1 cm to 4 cm), early crystallized potassium feldspar phenocrysts, surrounded by a matrix of later crystallized minerals, including plagioclase, quartz, biotite, hornblende, and sphene (Volborth, 1962). Rapakivi texture, with plagioclase rimming the alkali feldspar phenocrysts, is common, but not ubiquitous. The potassium feldspar phenocryst abundance and the intrusive geometry of the granite change significantly from west to east across the pluton (Fryxell et al., 1992). The phenocryst content increases from typically less than 20% in the western outcrops to nearly 70% in the easternmost outcrops. The western outcrops form a complex wormy pattern within the metamorphic country rock, whereas the eastern outcrops are part of a large continuous body, with clearly defined contacts.

In addition to the Gold Butte granite, there are diabase dikes reported from the southern part of the Gold Butte crystalline complex that are probably of Middle Proterozoic age, based on regional correlation with other diabase dikes (Howard, pers. comm.). There are also numerous mica-bearing pegmatite dikes that intrude many of the mappable units but, due to their generally small outcrop area, they were not mapped by Fryxell et al. (1992) or earlier workers. The age of these dikes is uncertain, since they have not been reliably isotopically dated (for a more detailed discussion, see Fryxell et al., 1992).

2.3.3 Mesozoic to Cenozoic

The biotite-muscovite granite which crops out near the western edge of the crystalline complex was previously inferred to have a Proterozoic X age, although field relations were ambiguous (Fryxell et al., 1992). U-Th/Pb monazite dating is currently in progress to determine the absolute age of this intrusion. Preliminary results suggest that it has an age of approximately 64 Ma. It is a fine- to medium-grained equigranular to pegmatitic biotite-muscovite granite with relatively abundant apatite and monazite as accessory minerals.

In addition to the biotite-muscovite granite, there are a number of small post-diabase leucogranites that crop out in the southern part of the Gold Butte crystalline block. These may be of Mesozoic or Cenozoic age, since regionally there are no known post-diabase Proterozoic intrusions (Howard, pers. comm.)

2.4 Stratified Rock Units

2.4.1 Paleozoic to Mesozoic

Separated from the crystalline basement rocks by the sub-Cambrian unconformity is a roughly 2.5 to 3.5 kilometer thick succession of sedimentary rocks (Figure 4). These strata comprise a thin cratonal section, just east of the Cordilleran miogeocline.

These strata comprise four major sequences, with the lower two being carbonate dominated and the upper two being clastic dominated. The lowest sequence is bounded at its base by the Proterozoic to Lower Cambrian unconformity, and is composed of a

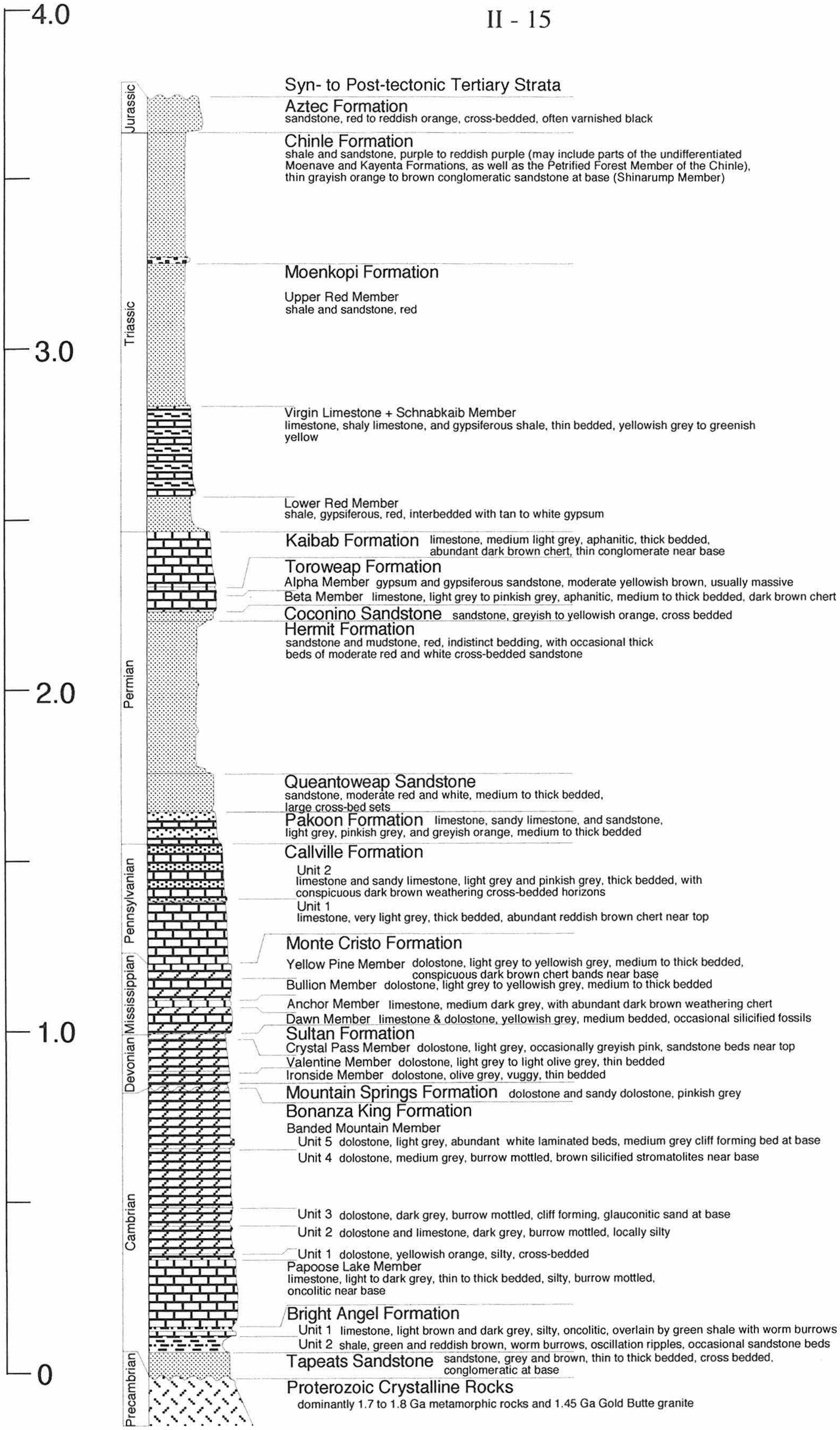

Figure 4. Stratigraphic section from the South Virgin Mountains, thicknesses calculated from map data.

basal clastic succession and an overlying carbonate succession. The basal succession includes the Lower Cambrian Tapeats Sandstone and overlying shales and limestone of the Middle Cambrian Bright Angel Formation (Schenck and Wheeler, 1942; Wheeler, 1943; McKee, 1945; Wheeler and Beasley, 1948). The thickness of this succession is approximately 140 meters, with significant variability due to tectonic thickening and thinning of the Bright Angel shales. The overlying carbonate-dominated succession varies in thickness from approximately 650 meters in Lime Ridge to approximately 520 meters in Wheeler Ridge. It is entirely composed of the Middle to Upper Cambrian (McKee and Resser, 1945; Longwell, 1949; Longwell et al., 1965) Bonanza King Formation, the lowest member of which is limestone (the Papoose Lake Member), with the remainder of the unit being dominantly dolostone.

The top of the first sequence, and the base of the second sequence, occurs at the Upper Cambrian to Devonian unconformity. The second sequence is composed of a carbonate dominated succession, overlain by a clastic succession, in turn overlain by a second carbonate succession. The lower carbonate succession is approximately 800 meters thick, and is composed of the Devonian Mountain Springs and Sultan Formations (McNair, 1951), the Mississippian Monte Cristo Formation (Langenheim, 1963), the Pennsylvanian Callville Formation (Longwell, 1921; McNair, 1951; Lumsden et al., 1973) and the Permian Pakoon Formation (McNair, 1951; McKee, 1975). All of these units are generally described as limestones, but the Devonian and Mississippian units tend to be heavily altered to dolostone in the South Virgin Mountains. The middle clastic succession has an average thickness of about 530 meters and is composed entirely of Permian rocks (White, 1929; McKee, 1933, 1969, 1975). It includes the Queantoweap Sandstone, the Hermit Formation, and the Coconino Sandstone. All three of these units show highly variable thicknesses throughout the map area due to variability in depositional thickness as well as probable tectonic thickening and thinning, particularly within the incompetent mudstones and fine sandstones of the Hermit Formation. Above this is the upper succession of limestone, made up of the Permian Toroweap and Kaibab Formations (Middle Permian; McKee, 1938). It has a maximum thickness of approximately 270 meters and thins toward the southeast, reaching zero thickness within the southeastern part of the South Virgin Mountains.

The boundary between the second and third sequences is defined by the Middle Permian to Lower Triassic unconformity. The third sequence is composed entirely of clastic rocks with a maximum total thickness of about 1100 meters, and a minimum thickness of zero meters, with the southeasternmost outcrops occurring on the east side of Azure Ridge. It includes the Lower to Middle Triassic Moenkopi and Chinle Formations (Gregory, 1915; Gregory and Williams, 1947; Poborski, 1954; Stewart, 1957).

The third and fourth sequences are separated by the base Jurassic unconformity. The fourth sequence includes only the Jurassic Aztec Formation. The Aztec Formation is nearly 200 meters thick in the northern part of the South Virgin Mountains, but pinches out to zero thickness within the central South Virgin Mountains, and is not exposed anywhere south of Tramp Ridge.

All thickness estimates presented herein are based on averaging the mapped thickness from several locations. Most of these strata, as they occur in the South Virgin Mountains, are described in more detail by Morgan (1968) and Matthews (1976), as well as in a measured section by Rowland and Korolev (unpublished data).

2.4.2 Tertiary

Two major sequences of Tertiary strata are present, one that lies disconformably on Paleozoic and Mesozoic strata and is tilted, the other in angular unconformity on all older rocks and still more-or-less flat-lying. The tilted sequence comprises the Miocene Horse Spring Formation (Bohannon, 1984; Beard, 1996). Within the mapped area, most of the outcrops are the Rainbow Gardens Member of the Horse Spring Formation, with exposures of the Thumb Member being less common due to erosional removal or burial by younger sediments. The thickest exposed Horse Spring section, at Horse Spring Ridge, is approximately 600 meters thick. Although the basal Horse Spring beds dip nearly concordantly with underlying Paleozoic strata, and therefore pre-date large magnitude extension and tilting, they are herein classified as early syn-tectonic strata. This classification is based on the fact that the lowest Rainbow Gardens beds exhibit growth-fault fanning of dips where they crop out near the north end of Wheeler Ridge (Figure 5 and Plate 1e). Bedding within the overlying Thumb Member fans slightly up-section, and is therefore also considered to be syn-tectonic (Beard, 1996).

In sharp angular unconformity above the Horse Spring Formation are the more-or-less flat lying "rocks of the Grand Wash trough" (Lucchitta, 1966; Bohannon, 1984). They include a unit composed of red sandstone and siltstone with occasional tuff beds, overlain by interfingering gypsum, conglomerates and basalts. The red sandstone unit is approximately correlative in age with the red sandstone unit of White Basin and Frenchman Mountain in the western Lake Mead region, but was probably not part of a connected depositional system, as all three localities were apparently isolated basins at the time of deposition (Bohannon, 1984). Immediately overlying the red sandstone in Grand Wash Trough are the Basalts of Grand Wash Trough (~4 - 7 Ma; Cole, 1989) and a succession of generally flat-lying conglomeratic units. The conglomerates were broken into three types by Lucchitta (1966); one type that includes clasts of Gold Butte granite as well as other crystalline clasts, a second type that includes crystalline clasts but no Gold Butte granite, and a third type that includes dominantly sedimentary clasts. Within the mapped area, most of the conglomerates are of the type that contains clasts of Gold Butte granite. The sedimentary-clast-dominated conglomerates occur closer to the Grand Wash Cliffs, and the conglomerate with crystalline clasts, but no Gold Butte granite clasts, occurs further south in the Grand Wash Trough (Lucchitta, 1966; Bohannon, 1984). Overlying these conglomerates is the Hualapai Limestone, the age of which is not directly known, but has been inferred based on its relationship to datable rocks elsewhere (~10.8 - 3.8 Ma; Blair, 1978; Blair and Armstrong, 1979; Bohannon, 1984; Faulds et al., 1997).

Conglomerates similar to those included in the "rocks of the Grand Wash Trough" are abundant on the west flank of the South Virgin Mountains, and are generally included in the Muddy Creek Formation (Longwell, 1936; Bohannon, 1984). Near the western end of the Gold Butte Fault, these conglomerates are overlain by the Gold Butte basalt (~ 9 - 9.5 Ma; Cole, 1989). Except for where they are overlain by the Gold Butte basalt, there are no known constraints on the age of the conglomerates, and their ages could extend into the Quaternary (the Muddy Creek Formation is considered by Bohannon (1984) to range from about 11.9 Ma to 10.6 Ma). West of Lime Ridge, these conglomerates are affected by late stage normal faulting (Quaternary?).

Stratigraphically above the "rocks of the Grand Wash Trough" and the Muddy Creek(?) conglomerates are a number of younger conglomerates, gravels, and sands. Some of these deposits, including an outcrop of Chemehuevi Formation at Sandy Point and scattered roundstone gravels, are probably ancient Colorado River deposits. There are

Figure 5. Photograph looking south at basal conglomerates of the Tertiary Horse Spring Formation, Rainbow Gardens Member, in Pigeon Wash near the north end of Wheeler Ridge. Note the fanning of dips, characteristic of strata in growth fault basins. Hammer is approximately 40 cm long.

also numerous levels of Quaternary alluvium. Within individual drainages there are commonly two to four different levels of Quaternary alluvial terraces, but these can not easily be correlated from drainage to drainage.

2.5 Structure

The South Virgin Mountains were essentially undeformed by Mesozoic compressional events, but strongly deformed by Tertiary extension and strike-slip faulting. The only structures within the mapped area that were probably formed by Mesozoic compression are a series of small amplitude (~ 10 meter) folds in Permian to Triassic strata of northeastern Lime Ridge (Plate 1b). North of the mapped area (but still within the South Virgin Mountains), there is a thrust fault adjacent to the Bitter Ridge Fault (Figure 3) of the Lake Mead Fault System that places Pennsylvanian strata over Triassic and Jurassic strata. While it is possible that this is a sliver of a Mesozoic thrust, its proximity to the Bitter Ridge Fault, and the geometry of the Bitter Ridge Fault, suggest that it is more likely due to oblique compression during Miocene strike-slip faulting (Campagna and Aydin, 1994). Most other structures within the South Virgin Mountains are almost certainly due to Miocene extension and/or strike-slip deformation.

The extensional structures are divisible into three categories, the first including large-offset, west-dipping normal faults that bound large ridge-forming fault blocks, the second including numerous, dominantly west-dipping imbricate normal faults which internally disrupt the major fault blocks and usually sole into the ridge-bounding faults, and the third including steeply east-dipping faults which cross-cut all other structures. Stereonet analysis of slip lineations from all three of these fault sets shows that they are predominantly dip-slip normal faults (Figure 6). In addition to the extensional

Figure 6. Fault orientation and slip lineation data. a) Kamb contoured stereoplot of poles to normal faults. This includes only those surfaces which were exposed and measured directly, no three point solutions. Note that mean fault dip direction is 302°, or N58W. b) Kamb contoured stereoplot of measured slip lineations; mean slip direction is approximately 301°, or N59W. c) Rose diagram of slip lineation trends. Together with a) and b), this suggests deformation by dominantly dip slip normal faulting, with extension oriented approximately 300° or N60W. d) Stereoplot of slip lineations and fault planes from the Gold Butte Fault, suggesting left-oblique normal faulting.

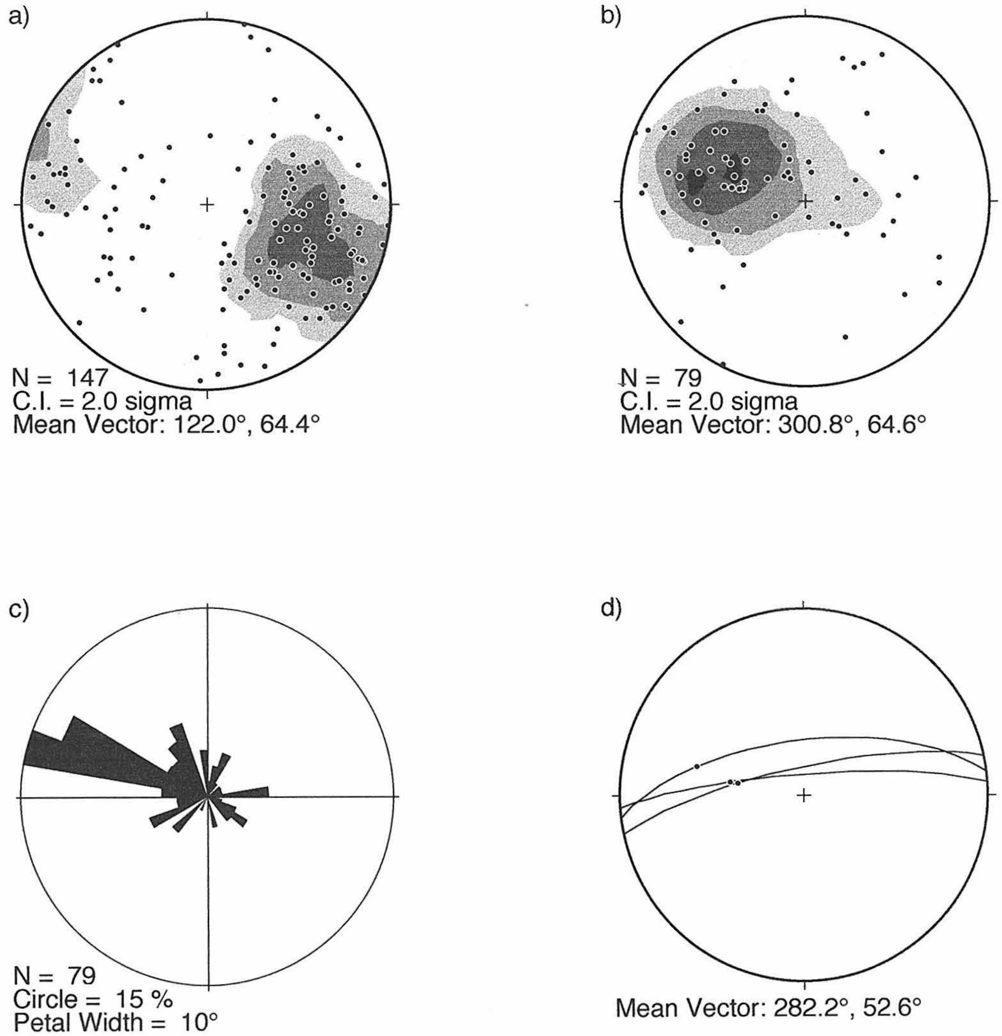
a)
N = 147
C.I. = 2.0 sigma
Mean Vector: 122.0°, 64.4°
b)
N = 79
C.I. = 2.0 sigma
Mean Vector: 300.8°, 64.6°
c)
N = 79
Circle = 15 %
Petal Width = 10°
d)
Mean Vector: 282.2°, 52.6°

structures, there are three steeply dipping, southwest-northeast striking faults and three steeply plunging folds within the South Virgin Mountains.

2.5.1 Ridge-Bounding Faults and Related Folds

South of the Lime Ridge Fault (Figure 3), the South Virgin Mountains include seven major ridge-forming fault blocks, bounded by normal faults which have each accommodated a kilometer or more of offset (Figure 3, Plate 1 and Plate 3). These faults, listed in ascending structural order, include the Grand Wash Fault Zone, the Wheeler Ridge Fault, the Iceberg Canyon Fault, the Indian Hills Fault, the Million Hills Wash Fault, the Garden Wash Fault, the Lime Canyon Fault, and the Maynard Spring Fault.

The easternmost and structurally lowest of these faults is the inferred Grand Wash Fault Zone. This zone separates the Wheeler Ridge block from the adjacent Colorado Plateau (Plate 1e). Since the strata of Wheeler Ridge are downthrown by about 3.5 kilometers relative to the plateau and folded into a rollover anticline, there must be at least one, and possibly more, normal faults separating Wheeler Ridge from the edge of the Colorado Plateau (Plate 3, Section B-B'). However, the fault or faults are nowhere exposed due to burial under the alluvium of Grand Wash Trough.

The next ridge-bounding fault to the west of, and structurally above, the Grand Wash Fault Zone is the Wheeler Ridge Fault (Plate 1d and Plate 1e). This structure was first mapped by Longwell (1936) as a fault surface dipping 60° to the west where it crossed the Colorado River, in outcrops now submerged beneath Lake Mead. The normal offset accommodated on this structure where it crosses Lake Mead is approximately 2.1 kilometers. The Wheeler Ridge fault seems to be a single fault plane which continues to the north for a minimum of approximately 20 kilometers and to the south for approximately 8 kilometers (Plate 1). Beyond the north end of the clearly exposed bedrock of Wheeler Ridge the fault remains visible for about 12 kilometers, juxtaposing Tertiary Horse Spring strata in its footwall and younger conglomerates of the "rocks of the Grand Wash Trough" in its hanging wall (Lucchitta, 1966). This is probably a depositional, rather than tectonic contact, with the rocks of the Grand Wash Trough lapping against the fault scarp. Further to the north, the Wheeler Ridge Fault becomes buried under younger Tertiary conglomerates and gravels, so its location is unknown. To the south, the fault splits into several strands near the south ends of Wheeler and Iceberg Ridges, where some of the displacement on the Wheeler Ridge fault is transferred to a structure which cuts across to the east side of Wheeler Ridge, and becomes buried under Grapevine Mesa (the Airport Fault of Matthews; 1976) (Plate 1d). The rest of the displacement is distributed onto two major, and a number of minor, fault strands which lose displacement southward and eventually merge again near South Cove. One of these two major faults is the South Cove Fault, which was originally mapped by Matthews (1976) as a southwest-northeast trending left-lateral strike-slip fault which cut entirely across southern Iceberg Ridge. More detailed mapping has shown that this fault turns southward and runs along the east side of southern Iceberg ridge, and is continuous with the Sunfish Cove Fault of Matthews (1976). Both parts of this fault are labeled as the South Cove Fault on Plate 1d. The other major strand is the Sheep Canyon Fault, which merges again with the South Cove Fault to the east of South Bay, essentially as interpreted by Matthews (1976). Southward, the Wheeler Ridge Fault is poorly understood, as it disappears under alluvium near South Cove.

The third major fault in the imbricate stack is the Iceberg Canyon Fault, first mapped by Longwell (1936) prior to the filling of Lake Mead and more fully described in a later paper by Longwell (1945). This fault accommodates approximately 1.2 kilometers of normal offset, is gently listric in cross-section, and is seen to cut bedding in its hanging wall at 60° to 90°. It dips approximately 35° to the west where it cuts through the Permian limestones in the hanging wall, and its dip decreases to about 10° to the west where it cuts through Mississippian strata in the hanging wall (Longwell, 1936; 1945).

The fourth fault in the structural stack is the Indian Hills Fault, which dips between 0° and 12° to the east and therefore has a very sinuous fault trace which runs generally north-northeast through the Indian Hills. It forms several klippe of Cambrian rocks on Pre-Cambrian basement and of Mississippian strata on Cambrian (Plate 1d). Where it crosses the line of cross-section A-A' shown in Plate 3, it accommodates a normal separation of the Tapeats Sandstone of approximately 1.5 kilometers. Hanging wall bedding cut-off angles range from about 50° to 70°, except in part of the western Indian Hills, where the fault forms a hanging wall flat for approximately 200 meters in the shales of the Bright Angel Formation. West of this hanging wall flat, the fault again cuts downsection to the west, giving it an overall ramp-flat-ramp geometry. Immediately above this hanging wall flat is an extremely tight rollover anticline that affects the upper unit of the Bright Angel Formation as well as higher Cambrian units (Figure 7).

The fifth fault in the stack, and the last one to crop out east of the Gold Butte crystalline block, is the Million Hills Wash Fault, which apparently increases in offset from south to north. This fault has a well-exposed surface trace which defines the south end and southwest margin of the Azure Ridge block, just north of Connoly Wash. It has an average dip of approximately 12° to the northwest, but there is some variation of dip along the surface trace, and it is slightly listric in cross-section. Bedding cut-off angles in the hanging wall are typically between 70° and 90°. Normal offset on the Million

Figure 7. Photograph looking north at a sharp rollover in the western Indian Hills. The fold formed above a ramp-flat-ramp in the Indian Hills Fault. Strata involved are upper Bright Angel Formation to middle Bonanza King Formation. Field of view across the middle of the photograph is approximately one kilometer. Stratigraphic labels are explained in the legend included in Figure 8.

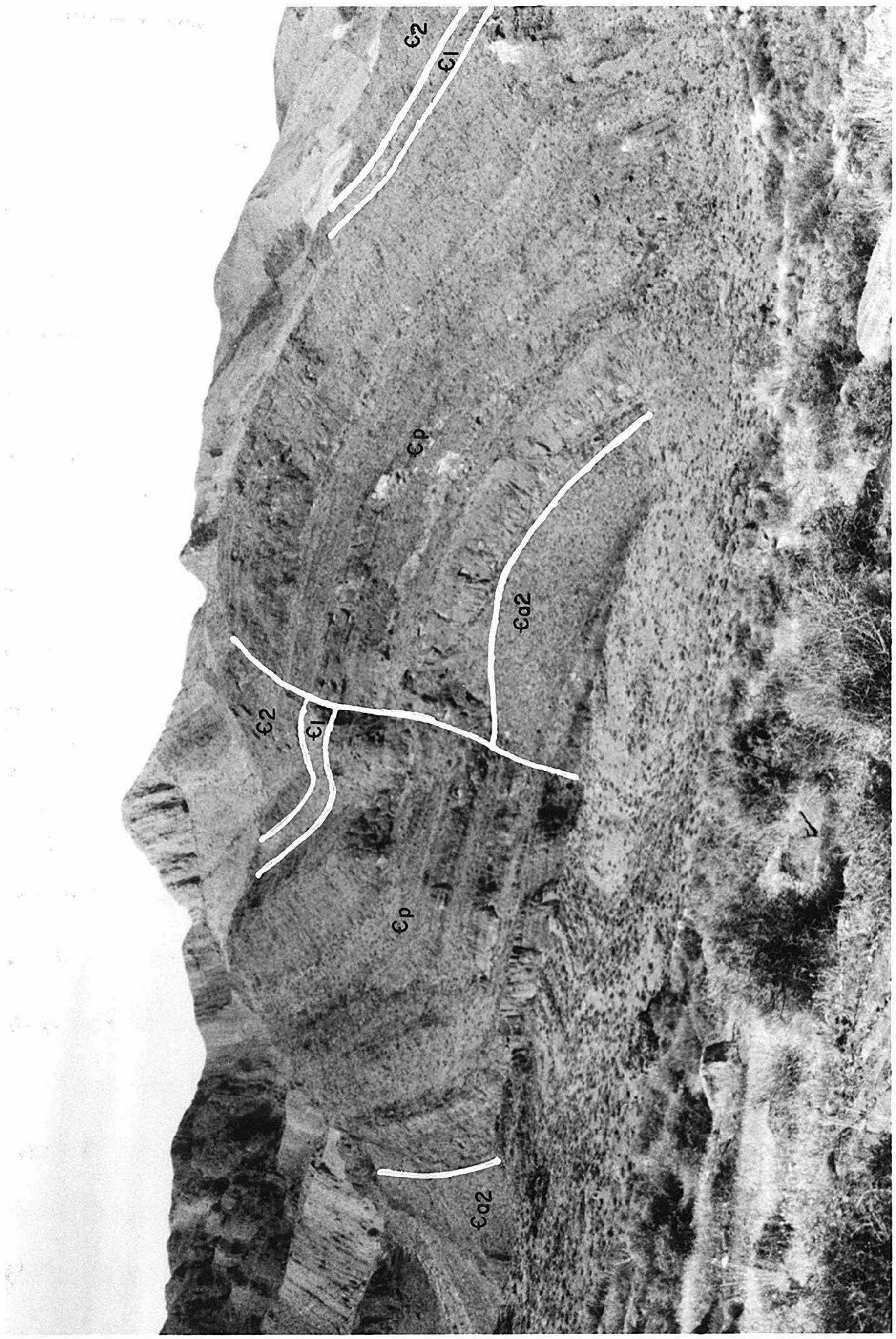
Є2
Є1
Єp
Єa2
Є2
Є1
Єp
Єa2

Hills Wash Fault is less than 100 meters where it occurs as a small klippe just south of Connoly Wash, and increases to approximately 1.1 kilometers at the south end of Azure Ridge, and to slightly greater than 2.4 kilometers under central Azure Ridge (Plate 1 and Plate 3).

Structurally above the Million Hills Wash Fault is the Garden Wash Fault, which is responsible for translating Tramp Ridge, Lime Ridge and the northernmost outcrops of Azure Ridge westward relative to the rest of Azure Ridge (Fryxell et al., 1992). Detailed mapping of Azure, Tramp, and Lime Ridges generally corroborates the earlier mapping of the Garden Wash Fault by Fryxell et al. (1992), but it was necessary to modify and add a few details to their mapping. At the northern end of Azure Ridge, Fryxell et al. mapped a piece of the Garden Wash Fault as a low angle structure placing Mississippian Redwall Limestone (equivalent to the Monte Cristo Formation) over Cambrian dolostone. This outcrop was re-mapped as Permian Toroweap and Kaibab limestones over Cambrian Bonanza King dolostones. In addition to this change, a small outcrop immediately east of Horse Spring Ridge, mapped by Fryxell et al. (1992) and Morgan (1967) as Permian limestone, is instead Mississippian Anchor Member of the Monte Cristo Formation. Just to the east of this outcrop, a large area of Thumb Member of the Horse Spring Formation is irregularly mantled by a thin veneer of gravel. Still further to the east, ~ 1.4 kilometers north of Azure Ridge, small outcrops of Permian Toroweap Limestone were found, directly along strike with those to the south in Azure Ridge. These outcrops are interpreted to be part of a continuous ridge of Permian strata, which is visible as a pale stripe on air photos for at least 3.1 kilometers to the north of Azure Ridge. This partially buried ridge of Permian limestone has an east-west separation of approximately 8 kilometers relative to equivalent strata on Tramp Ridge.

It is proposed here that the name Virgin Detachment be applied to the Garden Wash Fault, as well as the Lakeside Mine Fault (Fryxell et al., 1992), the Salt Spring Wash Fault and the Cyclopic Detachment (Cascadden, 1991), since these form an apparently continuous series of faults (Figure 3) which accommodated major top to the west normal motion during the Miocene. The Garden Wash Fault, which translates Tramp Ridge westward by approximately 8 kilometers relative to Azure Ridge, is probably linked with the Lakeside Mine Fault further to the south, which unroofed the Gold Butte crystalline block at ~ 15 Ma (Fitzgerald et al., 1991; Fryxell et al., 1992). Although partially buried under younger sediments, the Lakeside Mine Fault appears to be continuous southward with the Salt Spring Wash Fault, which also exposes Precambrian crystalline rocks in its footwall and carries ~ 16 Ma growth fault strata in its hanging wall (Cascadden, 1991). The Cyclopic detachment, exposed still further to the south, also has Precambrian crystalline rock in its footwall and is probably continuous with the Salt Spring Wash Fault (Cascadden, 1991).

Structurally above the Virgin Detachment is the Lime Canyon Fault, which separates the Lime Ridge and Tramp Ridge blocks. Overall, the Lime Canyon Fault dips to the west at about 10°, and has accommodated approximately 8 kilometers of westward separation of the Paleozoic section in western Lime Ridge relative to the corresponding section in Tramp Ridge (Plate 1b and Plate 3).

The Lime Canyon Fault appears to have evolved from two major faults and a number of minor anastomosing splays which all merged downward. This interpretation is based on a retrodeformable cross-section of the Lime Canyon and Perkin's Spring area (Plate 4). The westernmost of the two main splays crops out clearly around the head of Lime Canyon, where it is a well-exposed flat-lying fault, carrying relatively simple imbricate fault blocks of east-dipping Mississippian and Pennsylvanian strata in its hanging wall, with bedding cut-off angles between 35° and 45° (Plate 1b). The eastern splay crops out on westernmost Tramp Ridge, where it carries lower Cambrian units down against Precambrian basement (Plate 3, cross-section A-A'). This splay projects just above the basement block which separates Tramp Ridge from Lime Ridge, and may have merged with the detachment that underlies the Perkin's Spring area and Lime Canyon Fault farther west (Plates 1b, 3, and 4). In order for this projection to work, the offset on the fault that bounds the west side of the basement block between Tramp and Lime Ridges must be restored. This suggests that the basement block may be a later uplifted horst, from the footwall to the eastern splay of the Lime Canyon Fault.

The western splay of the Lime Canyon Fault may have a ramp-flat-ramp geometry, and this geometry may explain the relatively flat-lying, little extended strata of northern Lime Ridge. At Lime Canyon, the fault cuts bedding at a relatively low angle (approximately 40°), and is inferred to have cut through this part of the section with an initially moderate west dip. Its initial dip is less well constrained where the fault cuts down through the rest of the Paleozoic section; however, creation of an area-balanced cross-section seems to require the fault to have flattened to dips as low as 15° to 20° where it cut through the lowest part of the section, so it was apparently a shallowly dipping listric fault which included a flat near the base of the Cambrian section (Plate 4). A northward increase in the length of this flat might result in a wide block of hanging wall strata being carried westward over a flat surface, and undergoing only minor internal disruption and rotation. This would explain the wide block of little rotated Pennsylvanian strata seen in northern Lime Ridge.

Near Perkin's Spring, between Tramp Ridge and Lime Ridge, the Lime Canyon Fault is nearly flat lying, and its hanging wall is structurally complex (Figure 8 and Plate 1b). To the west of Perkin's Spring, a set of west-dipping, top-to-the-west normal faults within the hanging wall of the Lime Canyon Fault carry east-dipping panels of Cambrian strata down against Proterozoic basement. These panels of east-dipping Cambrian strata are structurally overlain by a west-dipping panel of Pennsylvanian Callville Formation, carried on a west-dipping normal fault. The structures to the east of Perkin's Spring dip in the opposite direction to those just described from the west of Perkin's Spring. To the east, a set of east-dipping, top-to-the-east normal faults, carry west-dipping panels of Cambrian strata down against Proterozoic basement. These are structurally overlain by an east-dipping panel of Permian Toroweap Formation, carried on an east-dipping fault.

The arrangement of fault slices seen near Perkin's Spring may have been achieved by collapsing a stack of imbricate fault slices, bounded by predominantly west-dipping, west-side-down normal faults, onto a shallowly dipping detachment (Figure 8). In order to achieve their present configuration, the imbricate slices must have initiated in an eastward-stepping and down-stepping sequence. This would result in slices of stratigraphically higher Pennsylvanian Callville Formation being carried downward, and to the west of, the stratigraphically lower slices from the Banded Mountain Member of the Bonanza King Formation, which would in turn be carried downward and to the west of slices of the Papoose Lake Member of the Bonanza King Formation. All of these fault slivers would then be carried westward and downward against Proterozoic basement rocks. The occurrence of west-dipping panels, separated by east-dipping, top-to-the-east normal faults can be explained by top-to-the-west simple shear within the fault bounded imbricate slices. Within each fault sliver shown on Figure 8, it is reasonable to expect a top-to-the-west rotation of blocks, bounded by top-to-the-east faults.

Figure 8. Detailed cross-section and restoration of the Perkin's Spring area. This cross-section coincides with part of cross-section A-A' from Plate 3. Across the entire section, shallowly dipping normal faults separate a thin veneer of extensionally imbricated Paleozoic rocks from Precambrian basement. These shallowly dipping faults are all considered to be part of the Lime Canyon Fault, although only the western strand, which crops out at Lime Canyon, is labeled on the section.

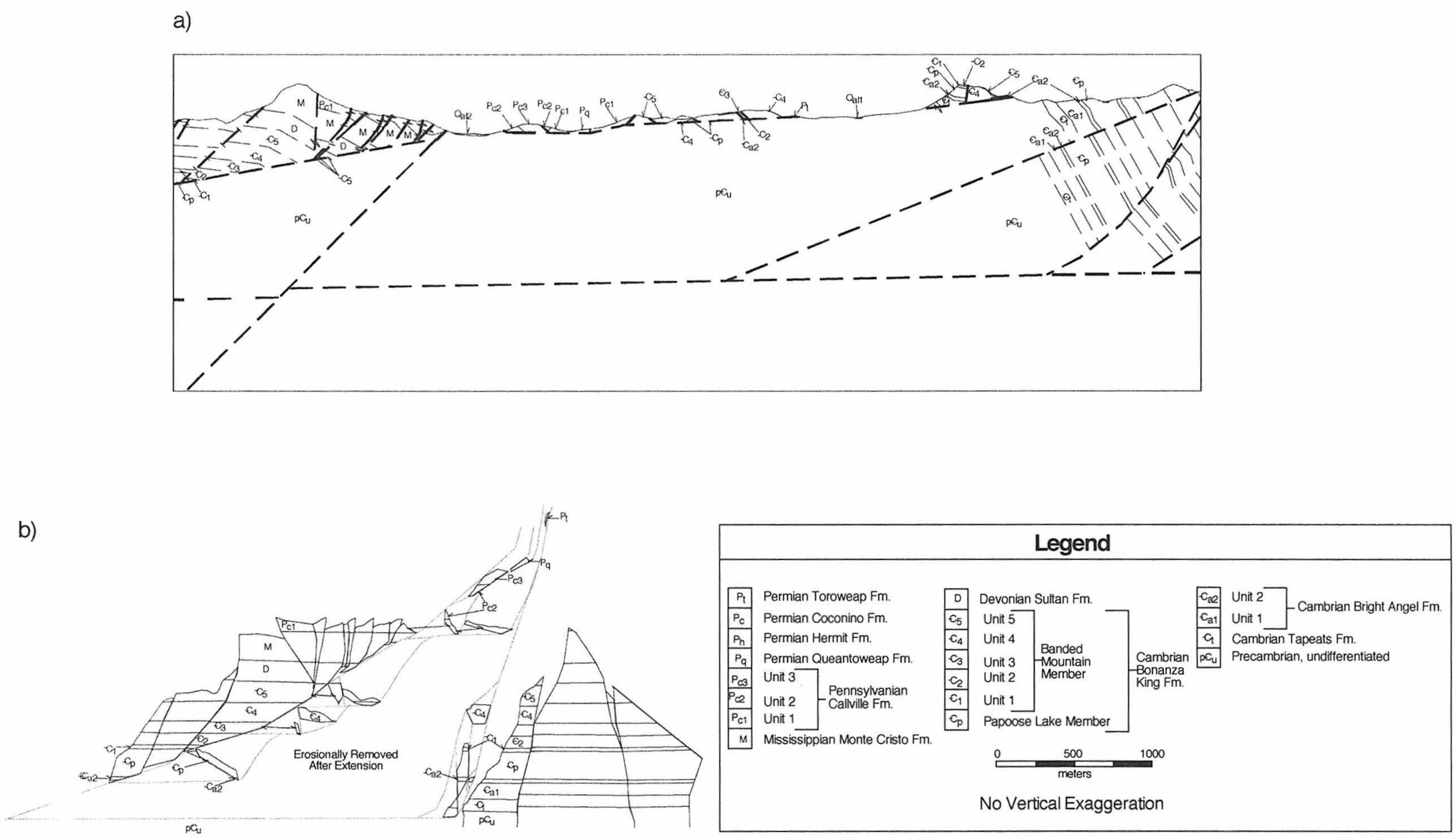
a)
b)
Erosionally Removed After Extension
Legend
Permian Toroweap Fm.
Permian Coconino Fm.
Permian Hermit Fm.
Permian Queantoweap Fm.
Unit 3
Unit 2
Unit 1
Pennsylvanian Callville Fm.
Mississippian Monte Cristo Fm.
Devonian Sultan Fm.
Unit 5
Unit 4
Unit 3
Unit 2
Unit 1
Banded Mountain Member
Papoose Lake Member
Cambrian Bonanza King Fm.
Unit 2
Unit 1
Cambrian Bright Angel Fm.
Cambrian Tapeats Fm.
Precambrian, undifferentiated
0
500
1000
meters
No Vertical Exaggeration

The westernmost and structurally highest ridge-bounding fault is the Maynard Spring Fault. This fault separates the roughly north-south striking strata of Lime Ridge from the northeast-southwest striking strata which comprise the westernmost outcrops of the range. The Maynard Spring fault is well exposed starting just south of the Lime Ridge Fault and continuing southward for approximately a kilometer, where it becomes buried under alluvium. For an additional 1.4 kilometers to the southeast, several small exposures of fault-bounded Permian Toroweap Limestone are found; these are probably part of the hanging wall of the Maynard Spring Fault. This fault differs from other ridge-bounding faults in so far as the strike of hanging wall strata is markedly different from foot wall strata. Hanging wall strata strike approximately N65E, whereas strata in the adjacent parts of Lime Ridge strike due north, suggesting clockwise rotation of the hanging wall rocks of about 65° about a vertical axis, in addition to extension.

2.5.2 Minor Imbricating Faults and Related Folds

Within each of the major fault blocks bounded by large offset faults are numerous smaller offset normal faults. These faults typically have offsets in the range of 5 meters to 100 meters, with a few having offsets of several hundred meters. These faults accommodate internal deformation and extension of the major fault blocks and usually merge downward with the major ridge-bounding normal faults (Figure 9). They dip more steeply and usually have higher bedding cut-off angles than the ridge bounding faults. Most of these smaller offset faults have hanging wall bedding cut-off angles of about 90°, with some having cut-off angles greater than 115° (Figure 10).

Nearly all of these smaller offset faults merge with, or are truncated by, shallowly-dipping, large-offset ridge-bounding faults. Of 27 cases where a more steeply dipping fault clearly intersects a shallowly dipping ridge-bounding fault, the more steeply dipping fault is truncated by, or merges with, the shallowly dipping fault in 25 cases. There are only two cases in which the more steeply dipping faults cut the shallowly dipping, block-bounding fault. These two more steeply dipping faults are close together, sub-parallel, and each accommodates roughly 30 meters of west side down normal separation. They cut through the southern end of the Mississippian on Cambrian klippe formed by the Indian Hills Fault just north of Devil's Cove. The intersection of these faults with the underlying Iceberg Canyon Fault is not exposed, so it is unclear whether or not they also cut it. It is certainly possible that they splay upward from the Iceberg Canyon fault and cut only the Indian Hills Fault.

Nearly all of the minor imbricating normal faults are synthetic to the ridge bounding detachments. There are a few antithetic faults, all of which have been rotated so that they now appear to be reverse faults (the two most significant of these can be seen on cross-section A-A' of Plate 3, one under eastern Azure Ridge, and one under central Tramp Ridge).

Upward fanning synthetic faults are associated with two large amplitude, broadly folded, rollover anticlines in the strata of the western half of Azure Ridge and the eastern part of Lime Ridge (cross-section A-A', Plate 3). Rather than being due to folding of any individual panel of strata, these antiforms result from a gradual decrease in dip of small imbricate fault blocks as one moves structurally upward.

Figure 9. a) Map of the southern tip of Azure Ridge, showing anastomosing moderately dipping faults soling into the nearly horizontal Million Hills Wash Fault. The moderately dipping faults typically dip between 20° and 40° to the west; bedding mostly dips between 45° and 60° to the east; hanging wall bedding cut off angles are mostly between about 65° and 100°. b) Photograph looking north at the south end of Azure Ridge, showing approximately the eastern half of the area mapped in a). The Million Hills Wash Fault runs along the break in slope at the base of the Paleozoic strata.

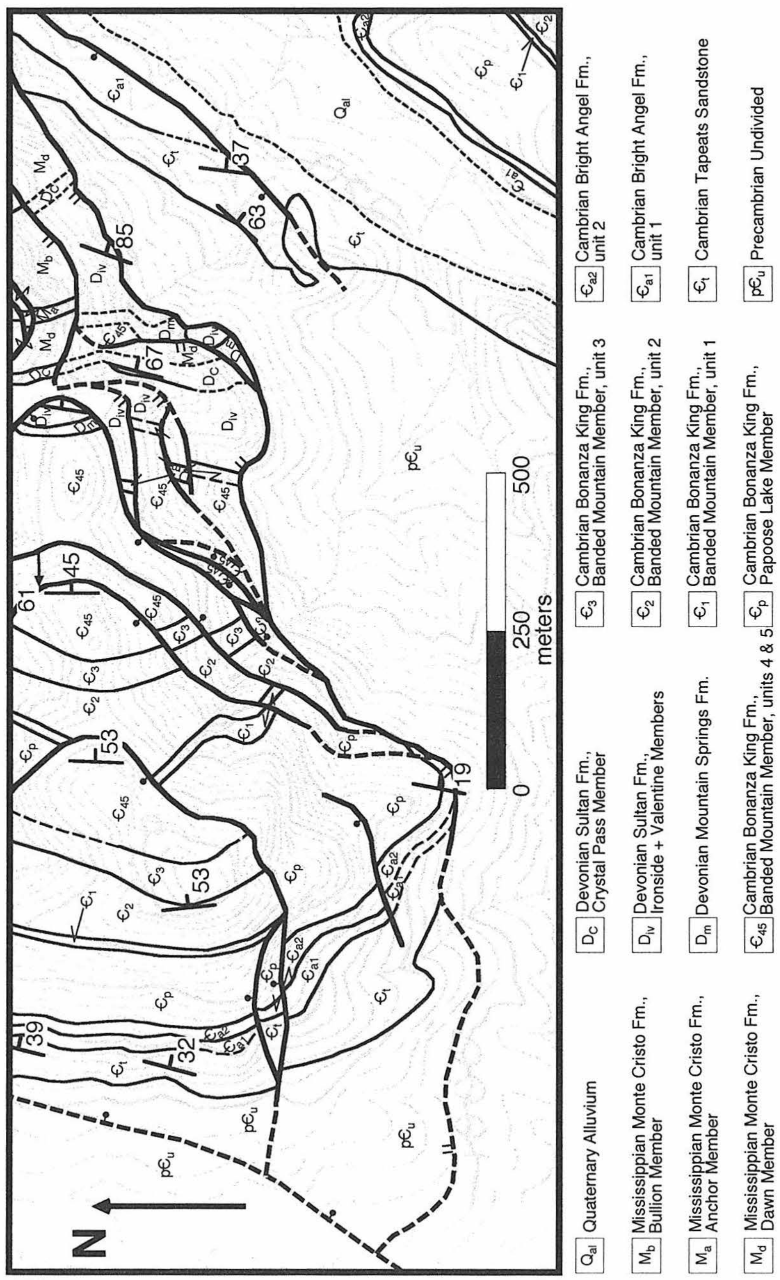
N
0 250 500
meters
Qal Quaternary Alluvium
Mb Mississippian Monte Cristo Fm., Bullion Member
Ma Mississippian Monte Cristo Fm., Anchor Member
Md Mississippian Monte Cristo Fm., Dawn Member
Dc Devonian Sultan Fm., Crystal Pass Member
Div Devonian Sultan Fm., Ironside + Valentine Members
Dm Devonian Mountain Springs Fm.
Ꞓ45 Cambrian Bonanza King Fm., Banded Mountain Member, units 4 & 5
Ꞓ3 Cambrian Bonanza King Fm., Banded Mountain Member, unit 3
Ꞓ2 Cambrian Bonanza King Fm., Banded Mountain Member, unit 2
Ꞓ1 Cambrian Bonanza King Fm., Banded Mountain Member, unit 1
Ꞓp Cambrian Bonanza King Fm., Papoose Lake Member
Ꞓa2 Cambrian Bright Angel Fm., unit 2
Ꞓa1 Cambrian Bright Angel Fm., unit 1
Ꞓt Cambrian Tapeats Sandstone
pꞒu Precambrian Undivided


D
Є45
Є3
Є2

Figure 10. Photograph looking north obliquely across a canyon at moderately to steeply west-dipping imbricate normal faults in the hanging wall of the Indian Hills Fault. These faults merge downward with the Indian Hills Fault. Note the bedding cut off angle of about 115° in Pennsylvanian strata in the hanging wall of the most steeply dipping fault (photograph is looking approximately along strike of this bedding-fault intersection). See the legend in Figure 8 for an explanation of stratigraphic labels.

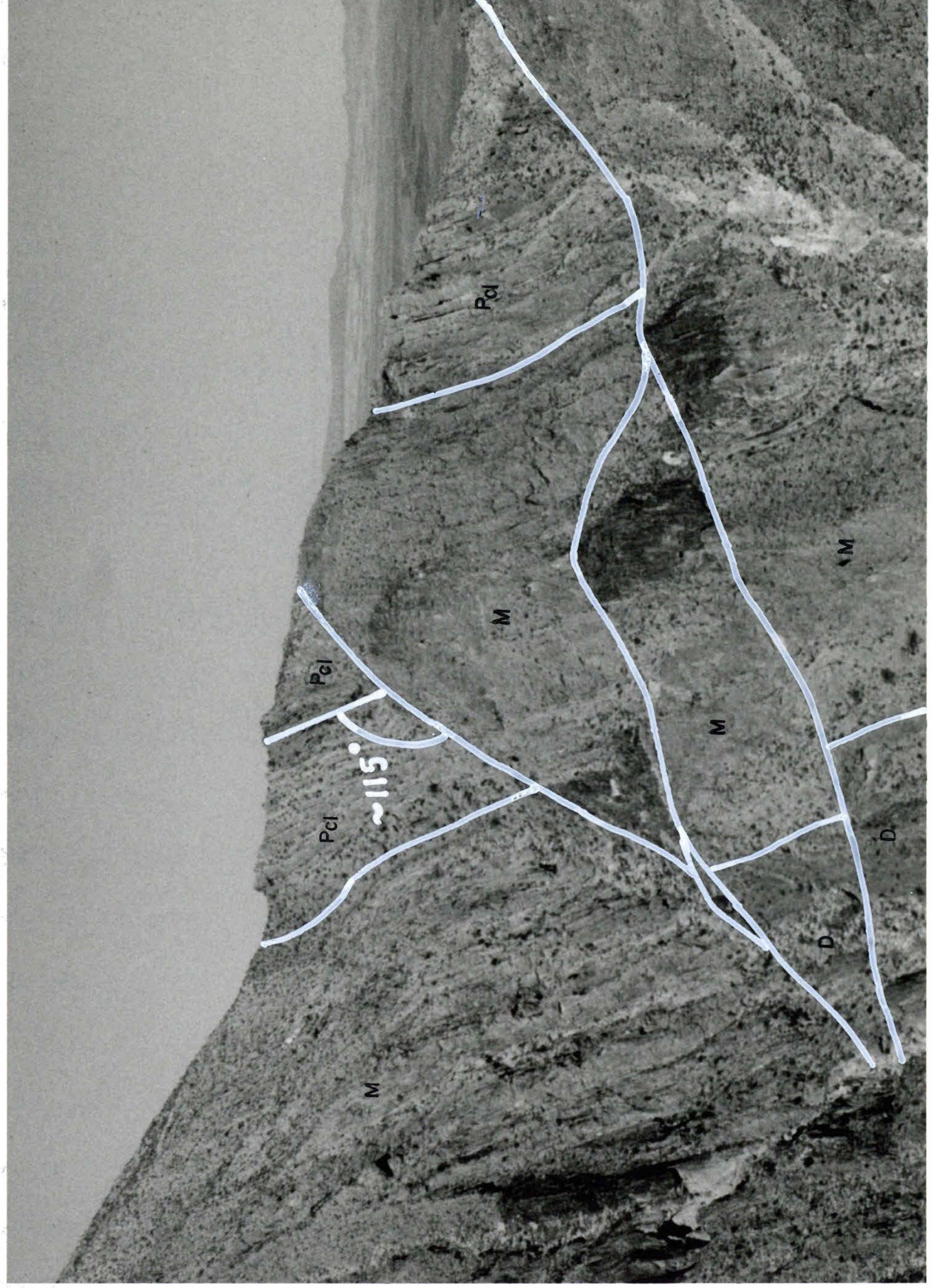
Pcl
Pcl
Pcl
~115°
M
M
M
M
D
D

2.5.3 Cross-cutting Faults

The extensional structures recognized in the South Virgin Mountains include a number of sub-vertical faults that cut all other normal faults and are upthrown on the side closest to nearby crystalline blocks. East of the Gold Butte crystalline block these faults are consistently east-side-down, i.e. they are upthrown on the side closest to the main Gold Butte crystalline block. North of the Gold Butte Block, within the Tramp Ridge - Lime Ridge area, steeply east- and west- dipping cross-cutting faults bound a horst of crystalline rocks between Tramp Ridge and Lime Ridge. There are also two steeply west-dipping faults within Lime Ridge that cut across moderately and shallowly dipping faults, and are upthrown on the east side, i.e. the side closest to the crystalline block between Tramp Ridge and Lime Ridge.

Many of the steep cross-cutting normal faults are localized along the basement-cover contact. An en-echelon series of these faults is located along the western edge of Azure Ridge, and a similar fault was mapped by Longwell (1936) near the south end of Iceberg Canyon. The faults bounding Azure Ridge dip vertically to steeply eastward and have east side down normal separations ranging from a few meters to greater than 150 meters. The fault near the south end of Iceberg Canyon, as described by Longwell (1936), is a steeply west-dipping structure which places Proterozoic granite against mid-(?) Bonanza King, making this a steep reverse fault with approximately 500 meters of dip-slip movement. The faults that bound the horst between Tramp Ridge and Lime Ridge accommodate between a few meters and greater than 500 meters of normal separation, bringing Paleozoic strata ranging from the Cambrian Tapeats Sandstone to highest Cambrian Bonanza King down against Proterozoic crystalline rocks.

There are also a number of steeply dipping, cross-cutting faults found within the ridges of Paleozoic strata as bedding-parallel shear surfaces. These structures are difficult to observe, except where they offset younger normal faults (Figure 11). These bedding-parallel faults, with normal separations of a few meters to a few tens of meters, were only found east of the Gold Butte crystalline complex. They apparently decrease in abundance and offset with increasing distance from the crystalline complex, with no examples being found east of Iceberg Canyon.

2.5.4 Steep SW-NE Striking Faults

Three major southwest-northeast striking faults appear on previous maps of the South Virgin Mountains. From north to south, these include the Bitter Ridge Fault, the Lime Ridge Fault, and the Gold Butte Fault (Anderson, 1973; Bohannon, 1979, 1984; Beard, 1996) (Figure 3). All are considered to be steeply dipping strands of the left-lateral Lake Mead Fault System. Recent work by Campagna and Aydin (1994) showed that the Bitter Ridge Fault is a sub-vertical structure with slickenlines plunging gently to the southwest, supporting the interpretation that this is a strand of the Lake Mead Fault System. However, Fryxell et al. (1992) re-interpreted the Gold Butte Fault as a right-lateral tear fault in the hanging wall of the Garden Wash Fault Zone, suggesting that it is not a branch of the Lake Mead Fault System.

The Gold Butte Fault was completely re-mapped during this study. The mapping showed it to be a vertical to steeply north-dipping structure, with slip lineations plunging steeply to the north (Figure 6 d).

Figure 11. Photographs of late, east-side down, east-dipping faults. Stratigraphic labels are explained by the legends shown in Figures 8 and 9. a) West-dipping fault offset by approximately 40 meters of slip along a surface parallel to the base of the Mississippian Anchor Member, central Indian Hills. b) West-dipping fault offset by approximately three meters of bedding-parallel slip within the Pennsylvanian Callville Formation, northern Azure Ridge. c) Sliver of Mississippian Anchor Member along the Indian Hills Fault, offset by a slip surface which is parallel to bedding in the structurally lower Cambrian Bonanza King Formation and sub-parallel to bedding in the structurally higher Pennsylvanian Callville Formation, northeastern Indian Hills. d) Bedding parallel shear zone within the Pennsylvanian Callville Formation, eastern Azure Ridge. Pocket knife for scale is approximately eight centimeters long.


Mb
Ma
Mb
Md
Ma
Dc
My
Div
Md
ridgeline
Mb
Mb
Dm
Md
€45
Md
Dc
Div

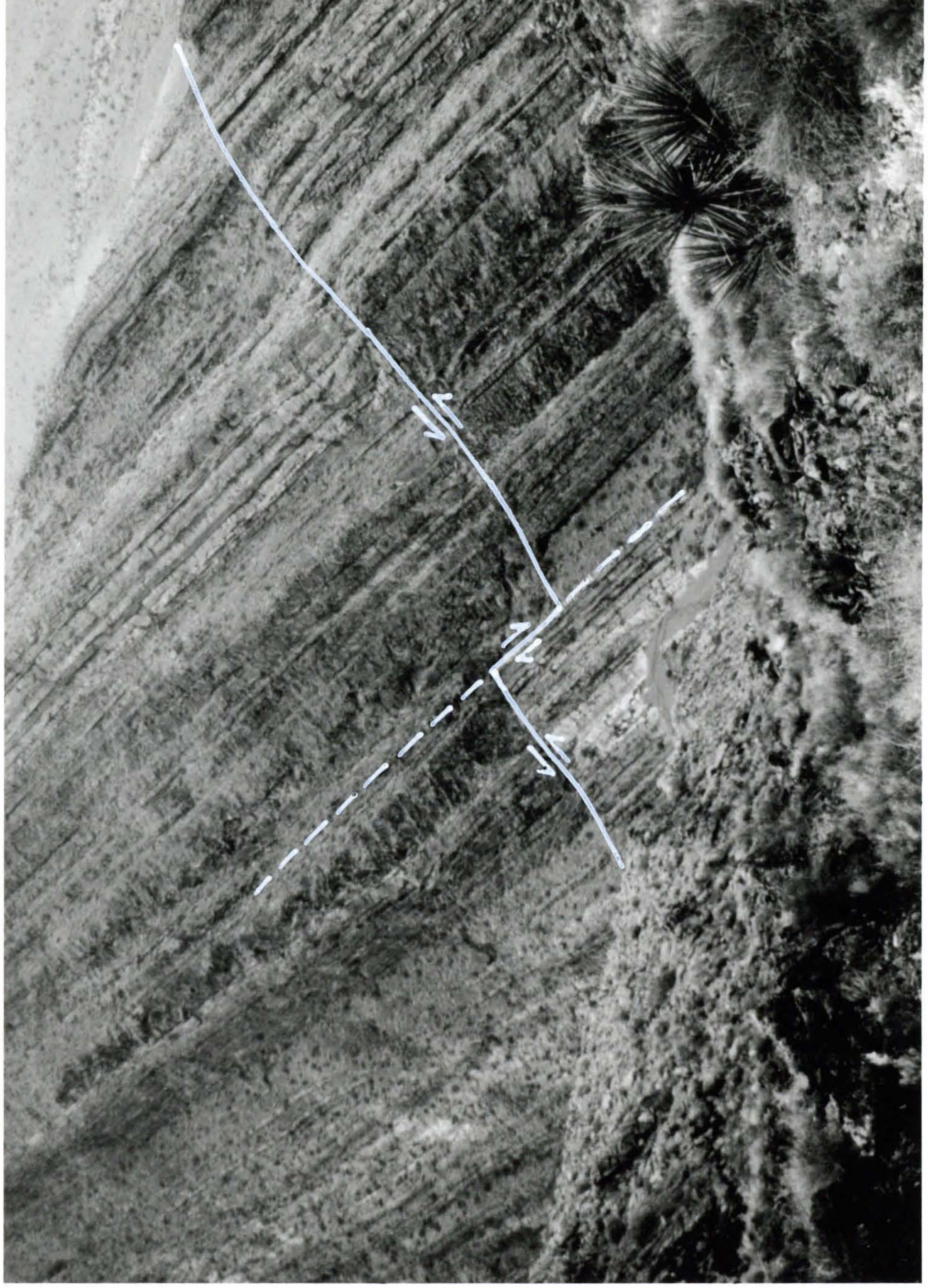

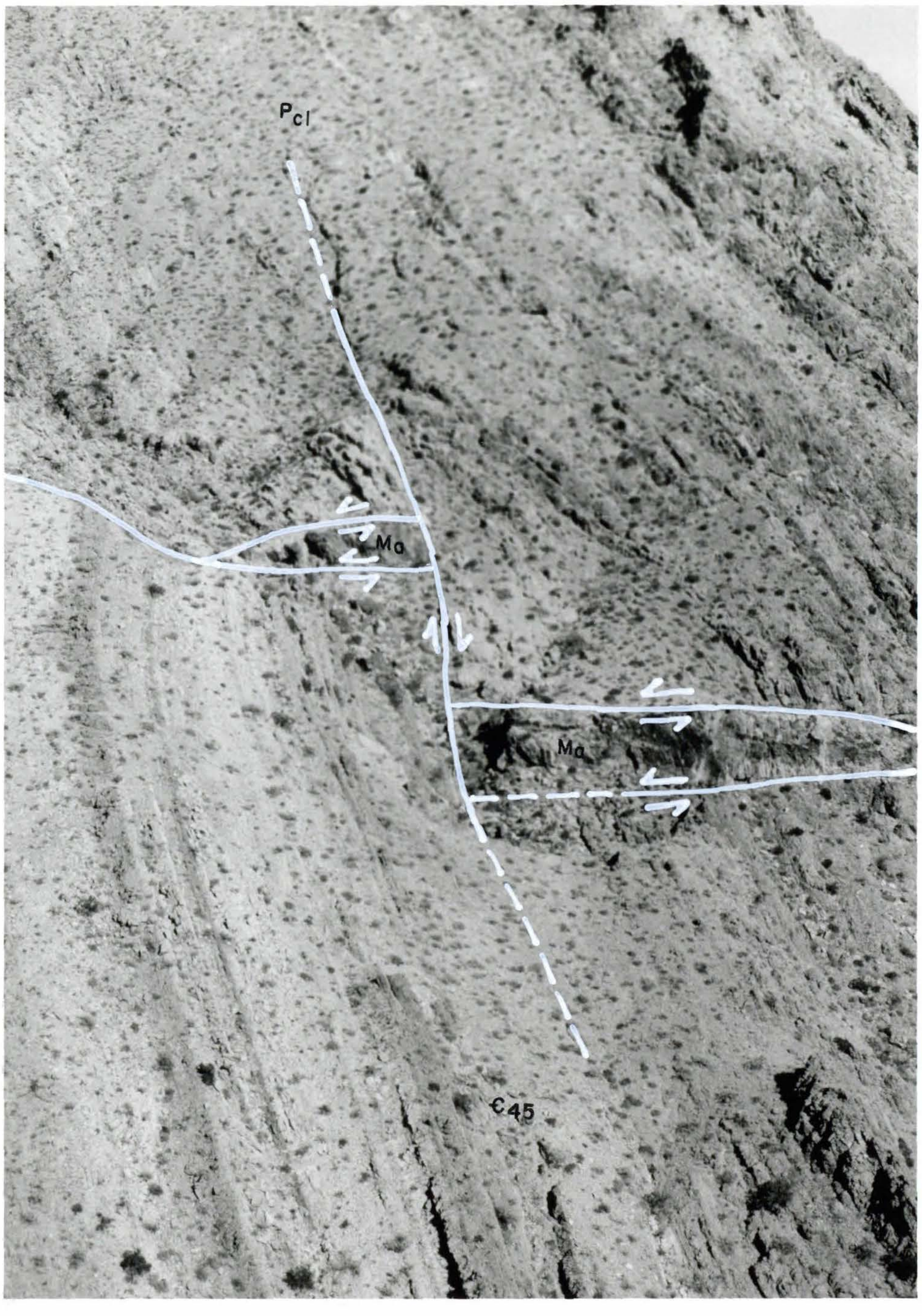
Pcl
Ma
Ma
€45

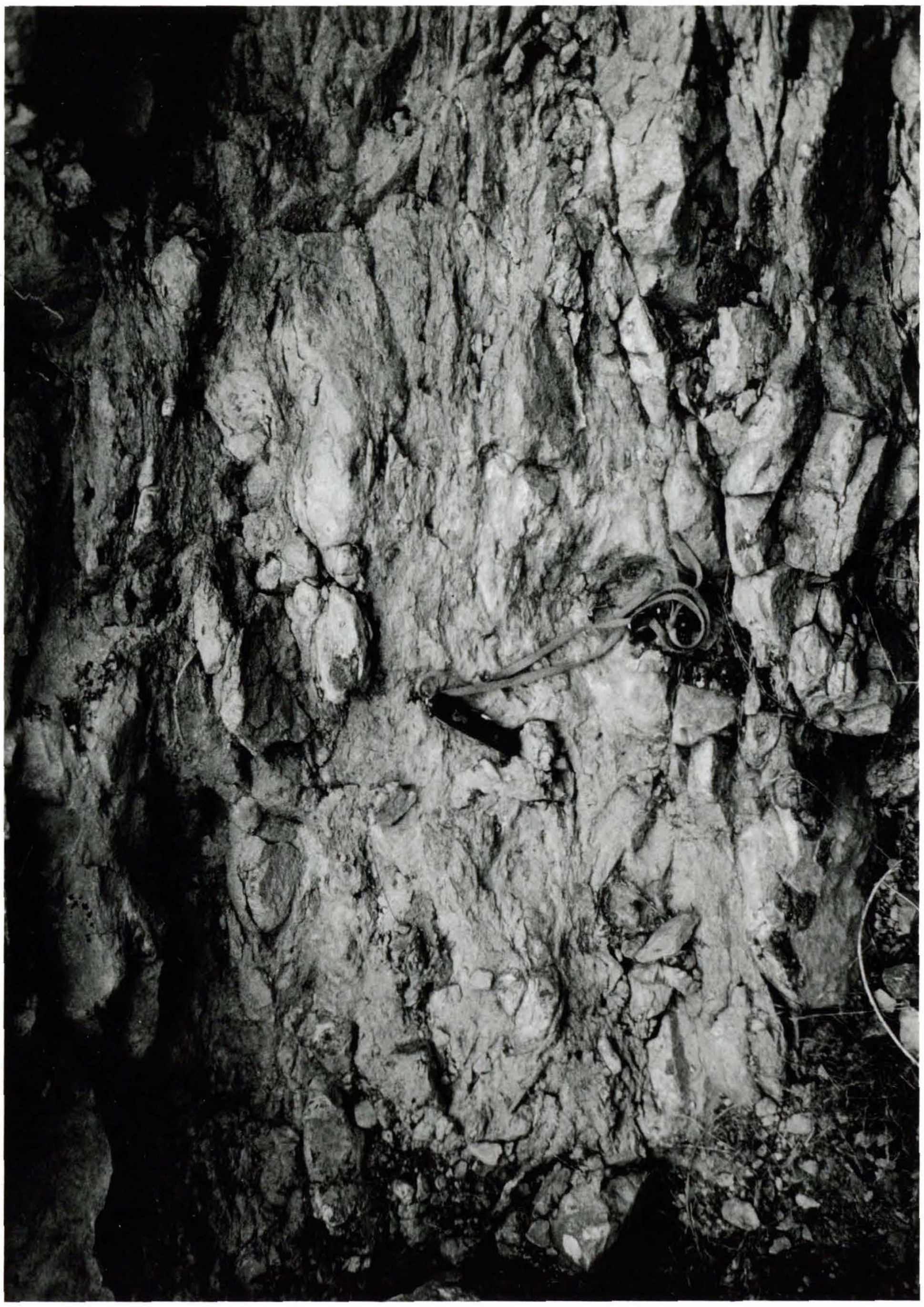

New mapping along part of the Lime Ridge Fault shows that it is not a simple, steeply northwest-dipping plane. Where re-mapped at the north end of Lime Ridge (Plate 1), the fault exhibits a sinuous trace, and based on its outcrop pattern where it cuts up and over eastern Lime Ridge, its dip is only about 50° to the northwest.

2.5.5 Steeply Plunging Folds

There are three large steeply plunging folds within the South Virgin Mountains, all clearly visible in map view, which appear to be either right-lateral or left-lateral deflections of steeply tilted ridges adjacent to fault zones. Two of these occur north of and immediately adjacent to the Gold Butte Fault, producing right-lateral deflection of Horse Spring strata in Horse Spring Ridge and basal Cambrian strata in southernmost Lime Ridge (Plate 1a and Plate 1c). The third fold is apparently left-lateral, and is outlined by a gradual change in strike of bedding in the ridges east of the Gold Butte crystalline block. The average strike of bedding changes northward from approximately N30E in Wheeler Ridge, Iceberg Ridge, and the southern Indian Hills to approximately N05E in northern Azure Ridge (Plate 1).

2.6 Interpretation of Subsurface Geometries of Concealed Faults

Most of the major normal faults of the South Virgin Mountains are well exposed, but three of the major ridge-bounding normal faults or normal fault zones are concealed by alluvium along much or all of their traces. These three faults are the Grand Wash Fault Zone, the Wheeler Ridge Fault, and the Garden Wash Fault. In addition, the late, steep cross-cutting fault of southern Iceberg Canyon is covered by the waters of Lake Mead. Nevertheless, the location, geometry, and offset of all of these faults can be constrained reasonably well using a variety of geologic arguments. The locations and geometries of the Wheeler Ridge Fault and the steep cross-cutting fault of southern Iceberg Canyon are constrained by the observations of Longwell (1936), made prior to the filling of Lake Mead.

The Grand Wash Fault Zone must include one or more, west-side-down normal faults. These faults are inferred to be relatively steep listric structures that have only been rotated a few degrees from their initial orientations. The inference of only minor rotation of these faults is based on the absence of structurally lower faults with major offset, and the observation that the next higher structure (the Wheeler Ridge Fault) is apparently only slightly rotated from its original orientation. The inference that the fault or faults of the Grand Wash Fault Zone initiated as steeply dipping listric structures is based on the observed rollover geometry of Wheeler Ridge and on analogy with higher and lower normal fault zones, where listric curvature is directly observed. These include the Hurricane Fault and Iceberg Canyon Fault, both of which had initially steeply dipping listric geometries. The Hurricane Fault cuts the Colorado Plateau approximately 65 kilometers east of the Grand Wash Fault Zone, is vertical where it cuts Permian strata and shallows to approximately 60° westward dip where it cuts through the lower part of the Cambrian section (Hamblin, 1965). 30° of shallowing across approximately two kilometers of section is similar in curvature to the Iceberg Canyon Fault, which shallows at a rate of ~ 16° per kilometer.

Our preferred interpretation of the Grand Wash Fault Zone is that it includes at least two normal faults, which have served to downdrop the east side of the Wheeler Ridge block by approximately 3.5 kilometers relative to the Colorado Plateau. Projection of beds from Wheeler Ridge to the inferred location of the western fault strand of the Grand Wash Fault Zone suggests that almost all of this 3.5 kilometer offset can be accommodated on the western strand. The amount off offset on the inferred fault further to the east is unknown, but is probably relatively small. The offset on the eastern fault is inferred to be small for two reasons: 1) Large offset on a listric fault should have resulted in hanging wall rotation and consequent creation of a tilted fault block ridge where the Grand Wash Trough currently exists, and none is observed; 2) Interpreted gravity data suggest that the Grand Wash Trough is a more-or-less symmetrical basin which deepens northward, being only about half a kilometer deep immediately east of Wheeler Ridge on the line of cross-section B-B' (Plate 3), and reaching three or four kilometers depth about 40 kilometers farther north (Saltus and Jachens, 1995).

The location of the western strand of the Grand Wash Fault Zone, as shown in Plates 1 and 3, is based on an assumption of high bedding cut-off angles in the Wheeler Ridge hanging wall, as seen in most other hanging wall blocks in the region, combined with the inferred steep dip of the fault and the observed rollover of strata within the Wheeler Ridge block. Note that the location of this strand, as shown in Plates 1 and 3, is near its easternmost allowable position, since strata are shown as having cut-off angles greater than 90°, and these cut-off angles would become unreasonably large if the fault was drawn further to the east and strata in Wheeler Ridge continue to roll over. This preferred interpretation does allow a hanging wall cut-off angle of slightly more than 90°, which is not reasonable for an initially west dipping fault, unless some small amount of increase in cut-off angle beyond 90° resulted from collapse of the hanging wall into the potential void adjacent to the listric fault surface. However, this assumption is necessary if the fault had an initial orientation similar to that of the Hurricane Fault, since the only way to avoid hanging wall cut-off angles in excess of

90° is to draw the fault further west in the cross-section. This, in turn, would require its exposure at surface, within the bedrock of Wheeler Ridge, which clearly does not occur.

The location of the eastern strand of the Grand Wash Fault Zone is inferred from a number of small scarps in alluvium, approximately one kilometer from the exposed bedrock of the Grand Wash Cliffs. These scarps are visible on air photos of the region, and are consistent with formation by a west-side down normal fault, but they do not form a continuously exposed feature and are therefore suggestive, rather than compelling, evidence.

An alternate interpretation of the Grand Wash Fault Zone as consisting of only one fault that projects to surface near the eastern edge of the Grand Wash Trough can not be entirely ruled out, but is not preferred. This fault would have to flatten at a very shallow depth and slip earlier than the ridge-bounding faults further to the west. To be consistent with the interpreted shallow depth of the Grand Wash Trough (Saltus and Jachens, 1995), and to avoid hanging wall cut-off angles of much greater than 90° with the rolling over strata of Wheeler Ridge, the fault would have to flatten at a depth of about one kilometer. It would be required to slip earlier than the faults further to the west because palinspastic restoration of such a shallow flattening fault requires that the structurally higher faults be back-rotated through vertical to initial east dips. Since it is unlikely that the faults initiated as east-dipping reverse faults, this would suggest that they initiated after the strata in Wheeler Ridge had been rolled over above the Grand Wash Fault. This alternative interpretation is not preferred because: 1) It requires the Grand Wash Fault to have a geometry much different from that of better exposed nearby analogs, 2) It requires a diachroneity of slip on the major ridge-bounding normal faults, that can not be ruled out with the current data but seems unlikely, since there is no structural evidence for diachronous slip within the better exposed fault blocks farther to the west, and the available geochronologic evidence suggests that all of the major ridge bounding faults were active during a very short interval of time (see later discussion of geochronology), and 3) It would predict an asymmetric half-graben, inconsistent with the gravity model of Saltus and Jachens (1995).

As discussed earlier, the surface trace and dip of the Wheeler Ridge Fault is well constrained for a distance of approximately 5 kilometers where it cuts through southern Iceberg Ridge and Wheeler Ridge (Plate 1d) and by observations of Longwell (1936), where its trace is now covered by Lake Mead. However, its cross-sectional shape can only be inferred. As with the fault(s) of the Grand Wash Fault Zone, the Wheeler Ridge Fault is assumed to have a listric geometry similar to the Hurricane Fault further to the east and the Iceberg Canyon Fault further to the west.

The Garden Wash Fault, the northernmost part of the Virgin Detachment, is mostly buried, yet its location and offset are reasonably well constrained by geologic mapping north of Azure Ridge. At least one major normal fault lies to the east of, and roughly parallel to, Horse Spring Ridge. This fault separates the Tertiary strata that crop out on Horse Spring Ridge and immediately to its east from the partially buried ridge of Permian Toroweap Formation that continues north from Azure Ridge (Plate 1). The normal offset on this fault must be equal to or greater than the 8 kilometer separation of Permian strata in the Azure Ridge block from equivalent strata in Tramp Ridge. Farther to the south, across the Gold Butte Fault, the Virgin Detachment is interpreted to have unroofed the Gold Butte crystalline complex. The Gold Butte crystalline block is a more-or-less intact upper crustal section, through which the unroofing fault cut with an initial dip of approximately 60° (Fryxell et al., 1992). The fault is not currently exposed, except as a zone of chlorite breccia near the margins of the Gold Butte Block, but presumably dips gently away from the domiform Gold Butte Block. In order to denude the crystalline block and exposed chlorite breccias along the western margin, a minimum normal offset roughly equal to the width of the block is required (Wernicke and Axen, 1988). Assuming a 60° initial dip of the denuding fault zone and a currently exposed width of ~ 18 kilometers (basement plus cover), the minimum offset on the denuding fault zone is ~ 15 kilometers (Fryxell et al., 1992). This interpretation of very large normal offset on the Virgin Detachment is supported by the fact that to the north of the Gold Butte crystalline block, where hanging wall blocks are still present, the cumulative westward translation of strata in the Maynard Spring block relative to equivalent strata in the Azure Ridge block is ~ 19 kilometers (Plate 1).

Within Tramp Ridge, which is the hanging wall to the Garden Wash Fault, the amount of extension and structural style changes northward. The southern end of Tramp Ridge is significantly internally extended on moderately west-dipping normal faults. Farther north, it is very little extended on steeply dipping normal faults. Given that the relatively steeply east-dipping strata along the east side of Tramp Ridge have a more-or-less constant strike of about N20E, and assuming that the correlative strata in the buried northward continuation of Azure Ridge maintain a constant strike of about N10E, then the total westward displacement of strata within Tramp Ridge relative to the strata of Azure Ridge would change very little from south to north. Therefore, the normal offset accommodated on the Garden Wash Fault apparently remains fairly constant from south to north. The width of the Tramp Ridge block also remains fairly constant from south to north, despite the fact that the degree of internal extension of the Tramp Ridge block decreases significantly to the north. This may indicate a northward change in the initial geometry of the Garden Wash Fault. If it initiated as a steeply dipping listric fault near its south end, but developed a ramp-flat-ramp geometry further to the north, it would result in a wide, relatively untilted northern Tramp Ridge Block with a rollover on its east side (Plate 1). A smaller scale analog is seen in the southern Indian Hills, discussed above, where the Indian Hills Fault forms a flat in the Bright Angel Shale, above which a rollover anticline is developed (Figure 7).

The steep reverse fault of southern Iceberg Canyon, described by Longwell (1936), is now covered by the waters of Lake Mead. This fault is the only significant, apparent compressional structure reported from the South Virgin Mountains. Since all other faults in the area are normal faults, rather than reverse faults, it is reasonable to suggest that this structure was also active as a normal fault. This fault was probably active as a steeply east-dipping normal fault, and was later rotated a few degrees into a steeply west-dipping, apparently reverse orientation. This rotation could have occurred either by late stage slip on the Wheeler Ridge Fault and/or Grand Wash Fault Zone, or as a result of upflexing of the crust adjacent to the uplifting Gold Butte crystalline complex.

2.7 Geochronologic Data

A transect of five samples was collected across the Gold Butte crystalline block (Figure 12). Three of these samples were collected from coarse grained pegmatite dikes (samples 16-1-88, 47-5-89, and 52-1-89) and two were from retrograde mylonitic garnet gneiss (samples 1-10-88, and 5-10-88). $^{40}Ar/^{39}Ar$ step heating experiments were performed on muscovite separates at the University of Maine (Appendix A). The data were combined with two K/Ar ages from muscovite in coarse grained pegmatite dikes (recalculated from Wasserburg and Lanphere; 1965, using constants from Faure; 1977). The resulting data set shows that muscovite cooled through its closure temperature of approximately 350° - 425°C (Hodges, 1991) at times varying from approximately 1.4 Ga near the eastern edge of the Gold Butte crystalline complex to about 90 Ma near its western edge (Figure 12 and Table 1).

The two samples from the eastern part of the crystalline block both produced Precambrian plateaus in the model age of released gas, assuming an initial atmospheric $^{40}Ar/^{36}Ar$ ratio of 295.5 (Appendix A). These $^{40}Ar/^{39}Ar$ ages are consistent with the Precambrian K/Ar ages from the eastern Gold Butte crystalline block.

The three samples from the western side of the crystalline block produced comparatively complex release spectra. The sample from the pegmatite dike (16-1-88) produced a release spectrum with a plateau, with a model age of 89.81 ±1.09 Ma. The step heating experiments on the other two samples (1-10-88 and 5-10-88) of mylonitic gneiss did not yield plateaus, with ages increasing with increasing temperature. All three western samples yielded total gas ages of approximately 90 Ma. Given that muscovite in samples from the western side of the crystalline block may have been deformed during Tertiary Basin and Range extension, it is possible that the $^{40}Ar/^{39}Ar$ ages include the effects of $^{40}Ar^*$ loss due to deformation of the muscovite crystals (e.g. Hames and Hodges, 1993; Hames and Cheney, 1997). In this case, the cooling age of the samples may be somewhat older than the $^{40}Ar/^{39}Ar$ model ages. However, these effects would have to be extensive in order to greatly affect the total gas ages. The deformation effects would also have to be peculiarly uniform in order to yield about the same total gas age for all three samples. On the basis of the 90 Ma plateau age and the consistency of the three total gas ages, we interpret the data to indicate the western part of the crystalline block was at or above the Ar closure temperature for muscovite as recently as 90 Ma..

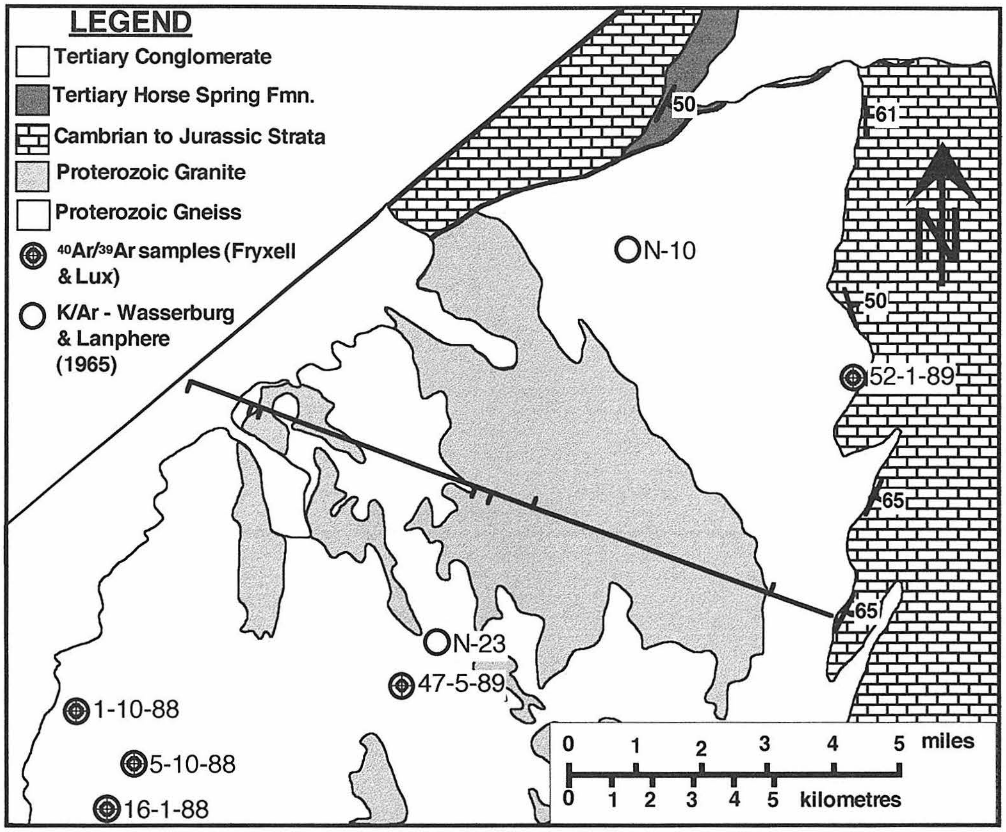

Figure 12. Simplified geologic map of the Gold Butte crystalline block, showing muscovite $^{40}Ar/^{39}Ar$ sample locations and muscovite K/Ar sample locations from Wasserburg and Lanphere (1965). Heavy black line was used as a depth axis for Figure 13; all samples were projected onto this line in a direction perpendicular to it (see tick marks on line for resultant locations).

Sample Number	Plateau Age (Ma)	Total Gas Age (Ma)
52-1-89	1374.4 ±13.0	1368.5 ±11.7
47-5-89	994.8 ±11.4	999.8 ±8.8
5-10-88	No Plateau	88.50 ±1.16
16-1-88	89.81 ±1.09	92.63 ±1.05
1-10-88	No Plateau	92.69 ±1.16

Table 1. Muscovite $^{40}Ar/^{39}Ar$ ages from the Gold Butte crystalline block.

In addition to the $^{40}Ar/^{39}Ar$ data discussed above, a new isotopic age of 65.2 ±0.6 Ma has been determined for the biotite-muscovite granite that crops out near the western edge of the crystalline block. This age represents cooling through the closure temperature for Pb in monazite of approximately 725 ±25 °C (Copeland et al., 1988; Parrish, 1988), and is based on U/Pb analyses of six single grains of monazite, with further analyses still in progress (Figure 13 and Appendix B).

2.8 Implications of the Geochronologic Data

In order to use the $^{40}Ar/^{39}Ar$ and K/Ar muscovite ages to examine the tectonic history of the South Virgin Mountains, the paleodepth of each of the samples was calculated. The sample locations were projected onto a N60W trending line, since this is the extension direction inferred from slip lineations on Tertiary normal faults (Figure 6), and therefore the inferred dip line for the dip-slip normal fault which is interpreted to have unroofed the Gold Butte crystalline complex. The paleodepth was then calculated by assuming that this line originally lay along a 60° WNW dipping fault surface, essentially as interpreted by Fryxell et al. (1992). The resulting age vs. depth profile is shown in Figure 14.

Combining the five muscovite $^{40}Ar/^{39}Ar$ ages with previous K/Ar ages (Wasserburg and Lanphere, 1965) yields a seven-sample transect of muscovite Ar ages from across the crystalline block with ages ranging from 1.4 Ga to 90 Ma, decreasing with structural depth. The three deepest samples (13-15 km projected depth) yielded total gas ages of ~ 90 Ma. The pattern of ages with projected depth (Figure 14) suggests that the interval from 7 kilometers to 11 kilometers depth may represent a fossil partial retention zone related to Late Cretaceous cooling of the Cordilleran crust. This time

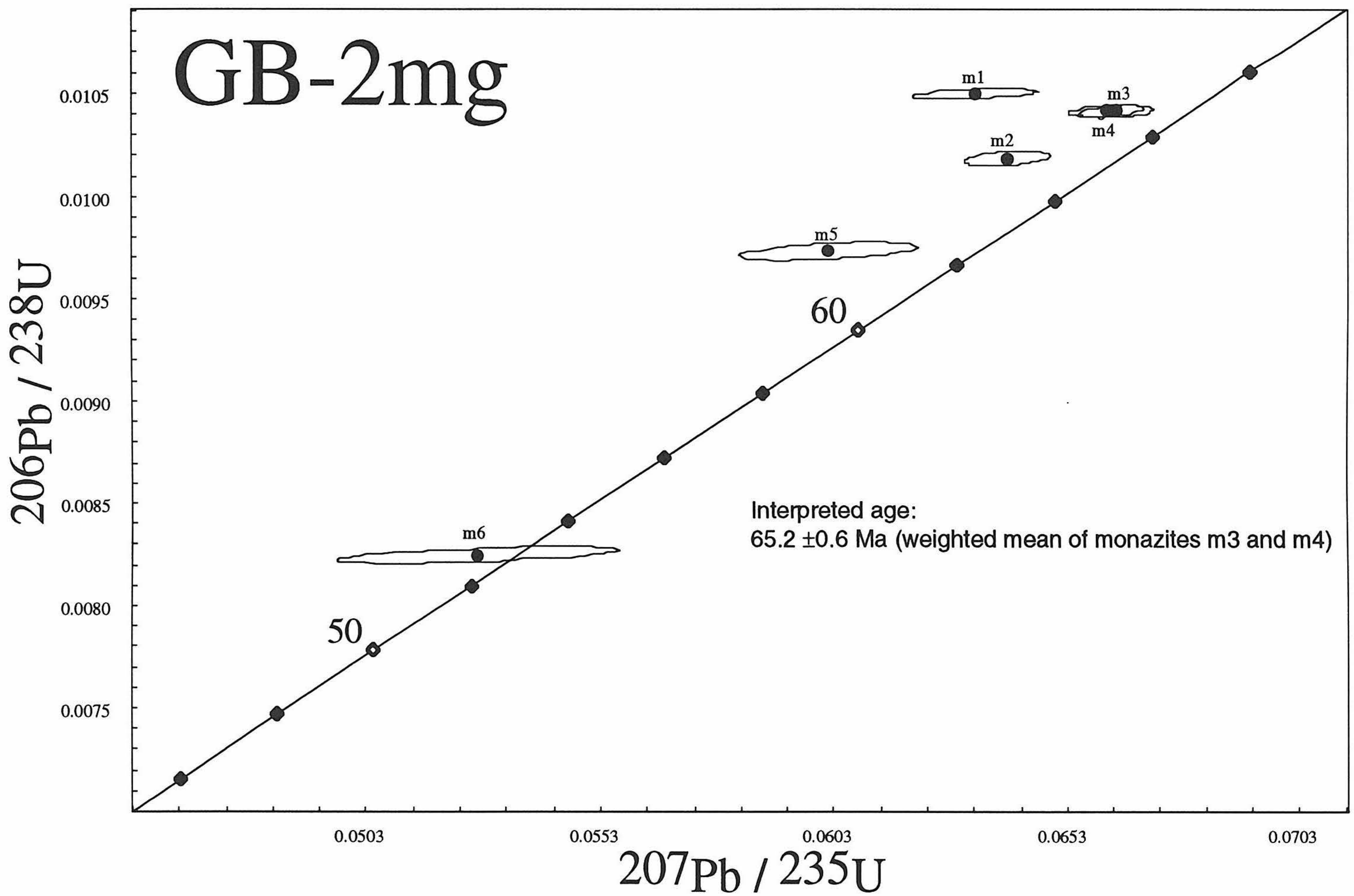

Figure 13. Concordia diagram showing data from six different single grain analyses of monazite crystals from the biotite-muscovite granite in the Gold Butte crystalline block.

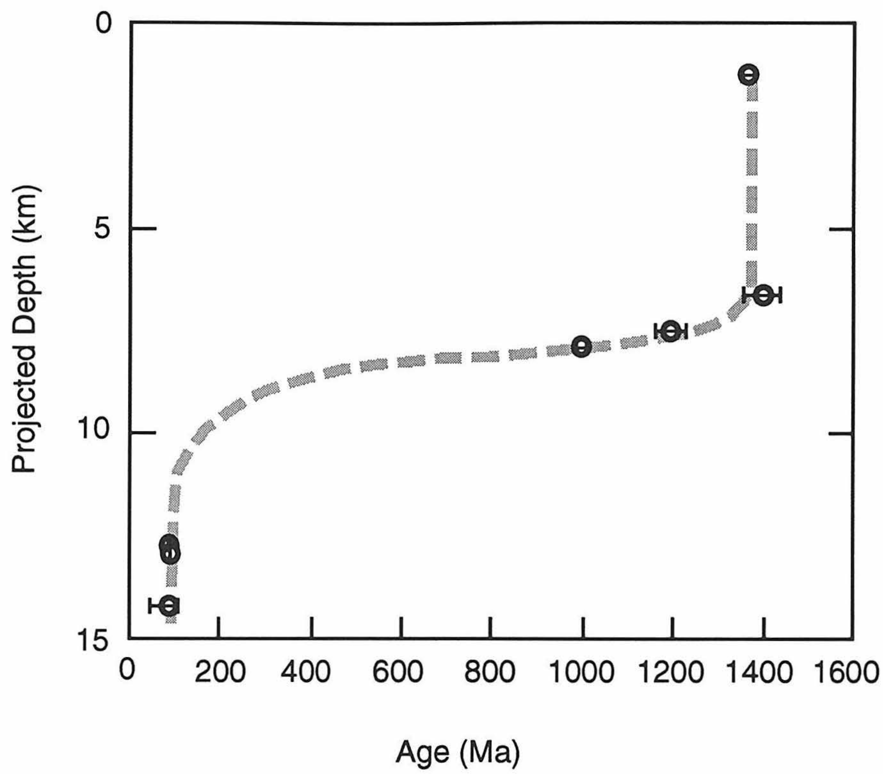

Figure 14. Age vs. projected depth for muscovite $^{40}Ar/^{39}Ar$ and K/Ar ages from the Gold Butte crystalline block, assuming the crystalline block represents an originally 60° west dipping crustal section.

period corresponds to the cessation of Sevier thrusting (Burchfiel and Davis, 1991) as well as the shutoff of intense plutonism in the Sierra Nevada, and associated lowering of the geothermal gradient at that time (Dumitru, 1990; House et al., 1997). Regardless of the cause of the late Mesozoic resetting event, the muscovite Ar ages demonstrate that the west end of the crystalline block was at mid-crustal depths at about 90 Ma. Assuming muscovite closure at 350-425 °C and a paleogeotherm of 25-30 °C/km, a paleodepth of 11-17 km is obtained, consistent with (Fryxell et al., 1992; Brady et al., 1996).

The monazite U/Pb age of ~ 65 Ma from the west end of the Gold Butte crystalline block is also consistent with the interpretation that the block is a more-or-less intact crustal section which has been denuded and tilted. Although the depth of crystallization of the biotite-muscovite granite is not well known, it is certainly not a hypabyssal granite, and its presence requires the west end of the crystalline block to have been at several kilometers depth at ~ 65 Ma.

The muscovite $^{40}Ar/^{39}Ar$ and monazite U/Pb ages constrain the timing of exhumation of the west end of the block as post-65 Ma. The only known tectonic event to affect the region later than 65 Ma is mid-Miocene extension. On the basis of tilting of Miocene strata at shallow levels at the same time as tilting of the Proterozoic strata, and on the 15 Ma unroofing ages observed from the apatite fission-track profile (Fitzgerald et al., 1991), exhumation of the western part of the crystalline block is also most likely mid-Miocene in age. There is evidence of some structural relief on the basal Tertiary unconformity, where it cuts downsection from Mesozoic strata to Precambrian basement from north to south across the region (e.g. Bohannon, 1984). However, there is no evidence of major tilting or structural relief on the basement-cover contact prior to ~ 16 Ma between the Sevier front and the Colorado Plateau.

In addition to the muscovite $^{40}Ar/^{39}Ar$ and monazite U/Pb data discussed above, there are other geochronologic data sets which are useful in constraining the absolute timing of extension within the Gold Butte breakaway zone. The initiation of motion on the Grand Wash Fault Zone is constrained by the age of the Rainbow Gardens Member of the Horse Spring Formation, which exhibits growth fault fanning of bedding where it crops out on northeastern Wheeler Ridge (Figure 5). The Rainbow Gardens Member has been dated elsewhere at approximately 19 Ma to 24 Ma (Bohannon, 1984; Beard, 1996), suggesting that faulting initiated at about 20 Ma. Since the Rainbow Gardens Basin is not thought to have been highly disrupted internally during active deposition (Bohannon, 1984; Beard, 1996), fault motion may have been relatively minor at this early stage.

2.9 Kinematic Evolution of the Gold Butte Breakaway Zone

The large-offset, block-bounding normal faults of the South Virgin Mountains apparently initiated as a set of sub-parallel west-dipping listric faults. The Iceberg Canyon Fault is one of the best documented and least disrupted of the large-offset, block-bounding faults. Its current listric geometry, combined with hanging wall bedding cut-off angles which range from about 90° where it cuts through the Permian limestones to about 70° where it cuts through the Mississippian to Pennsylvanian strata, show that it initiated as a steeply west-dipping listric fault, such that its initial geometry was similar to that of the Hurricane Fault. The Wheeler Ridge Fault also clearly initiated with a steep west dip, since it still dips 60° to the west. The Indian Hills Fault, the Million Hills Wash Fault, and the Maynard Spring Fault all have hanging wall bedding cut-off angles between 50° and 90°, consistent with initially steep west dips.

The hanging walls to these faults have been internally deformed, and they are not as well exposed as the Iceberg Canyon fault, so it is difficult to establish whether or not they were initially listric, but the mapped relationships permit this possibility. Because of the preponderance of evidence that the large-offset, block-bounding normal faults of the South Virgin Mountains initiated as steeply west-dipping listric structures, it is inferred that the buried Grand Wash and Virgin Detachments also initiated as steeply west-dipping listric structures.

Since absolute ages of initiation are not known for all of the block-bounding faults, it is certainly possible that there was some diachroneity in the timing of their initial slip. Nevertheless, since they do not cross-cut any other structures, they all have similar spacings and offsets, and other faults with lesser displacements and generally larger bedding cut-off angles sole into them, they are interpreted to be the earliest-formed structures to affect the region.

The smaller-offset imbricating faults that internally disrupt the major ridge forming blocks are interpreted to have initiated later. The hanging wall cut-off angles for these faults are typically near 90°, but reach values greater than 120° (Figure 10 and Table 2). This variation in cut-off angles may result from variations in initial dip of these faults or from variations in time of initiation, with higher cut-off angles resulting from faults initiating after some amount of rotation of the major fault blocks. These two possibilities are indistinguishable, since none of the minor imbricating faults cut each other. Rather, they tend to anastomose in map view and occasionally are seen to fan upwards. The cut-off angles greater than 90° require that the faults either initiated as reverse faults, then rotated to become normal faults or they initiated as normal faults after some amount of top-to-the-east rotation of bedding had already occurred due to slip on the ridge-bounding faults. The latter explanation is preferable, since it simply requires one evolving extensional fault system, whereas the former requires extension followed by compression then resumed extension, all accommodated on the same set of faults, with no other evidence of a compressional event being preserved.

In almost all cases where the intersection can be seen, imbricating faults clearly merge with the block-bounding faults, so they must have slipped synchronously. Because they had to slip synchronously, the hanging wall bedding cut-off angles of the imbricating faults can be used to constrain the dip at which the block-bounding faults were active. As the first generation faults and adjacent fault blocks were rotated, the hanging wall cut off angles of subsequent faults would have increased. The minimum amount of rotation of bedding and adjacent block-bounding faults, prior to initiation of the later faults, can be calculated by assuming the later faults initiated with 90° dips (Figure 15). For example, the later imbricating faults near the southern tip of Azure Ridge have bedding cut-off angles which range from approximately 70° to 124°. For the 124° case, if the initial dip of the splay was 90° or less, the Azure Ridge block and the faults bounding it must have rotated by at least 34° prior to initiation of this later imbricating fault. Thus, the block-bounding fault below Azure Ridge, which initiated with its deeper portions dipping at about 60°, was actively slipping with dips at least as low as 26° at the time of initiation of some of the internal imbricating structures. Similar arguments can be made to constrain the dip to which other block-bounding faults must have continued slipping (Table 2). This data set suggests that major block-bounding faults remained active at dips of less than 20°.

The interpretation that the smaller offset imbricating faults formed after some amount of slip and rotation of the block-bounding faults and intervening faults blocks may explain the observed pattern of intensity of internal deformation of major fault blocks. If the imbricating faults broke once a larger fault block had been tilted to some extent, then

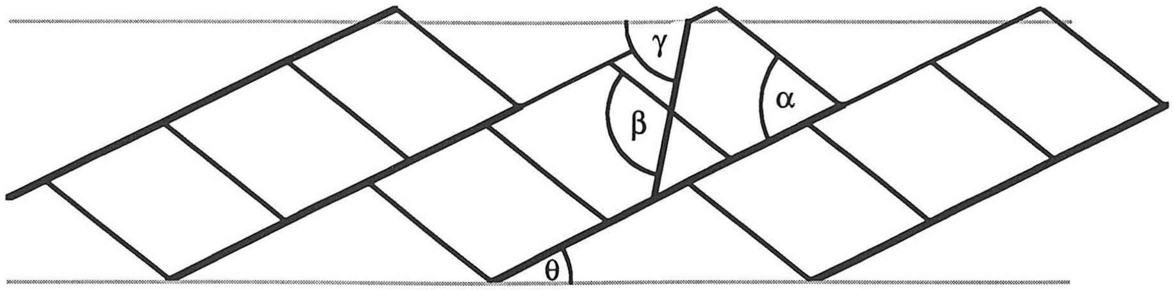

Figure 15. Diagram showing the relationship between the dip of active block-bounding normal faults and the hanging wall cut-off angles of bedding against the block-bounding and imbricating normal faults. The figure shows the fault system at the time of initiation of an imbricating fault. As the system continues to extend, fault and bedding dips will change, but the bedding cut-off angles will remain more-or-less the same. α = hanging wall cut-off angle adjacent to the block-bounding fault, β = hanging wall cut-off angle adjacent to the imbricating fault, γ = initial dip of the imbricating fault, and θ = dip of the active block-bounding fault. The amount of rotation (R) of the block bounding fault is the same as the amount of rotation of bedding in its hanging wall. If bedding was initially horizontal, then the amount of rotation of the block-bounding fault is given by:

$$R = \beta - \gamma$$

Since the present dip of the block-bounding fault is equal to its original dip minus its rotation, its dip can be calculated using:

$$\theta = \alpha - R = \alpha - (\beta - \gamma)$$

Since the imbricating normal faults had to initiate with dips of $\gamma = 90°$ or less, a maximum value for the dip of the active block-bounding fault (θmax) can be calculated using:

$$\theta\text{max} = \alpha - (\beta - 90°)$$

Bounding Fault	Max. Hanging Wall Cut-off Angle for Imbricating Faults in Superjacent Block (β)	Min. Required Rotation of Bounding Fault (R)	Max. Value of Lowest Initial Dip for Bounding Fault* (α)	Max. Value of Lowest Active Dip for Bounding Fault (θ)
Grand Wash Fault Zone	82°	0°	†60°	60°
Wheeler Ridge Fault	85°	0°	†60°	60°
Iceberg Canyon Fault	114°	24°	60°	36°
Indian Hills Fault	100°	20°	48°	28°
Million Hills Wash Fault	124°	34°	45°	11°
Garden Wash Fault	99°	9°	†60°	51°
Lime Canyon Fault	78°	0°	44°	44°

* - assumes that initial dip did not decrease below base of Cambrian strata

† - assumed - based on geometry of Hurricane Fault

Table 2. Maximum value of lowest active dip for the major block-bounding faults of the Gold Butte breakaway zone, South Virgin Mountains, Nevada. Variables correspond to those used in Figure 15.

these imbricating faults should be absent or at least less common in the relatively less tilted eastern fault blocks and they should be more abundant to the west. In fact, the abundance of small offset imbricating faults does increase from east to west, or upward in the structural stack of major fault blocks (Plates 1 and 3). Only a few imbricating faults affect most of Wheeler Ridge and Iceberg Ridge. The structurally higher and more tilted hanging wall to the Iceberg Canyon Fault includes a number of imbricating faults but is still a nearly intact homoclinal block. The still higher and more tilted fault blocks of the northern Indian Hills, Azure Ridge, Tramp Ridge, and Lime Ridge are all highly disrupted by imbricating faults.

As extension continued in the Gold Butte breakaway zone, the Virgin Detachment eventually became the dominant extensional structure. It accommodated the unroofing of the 17 kilometer wide Gold Butte crystalline block, as well as the ~ 8 kilometer westward translation of Tramp Ridge relative to Azure Ridge.

The hanging wall to the Gold Butte crystalline block has been translated further westward than the Tramp Ridge and Lime Ridge blocks. This requires a tear fault within the hanging wall of the Virgin Detachment. Since the large change in normal offset on the Virgin Detachment coincides with the Gold Butte Fault, the hanging wall tear fault must have been immediately above the Gold Butte Fault. This interpretation was originally suggested by Fryxell et al. (1992), and implies that the Gold Butte Fault was part of, or at least connected to, a right lateral structure in the hanging wall of the Virgin Detachment. The fact that the Gold Butte Fault clearly dips steeply to the north in at least the shallow subsurface suggests that it was not simply a tear fault in the hanging wall to a near-planar normal fault. The present northward dip of the Gold Butte Fault in the shallow subsurface can be explained in at least two ways: 1) The tear fault in the hanging wall of the Virgin Detachment may have coincided with a lateral ramp in the fault zone and/or 2) Isostatically driven uplift of the Gold Butte crystalline block was focused beneath the hanging wall tear fault due to the sharp gradient in amount of extension and therefore depth of unroofing.

The late, steep cross-cutting faults observed in the South Virgin Mountains are interpreted to be isostatic rebound structures, which have allowed uplift of extensionally denuded crystalline blocks in an area still being affected by regional extensional stresses. This interpretation is consistent with all of the observed features of these faults, including: 1) They have accommodated vertical movements of as much as several hundred meters, but relatively little extension, as evidenced by their little-rotated steep dips; 2) They are invariably upthrown on the side nearest to large extensionally denuded crystalline blocks; 3) Their abundance and magnitude of offset decreases away from the uplifted Gold Butte Block; and 4) They are the latest structures to affect the South Virgin Mountains, consistent with their formation being a response to extensional denudation.

In addition to the steep faults which accommodate uplift, the Gold Butte crystalline block probably moved upward by flexural folding of the upper crust. This folding is evident in the fanning of first generation fault dips within the fault blocks east of the crystalline complex. The near-surface dip of these faults decreases drastically from east to west, although they apparently initiated with parallel dips. Near surface fault dip for the first generation structures varies from a probable 60° to 90° dip for the fault(s) of the Grand Wash Fault Zone and Wheeler Ridge to a 12° east dip on the Indian Hills Fault, only 9 kilometers to the west (Plate 1 and Plate 3). While some of this fanning can be explained by active slip of a stack of listric dominos, at least some of it must be explained by another mechanism, since top-to-the-west normal faults almost certainly were not slipping with eastward dips. Much of the fanning of dips may be due to flexure caused by the uplift of the unroofed crystalline block. Unfortunately, the amount of rotation due to uplift is difficult to constrain, due to the difficulty of calculating the amount of rotation of faults which bound internally deforming listric dominos. If these calculations could be made, it would then be possible to accurately separate the effects of flexural rotation from rotation due to slip on a stack of listric domino blocks.

2.9.1 Alternative Interpretations of the Gold Butte Fault

As described above, the preferred interpretation of the Gold Butte Fault is that it coincided with a right lateral tear in the hanging wall of the Virgin Detachment. This tear may coincide with a ramp in the footwall and it was probably reactivated as an isostatic uplift fault after the Gold Butte crystalline block was unroofed. This scenario explains the steep north dip of the Gold Butte Fault, the dominantly dip-slip lineations observed on it, and the right-lateral map view folds of southernmost Lime Ridge and Horse Spring Ridge.

An alternative interpretation of the Gold Butte Fault is that it is a left-lateral strike-slip fault, apparently a splay of a left-lateral system of faults known as the Lake Mead Fault System (Anderson, 1973; Bohannon, 1979, 1984; Beard, 1996). This interpretation does not explain the observed right-lateral folds, or the slip lineations, and it is inconsistent with the apparent continuity of Permian strata northward from Azure Ridge. Furthermore, it does not explain the observed low angle contact of Tertiary Horse Spring Formation over Precambrian basement at the south end of Horse Spring Ridge (Plate 1b), unless the Gold Butte Fault has deviated southward at that point, and is entirely hidden within the Precambrian crystalline block. However, if the trace of the Gold Butte Fault does deviate southward into the crystalline block south of Horse

Spring Ridge, and deviate northward around the Permian subcrop at the north end of Azure Ridge, then it could still be interpreted as a left-lateral fault. If this alternative interpretation is correct, then Tramp Ridge may be the offset equivalent to Azure Ridge, as suggested by Longwell et al. (1965), Bohannon (1984), and Beard (1996). In this case, the Garden Wash Fault would be equivalent to the Million Hills Wash Fault, rather than being continuous with the Virgin Detachment. This interpretation places more emphasis on strike-slip faulting, and reduces the total extension calculated across the seven major fault blocks of the South Virgin Mountains. As measured from the cross-sections of Plates 3 and 4, the total extension across these blocks would change from ~15 kilometers if the Gold Butte Fault is interpreted as a lateral ramp to ~7 kilometers if it is interpreted as a later left-lateral strike-slip fault.

While this alternative significantly affects the total extension estimated along a transect across the Gold Butte Fault, it has no effect on the total extension estimated along a transect across the Gold Butte crystalline complex. Such a transect would require a minimum of approximately 4 kilometers extension across the fault blocks east of the crystalline complex, in addition to the approximately 17 kilometers of extension required to unroof the exposed width of the crystalline block, giving a total extension across the South Virgin Mountains of about 21 kilometers.

2.9.2 Kinematic Summary

Early extension within the Gold Butte breakaway zone was directed roughly east-west, and was accommodated on a set of steeply west-dipping, listric normal faults. After a significant amount of slip and rotation had been accommodated by this initial set of faults, a second set of steeply west-dipping, anastomosing normal faults developed in the higher fault blocks. These later faults sole into the earlier faults, rather than cross-cutting them. This requires that the earliest fault surfaces remained active to very shallow dips while the later faults were slipping. The earliest faults have accumulated normal offsets which range from about one kilometer to perhaps greater than 15 kilometers, and have been rotated to near horizontal dips. Some of the rotation of the originally steeply dipping faults can be attributed to folding accompanying isostatic uplift of the Gold Butte crystalline complex.

2.10 Relevance to Interpreting other Extended Regions

The observations that (1) slip on the imbricate normal faults continued to relatively low dips, and (2) rotation of faults and fault blocks did not occur on cross-cutting sets runs counter to both the "multiple-domino" models (e.g. Morton and Black, 1975; Miller et al., 1983) and flexural rotation models (e.g. Buck, 1988) where all slip is accommodated on steeply-dipping faults. This raises the question of whether either of these concepts is broadly applicable to the formation of normal fault systems with strongly rotated faults and fault blocks. Both are based on the assumption that slip on low-angle normal faults can not occur, rather than on kinematics of well documented normal fault systems themselves. Here, we evaluate published mapping from the highly extended southern Cherry Creek Range and Egan Range, Nevada (Gans and Miller, 1983), and from two areas previously regarded as examples of the multiple-domino model, the Yerington District, Nevada (Proffett, 1977; Proffett and Dilles, 1984) and the Lemitar Mountains, New Mexico (Chamberlin, 1982, 1983), in order to test whether or not the geology of these regions is consistent with the model of fault system evolution deduced for the Gold Butte breakaway zone.

The southern Cherry Creek Range and Egan Range comprise a series of tilted normal fault blocks, each of which is internally extended by fanning upward splays and bounded by an originally steeply east-dipping listric normal fault that has accommodated over a kilometer of offset (Gans and Miller, 1983). A sequential reconstruction of the region shows that the deeper portions of the major block-bounding faults remained active to dips as low as zero degrees (Figure 11 of Gans and Miller, 1983). Furthermore, the reconstruction suggests that the block-bounding faults were rotated through horizontal, to gentle westward dips, due to uplift of the adjacent highly attenuated Schell Creek Range and Snake Range. This structural evolution is virtually identical to that deduced for the Gold Butte breakaway zone.

For the case of the Yerington District, the primary source of data was the map and cross-sections of Proffett and Dilles (1984). A roughly east-west trending cross-section was constructed through most of the Singatse Range and just to the north of the Yerington Mine. This cross-section followed the exact same path as the eastern part of cross-section D-D' from Proffett and Dilles (1984). This cross-section, as interpreted by Proffett and Dilles, and as re-interpreted by us, is shown in Figure 16. The re-interpretation honors the geologic mapping presented by Proffett and Dilles, as well as the contacts intersected by boreholes and other contacts drawn as solid lines on their cross-section.

The re-interpretation of the Yerington District cross-section suggests that the model of normal fault evolution suggested for the Gold Butte breakaway zone is consistent with the faults of the Yerington District. It is possible to honor all of the geologic data and have the later, steeper normal faults merge into the earlier, more gently dipping structures. Only the Montana - Yerington fault demonstrably cuts the older, gently dipping structures, and this cross-cutting fault can not explain much rotation of the older structures, as it appears to be nearly planar and is shown as accommodating less than 400 meters of normal separation.

In examining the Lemitar Mountains, the map and cross-sections of Chamberlin (1982) were used. Cross-section D-D" from Chamberlin (1982) was partially restored by taking out the displacement on the latest stage of steeply dipping normal faults (Figure 17). These faults are probably related to the formation of the modern basins and ranges of the Socorro area, and formed at about 7 Ma to 4 Ma, whereas most extension in the region probably occurred between 31 Ma and 27 Ma (Chamberlin, 1983). With the effects of late stage faulting removed, the cross-section shows a pattern of normal faulting which is entirely consistent with that seen in the South Virgin Mountains and Yerington, in that no large-displacement faults that could have accommodated significant rotation are observed to cut the shallowest faults.

Overall, analysis of data sets from the southern Cherry Creek and Egan Ranges, as well as the Yerington District and the Lemitar Mountains, suggests that the normal fault systems which were responsible for Oligocene extension in these three widely separated regions evolved in the same manner as the Miocene normal fault system of the Gold Butte breakaway zone, as exposed in the South Virgin Mountains. This suggests that the model of normal fault evolution shown schematically in Figure 1c, and discussed throughout this paper, may be applicable to many extended continental regions.

Figure 16. Approximately west to east cross-section through the central Singatse Range, just north of the Yerington Mine. a) As interpreted by Proffett and Dilles (1984), with steeper faults generally cross-cutting shallower faults. b) Reinterpreted, assuming that steeper faults tend to merge into shallowly dipping faults. This reinterpretation honors all of the observations recorded in Proffett and Dilles (1984).

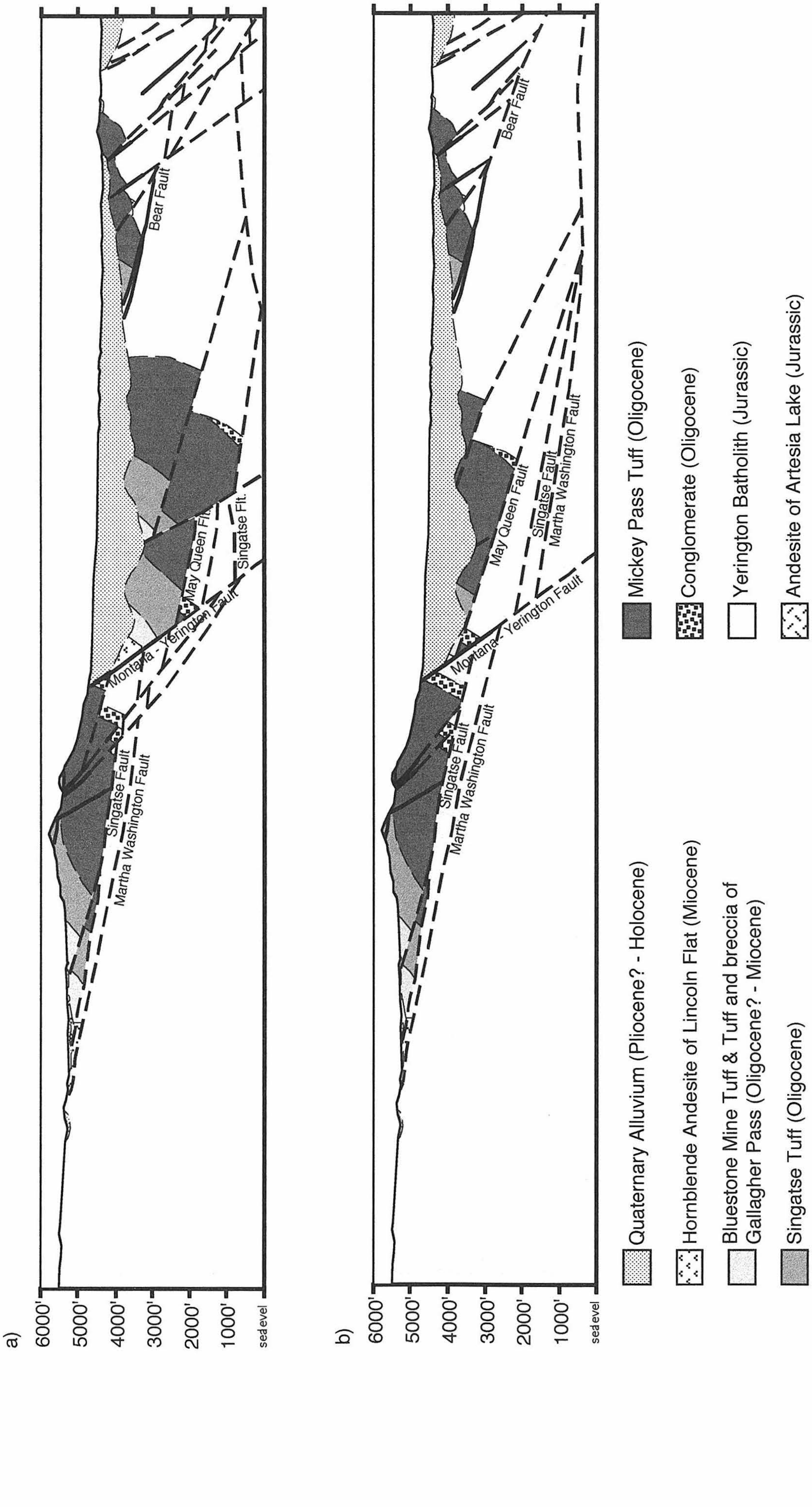
a)
6000'
5000'
4000'
3000'
2000'
1000'
sea level
Bear Fault
May Queen Flt.
Singatse Flt.
Montana - Yerington Fault
Singatse Fault
Martha Washington Fault
b)
6000'
5000'
4000'
3000'
2000'
1000'
sea level
Bear Fault
May Queen Fault
Singatse Fault
Martha Washington Fault
Montana - Yerington Fault
Singatse Fault
Martha Washington Fault
Quaternary Alluvium (Pliocene? - Holocene)
Hornblende Andesite of Lincoln Flat (Miocene)
Bluestone Mine Tuff & Tuff and breccia of Gallagher Pass (Oligocene? - Miocene)
Singatse Tuff (Oligocene)
Mickey Pass Tuff (Oligocene)
Conglomerate (Oligocene)
Yerington Batholith (Jurassic)
Andesite of Artesia Lake (Jurassic)

Figure 17. Approximately west to east cross-section through the Lemitar Mountains. a) As interpreted by Chamberlin (1982). b) With late stage (Pliocene) faults restored. Note that the steeply dipping faults merge into the shallowly dipping faults, rather than cutting them.

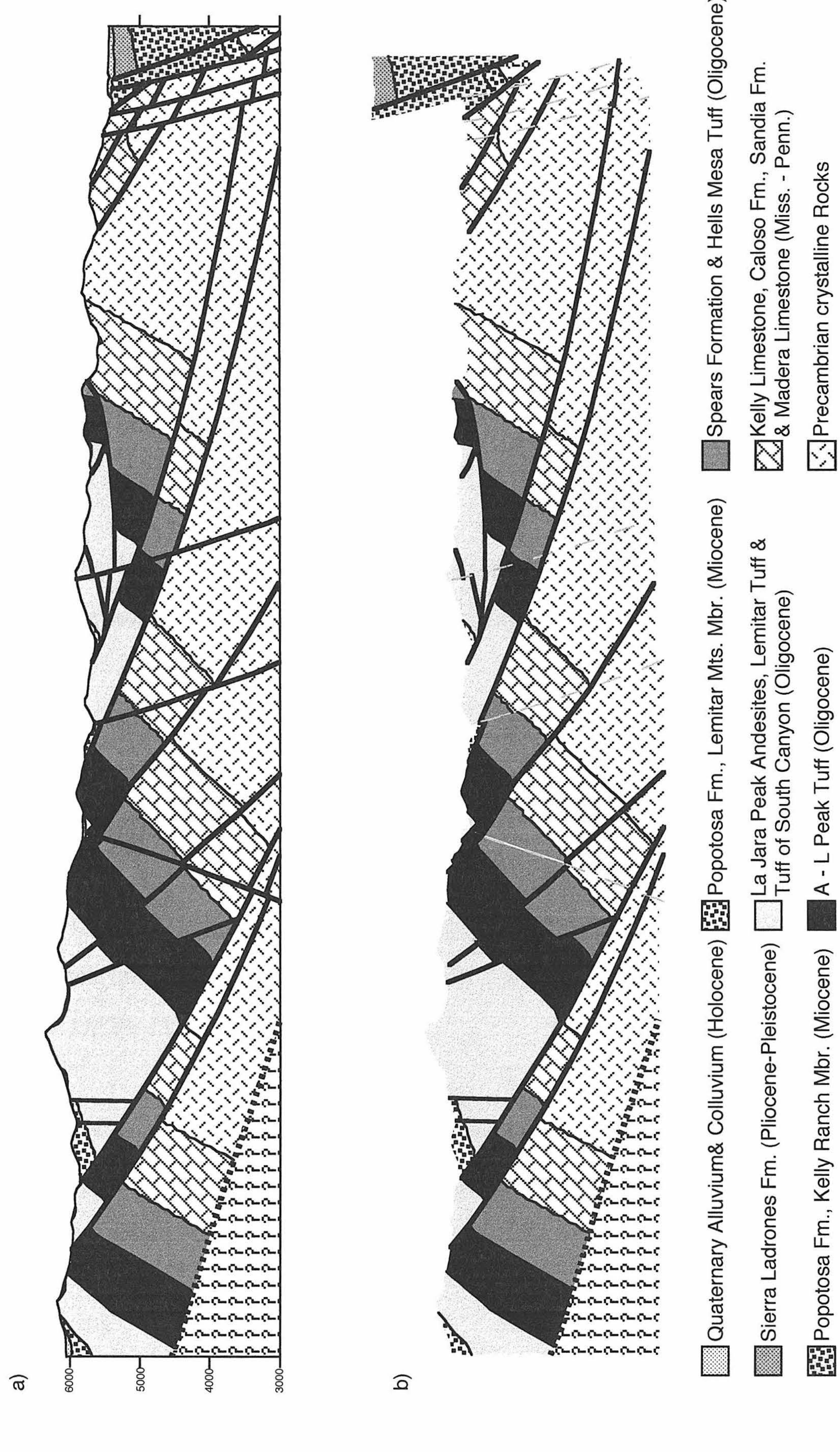
a)
6000
5000
4000
3000
b)
Quaternary Alluvium& Colluvium (Holocene)
Sierra Ladrones Fm. (Pliocene-Pleistocene)
Popotosa Fm., Kelly Ranch Mbr. (Miocene)
Popotosa Fm., Lemitar Mts. Mbr. (Miocene)
La Jara Peak Andesites, Lemitar Tuff & Tuff of South Canyon (Oligocene)
A - L Peak Tuff (Oligocene)
Spears Formation & Hells Mesa Tuff (Oligocene)
Kelly Limestone, Caloso Fm., Sandia Fm. & Madera Limestone (Miss. - Penn.)
Precambrian crystalline Rocks

2.11 References Cited

Agnon, A., and Reches, Z., 1995, Frictional rheology: hardening by rotation of active normal faults: Tectonophysics, v. 247, p. 239-254.

Anderson, E.M., 1942, The Dynamics of Faulting and Dyke Formation with Application to Britain: Edinburgh, Oliver and Boyd, 191 p.

Anderson, R.E., 1971, Thin skin distension in Tertiary rocks of southeastern Nevada: Geological Society of America Bulletin, v. 82, p. 42-58.

Anderson, R.E., 1973, Large-magnitude late Tertiary strike-slip faulting north of Lake Mead, Nevada: U.S. Geological Survey Professional Paper 794, 18 p.

Beard, L.S., 1996, Paleogeography of the Horse Spring Formation in relation to the Lake Mead fault system, Virgin Mountains, Nevada and Arizona: Geological Society of America Special Paper 303, p. 27-60.

Beard, L.S., and Campagna, D., 1991, Preliminary geologic map of the Devil's Throat 7.5 minute quadrangle, Clark County, Nevada: U.S. Geological Survey Open File Report OF 91-132, scale 1:24,000.

Bennett, V.C., and DePaolo, D.J., 1987, Proterozoic crustal history of the western United States as determined by neodymium isotopic mapping: Geological Society of America Bulletin, v. 99, p. 674-685.

Blair, W.N., 1978, Gulf of California in Lake Mead area of Arizona and Nevada during late Miocene time: American Association of Petroleum Geologists Bulletin, v. 62, p. 1159-1170.

Blair, W.N., and Armstrong, A.K., 1979, Hualapai Limestone Member of the Muddy Creek Formation - The youngest deposit predating the Grand Canyon, southeastern Nevada and northwestern Arizona: U.S. Geological Survey Professional Paper 1111, 14 p.

Bohannon, R.G., 1979, Strike-slip faults of the Lake Mead region of southern Nevada, *in* Armentrout, J.M., Cole, M.R., and TerBest, H., eds., Cenozoic paleogeography of the Western United States - Pacific Coast Paleogeography Symposium 3: Los Angeles, Pacific Section, Society of Economic Paleontologists and Mineralogists, p. 129-139.

Bohannon, R.G., 1983, Mesozoic and Cenozoic tectonic development of the Muddy, North Muddy, and northern Black Mountains, Clark County, Nevada, *in* Miller, D.M., Todd, R., and K.A. Howard, eds., Tectonic and stratigraphic studies in the eastern Great Basin, Geological Society of America Memoir, 157, p. 125-148.

Bohannon, R.G., 1984, Nonmarine sedimentary rocks of Tertiary age in the Lake Mead region: U.S. Geological Survey Professional Paper 1259, 72 p.

Brady, R.J., Wernicke, B.P., Fryxell, J.E., and Lux, D.R., 1996, Large magnitude Miocene extension in the Lake Mead region: Geological Society of America Abstracts with Programs, v. 28, no. 7, A-449.

Buck, W.R., 1988, Flexural rotation of normal faults: Tectonics, v. 7, p. 959-973.

Burchfiel, B.C., R.J. Fleck, D.T. Secor, R.R. Vincelette, and G.A. Davis, 1974, Geology of the Spring Mountains, Nevada, Geological Society of America Bulletin, v. 85, p. 1013-1022.

Burchfiel, B.C., and G.A. Davis, 1975, Nature and controls of Cordilleran orogenesis, western United States; Extensions of an earlier synthesis, American Journal of Science, v. 275-A, p. 363-396.

Burchfiel, B.C., and Davis, G.A., 1981, Mojave Desert and environs, *in*, Ernst, W.G., ed., The geotectonic development of California: Englewood Cliffs, New Jersey, Prentice-Hall, p. 217-252.

Campagna, D.J., and Aydin, A., 1994, Basin genesis associated with strike-slip faulting in the Basin and Range, southeastern Nevada, Tectonics, v. 13, p. 327-341.

Cascadden, T.E., 1991, Style of volcanism and extensional tectonics in the eastern Basin and Range Province; northern Mohave County, Arizona [Master's thesis]: Las Vegas, University of Nevada, 209 p.

Chamberlin, R.M., 1982, Geologic map, cross-sections, and map units of the Lemitar Mountains, Socorro County, New Mexico, New Mexico Bureau of Mines an Mineral Resources Open-file Report No. 169, 3 plates, scale 1:12,000.

Chamberlin, R.M., 1983, Cenozoic domino-style crustal extension in the Lemitar Mountains, New Mexico; A summary, in, Chapin, C.E., and Callender, J.F., eds., New Mexico Geological Society Guidebook, 34th Field Conference, Soccorro Region II: Soccorro, New Mexico Geological Society, p. 111-118.

Copeland, P., Parrish, R.R., and Harrison, T.M., 1988, Identification of inherited radiogenic Pb in monazite and implications for U-Pb systematics, Nature, v. 333, p. 760-763.

Dumitru, T. A., 1990, Subnormal Cenozoic geothermal gradients in the extinct Sierra Nevada magmatic arc: Consequences of Laramide and post-Laramide shallow-angle subduction, Journal of Geophysical Research, v. 95, p. 4925-4941.

Cole, E.D., 1989, Petrogenesis of late Cenozoic alkalic basalt near the eastern boundary of the Basin-and-Range: Upper Grand Wash trough, Arizona and Gold Butte, Nevada [Master's thesis]: Las Vegas, University of Nevada, 68 p.

Faure, G., 1977, Principles of isotope geology: New York, Wiley, 464 p.

Faulds, J.E., Schreiber, B.C., Reynolds, S.J., Gonzalez, L.A., and Okaya, D., 1997, Origin and paleogeography of an immense, nonmarine Miocene salt deposit in the Basin and Range (Western USA): The Journal of Geology, v. 105, p. 19-36.

Feuerbach, D. L., E. I. Smith, J. D. Walker, and J. A. Tangeman, 1993, The role of the mantle during crustal extension: Constraints from geochemistry of volcanic rocks in the Lake Mead area, Nevada and Arizona, Geological Society of America Bulletin, v. 105, p. 1561-1575.

Fitzgerald, P.G., Fryxell, J.E., and Wernicke, B.P., 1991, Miocene crustal extension and uplift in southeastern Nevada: Constraints from fission track analysis, Geology, v. 19, p. 1013-1016.

Fryxell, J.E., Salton, G.S., Selverstone, J.E., and Wernicke, B., 1992, Gold Butte crustal section, South Virgin Mountains, Nevada: Tectonics, v. 11, p. 1099-1120.

Gans, P.B., and Miller, E.L., 1983, Syle of Mid-Tetiary extension in east-central Nevada, *in* Gurgel, K.D., ed, Geologic excursions in the overthrust belt and metamorphic core complexes of the intermountain region, Guidebook - Part I, Utah Geological and Mineral Survey, Special Studies 59, p. 107-139.

Gregory, H.E., 1915, The igneous origin of the "glacial deposits" on the Navajo Reservation, Arizona and Utah, American Journal of Science, 4th ser., v. 40, p. 97-115.

Gregory, H.E., and Williams, N.E., 1947, Zion National Monument, Utah, Geological Society of America Bulletin, v. 58, p. 211-244.

Hamblin, W.K., 1965, Origin of "reverse drag" on the downthrown side of normal faults: Geological Society of America Bulletin, v. 76, p. 1145-1164.

Hames, W.E., and Hodges, K.V., 1993, Laser $^{40}Ar/^{39}Ar$ evaluation of slow cooling and episodic loss of ^{40}Ar from a sample of polymetamorphic muscovite, Science, v. 261, p. 1721-1723.

Hames, W.E., and Cheney, J.T., 1997, On the loss of $^{40}Ar^*$ from muscovite during polymetamorphism, Geochimica et Cosmochimica Acta, v. 61, p. 3863-3872.

Hodges, K.V., 1991, Pressure-temperature-time paths, Annual Review of Earth and Planetary Sciences, v. 19, p. 207-236.

House, M.A., Wernicke, B.P., Farley, K.A., and Dumitru, T.A., 1997, Cenozoic thermal evolution of the central Sierra Nevada, California, from (U-Th)/He thermochronometry, Earth and Planetary Science Letters, v. 151, p. 167-179.

John, B.E., and Foster, D.A., 1993, Structural and thermal constraints on the initiation of angle of detachment faulting in the southern Basin and Range: The Chemehuevi Mountains case study: Geological Society of America Bulletin, v. 105, p. 1091-1108.

Korolev, V.S., and Rowland, S.M., 1993, Age and correlation of the unclassified dolomites of the Grand Canyon: Geological Society of America Abstracts with Programs, v. 25, no. 5, A-63.

Kruse, S., M. McNutt, J. Phipps-Morgan, and L. Royden, 1991, Lithospheric extension near Lake Mead, Nevada: A model for ductile flow in the lower crust: Journal of Geophysical Research, v. 96, p. 4435-4456.

Langenheim, R.L., 1963, Mississippian stratigraphy in southwestern Utah and adjacent parts of Nevada and Arizona, p. 30-41, *in* Guidebook to the geology of southwestern Utah, Intermountain Association of Petroleum Geologists, 12th Annual Field Conference.

Longwell, C.R., 1921, Geology of the Muddy Mountains, Nevada, American Journal of Science, 5th ser., v. 1, p. 39-62.

Longwell, C.R., 1936, Geology of the Boulder Reservoir floor: Geological Society of America Bulletin, v. 47, p. 1393-1476.

Longwell, C.R., 1945, Low angle normal faults in the Basin and Range province: Transactions, American Geophysical Union, v. 26, p. 107-118.

Longwell, C.R., 1949, Structure of the northern Muddy Mountain area, Nevada, Geological Society of America Bulletin, v. 60, p. 923-966.

Longwell, C.R., E.H. Pampeyan, Bowyer, B., and Roberts, R.J., 1965, Geology and mineral deposits of Clark County, Nevada: Nevada Bureau of Mines Bulletin 62, 218.

Lucchitta, I., 1966, Cenozoic geology of the upper Lake Mead area adjacent to the Grand Wash Cliffs, Arizona [Ph.D. thesis]: University Park, Pennsylvania State University, 218 p.

Lumsden, D.N., Ledbetter, M.T., and Smith, G.T., 1973, Lithostratigraphic analysis of the Bird Spring - Callville Group and Pakoon Formation (Pennsylvanian - Lower Permian), southern Clark County, Nevada, Journal of Sedimentary Petrology, v. 43, p. 655-671.

Matthews, J., 1976, Paleozoic stratigraphy and structural geology of the Wheeler Ridge area, northwestern Mohave County, Arizona [Master's thesis]: Flagstaff, Northern Arizona University, 145 p.

McKee, E.D., 1938, The environment and history of the Toroweap and Kaibab formations of northern Arizona and southern Utah, Carnegie Institute Washington Pub. 492, 268 p.

McKee, E.D., 1945, Stratigraphy and ecology of the Grand Canyon Cambrian, Part I of Cambrian history of the Grand Canyon region, Carnegie Institute Washington Pub. 563, p. 5-168.

McKee, E.D., 1975, The Supai Group - subdivision and nomenclature, U.S. Geological Survey Bulletin 1395-J, 11 p.

McKee, E.D, and Resser, C.E., 1945, Cambrian history of the Grand Canyon region, Carnegie Institute Washington Pub. 563, 232 p.

McNair, A.H., 1951, Paleozoic stratigraphy of part of northwestern Arizona, American Association of Petroleum Geologists Bulletin, v. 35, p. 503-541.

Miller, E.L., Gans, P.B., and Garing, J., The Snake Range decollement; An exhumed mid-Tertiary ductile-brittle transition, Tectonics, 2, 239-263, 1983.

Nur, A., Ron, H., and Scotti, O., 1986, Fault mechanics and the kinematics of block rotations: Geology, v. 14, p. 746-749.

Parrish, R.R., 1988, U-Pb systematics of monazite and a preliminary estimate of its closure temperature based on natural examples, Geological Association of Canada, Programs with Abstracts, v. 13, A94.

Poborski, S.J., 1954, Virgin Formation (Triassic) of the St. George, Utah, area, Geological Society of America Bulletin, v. 65, p. 971-1006.

Powell, J.W., 1875, Exploration of the Colorado River of the west and its tributaries: Washington, Government Printing Office, 291 p.

Proffett, J.M., Jr., Cenozoic geology of the Yerington district, Nevada, and implications for the nature and origin of Basin and Range faulting, Geol. Soc. Am. Bull., 88, 247-266, 1977.

Proffett, J.M., Jr., and Dilles, J.H., 1984, Geologic map of the Yerington District, Nevada: Nevada Bureau of Mines and Geology, Map 77, scale 1:24,000.

Saltus, R.W., and Jachens, R.C., 1995, Gravity and basin-depth maps of the Basin and Range Province, Western United States, U.S. Geological Survey, Geophysical Investigations Map, GP-1012.

Sibson, R.H., 1985, A note on fault reactivation: Journal of Structural Geology, v. 7, p. 751-754.

Schenck, E.T., and Wheeler, H.E., 1942, Cambrian sequence in western Grand Canyon, Arizona, Journal of Geology, v. 50, p. 882-899.

Silver, L.T., Bickford, M.E., Van Schmus, W.R., Anderson, J.L., Anderson, T.H., and Medaris, L.G., Jr., 1977, The 1.4 - 1.5 b.y. transcontinental anorogenic plutonic perforation of North America, Geological Society of America Abstracts with Programs, v. 9, no. 7, p. 1176-1177.

Stewart. J.H., 1957, Proposed nomenclature of part of Upper Triassic strata in southeastern Utah, American Association of Petroleum Geologists Bulletin, v. 41, p. 441-465.

Stewart, J.H., 1980, Geology of Nevada, A discussion to accompany the geologic map of Nevada: Nevada Bureau of Mines and Geology Special Publication 4, 136 p.

Thomas, W.M., Clark, S.H., Young, E.D., Orrell, S.E., and Anderson, J.L., 1988, Proterozoic high-grade metamorphism in the Colorado River region, Nevada, Arizona and California, *in* Ernst, W.G., ed., Metamorphism and Crustal Evolution of the Western United States, Rubey Volume VII, Prentice Hall, Englewood Cliffs, N.J.

Volborth, A., 1962, Rapakivi-type granites in the Precambrian complex of Gold Butte, Clark County, Nevada: Geological Society of America Bulletin, v. 73, p. 813-832.

Wasserburg, G.J., and Lanphere, M.A., 1965, Age determinations in the Precambrian of Arizona and Nevada: Geological Society of America Bulletin, v. 76, p. 735-758.

Wernicke, B., and Axen, G.J., 1988, On the role of isostasy in the evolution of normal fault systems: Geology, v. 16, p. 848-851.

Wernicke, B., Walker, J.D, and Beaufait, M.S., 1985, Structural discordance between Neogene detachments and frontal Sevier thrusts, central Mormon Mountains, southern Nevada: Tectonics, v. 4, p. 213-246.

Wheeler, H.E., 1943, Lower and Middle Cambrian Stratigraphy in the Great Basin area, Geological Society of American Bulletin, v. 54, p. 1781-1822.

Wheeler, H.E., and Beasley, E.M., 1948, Critique of the time-stratigraphic concept, Geological Society of America Bulletin, v. 59, p 75-86.

Wolf, R.A., 1997, The development of the (U-Th)/He thermochronometer [Ph.D. thesis]: California Institute of Technology, 212 p.

Wolf, R.A., Farley, K.A., and Silver, L.T., 1996, Helium diffusion and low temperature thermochronometry of apatite: Geochimica et Cosmochimica Acta, v. 60, p. 4231-4240.

Young, R.A., 1966, Cenozoic geology along the edge of the Colorado Plateau in northwestern Arizona, [Ph.D. thesis], Washington University, St. Louis, Missouri, 155 p.

Young, R.A., 1979, Laramide deformation, erosion and plutonism along the southwestern margin of the Colorado Plateau, Tectonophysics, v. 61, p. 25-47.

Chapter 3

Crustal structure of the Basin and Range to Colorado Plateau transition in the Lake Mead region from BARGE seismic reflection data

Robert Brady, Brian Wernicke

Division of Geological and Planetary Sciences, California Institute of Technology, Pasadena, California 91125

Marcia McNutt

Department of Earth, Atmospheric, and Planetary Sciences, Massachusetts Institute of Technology, Cambridge, Massachusetts

John Mutter, Gustavo Correa

Lamont-Doherty Earth Observatory, Columbia University, Palisades, New York

(This chapter was re-formatted from a manuscript in preparation, for submission to the *Journal of Geophysical Research*)

Abstract. Approximately 120 kilometres of deep seismic reflection data were shot during a survey on the waters of Lake Mead in southeastern Nevada. The survey extends from near the abrupt eastern edge of the Basin and Range Province (BRP) to a point approximately 80 kilometres into the extended domain. Overall, the crust is much less reflective than is typically observed in the BRP. The upper two to four seconds of the data shows well defined reflections from sedimentary fill, but below that point, reflectivity is weak. Lower crustal reflectivity is generally absent under the eastern part of the survey, with a slight increase in reflectivity to the west. The

reflection Moho appears as a series of weakly defined, discontinuous reflections at 10 to 11 seconds. Previous reflection profiles from the BRP and Colorado Plateau have contrasted strongly, with BRP profiles showing a well defined Moho and strong deep crustal reflectivity, while the Plateau Moho is poorly defined and its deep crust is generally transparent. In light of these observations, we interpret our results to suggest a plateau-like deep crustal signature which persists 50 to 100 kilometres westward beneath the strongly extended Lake Mead region. Apparently, extension of the easternmost portion of the BRP did not produce the reflection fabrics typically observed under other strongly extended regions in the BRP and elsewhere. The interpreted crustal thickness immediately adjacent to the Colorado Plateau, when combined with other published data, suggests that a maximum of 900 km^2 of ductile crustal material was removed from an east - west cross section under the Plateau. When incorporated into mass balance calculations for the entire width of the central Basin and Range, the results indicate that ten or more kilometres of crustal thickness were probably removed from under the Sierra Nevada in response to Basin and Range thinning.

3.1 Introduction

The Basin and Range province of the western United States has experienced strongly heterogeneous Tertiary extension, partitioned between areas which have extended by only a few percent and others which have extended by over a hundred percent (e.g., Proffett, 1977; Guth, 1981; Wernicke et al., 1988; Chamberlin, 1983; Miller et al., 1983; Wernicke, 1992). Geophysical studies have shown that the crustal thickness under this variably extended region is more or less constant, typically 30 km to 35 km (e.g. Klemperer et al., 1986; Hauser et al., 1987b). In addition, most reflection profiles from the BRP show similar patterns of mid-crustal reflectivity and strong

Moho reflectivity, under both highly extended (e.g., Hauser et al., 1987a; McCarthy and Parsons, 1994) and moderately extended (e.g., Hauge et al., 1987; McCarthy and Parsons, 1994) domains.

Deep seismic reflection profiles also show that patterns of reflectivity under the stable Colorado Plateau and the BRP contrast strongly. The stable Colorado Plateau seismic character is probably best represented by COCORP line AZ6, which was acquired in the interior of the Colorado Plateau. It shows an uppermost crust composed of highly reflective layered sediments and a nearly transparent deeper crust, Moho, and uppermost mantle (Hauser and Lundy, 1989). A similarly transparent crust and unreflective Moho were observed under the eastern end of line AZ1, which crossed the transitional BRP to Colorado Plateau boundary in western Arizona (Hauser et al., 1987a).

Reflection profiles from the BRP have consistently shown patterns of reflectivity which are absent on Colorado Plateau data. The mid-crust of the BRP generally shows a pattern of gently dipping to sub-horizontal, discontinuous reflections. This reflection character has been observed in profiles which cross highly extended regions, such as the Snake Range (Gans et al., 1985) and Ruby-East Humboldt core complex (Valasek et al., 1989) in Nevada, as well as the Whipple Mountains and Buckskin-Rawhide core complexes of California and Arizona (Hauser et al., 1987a; McCarthy and Parsons, 1994). A similar, though more diffuse, pattern of mid-crustal reflectivity has been observed under less extended parts of the southern Basin and Range (McCarthy and Parsons, 1994). This reflection fabric has generally been interpreted to be the result of pervasive ductile deformation and mylonitization; this interpretation is strengthened by observations of similar reflection patterns in the upper crust which can be correlated with zones of shearing and mylonitization at surface (e.g. Gans et al., 1985; Valasek et al., 1989).

In addition to the reflective mid-crust, previous BRP profiles have shown a highly reflective deep crust. Most notably, reflection profiles show a strong, continuous band of reflections at 9 s to 11 s. This is interpreted as a nearly flat reflection Moho at depths of approximately 30 km to 35 km, and is seen on data from the northern BRP (e.g. Allmendinger et al., 1983; Klemperer et al., 1986; Hauge et al., 1987; Valasek et al., 1989), as well as the Death Valley region (Serpa et al., 1988; Wernicke et al., 1996), the southern BRP (Hauser et al., 1987a; McCarthy and Parsons, 1994) and the extended southern Canadian Cordillera (Cook et al., 1992). In many cases, the deep reflections are seen as two bright, continuous bands, approximately 1 s apart (e.g. Klemperer et al., 1986; Hauge et al., 1987; Valasek et al., 1987). The reflection Moho is probably a young feature, since it is found at the same depth under regions which have experienced different degrees of extensional thinning at different times during the Cenozoic. This interpretation is also consistent with the observation of dipping events being truncated by the reflection Moho on some data sets (Allmendinger et al., 1983; Klemperer et al., 1986). Overall, the reflection patterns seen on BRP seismic data strongly suggest that upper crustal extension has been accompanied by modification of the mid- to lower crust .

These observations raise the following question: Does the similarity of deep crustal reflection patterns seen on almost all BRP profiles indicate some common deep crustal response to extension, or does the deep crustal response to extension vary? One possibility is that the deep crustal response to extension, and therefore the character of the Moho, may change as a function of position in a decoupled strain system. This would be analogous to the changing degree of basement involvement in thrust belts from foreland to hinterland due to decoupling of the upper crust and non-involvement of the basement in foreland deformation. In order to test this proposal, it would be necessary to examine the character of the Moho at some clearly different position within the extended domain. All of the previous BRP reflection profiling experiments were conducted within the interior of the extended province, or across a diffuse, magmatically altered margin. One way to test the proposal that a spectrum of deep crustal processes may accompany extension is to acquire deep reflection seismic data across a clearly defined edge to the extended BRP and continuing into its interior.

There are a number of possible deep crustal responses to extension which might be seen in such a profile. Clearly, one possibility is that the crust might have an abrupt change in thickness which correlates with the abrupt change in degree of extension at the edge of the BRP. A second possibility is that the crust under the extended region may be rebuilt by flow of the adjacent lower crust, this should result in a flat Moho with no abrupt change in reflection character or thickness at the edge of the stable Plateau. A third possibility is that the lower crust might be rebuilt by voluminous magmatic underplating, which might result in significant lower crustal layering and reflectivity. One might also see evidence for some combination of lower crustal flow and magmatism, as has been suggested by many authors (e.g. Gans et al., 1989; Kruse et al., 1991; Wernicke, 1992).

During 1994 the Basin and Range Geoscientific Experiment (BARGE) collected over 120 km of deep seismic reflection data on the waters of Lake Mead, Nevada and Arizona (Fig. 1). The profiles cross over part of the Gold Butte breakaway zone (easternmost Lake Mead), which marks a transition at the surface from extended crust of the central BRP into unextended crust of the Colorado Plateau. The transition from extended to unextended crust is apparently more abrupt here than elsewhere along the

Figure 1. Location map, showing Lake Mead and the surrounding area, as well as major structural features and the locations of Lines 1,2,3,5,6,7 and 8. Numbers indicate the line locations. Light grey indicates the location of mountainous terrane. BM - Black Mountains, CP - Colorado Plateau, FM - Frenchman Mountain, GPT - Gass Peak Thrust, KT - Keystone Thrust, LMFS - Lake Mead Fault System, LMFZ - Lakeside Mine Fault Zone, LVR - Las Vegas Range, LVVSZ - Las Vegas Valley Shear Zone, MM - Muddy Mountains, MMT - Muddy Mountains Thrust, NVM - North Virgin Mountains, SR - Sheep Range, SVM - South Virgin Mountains.

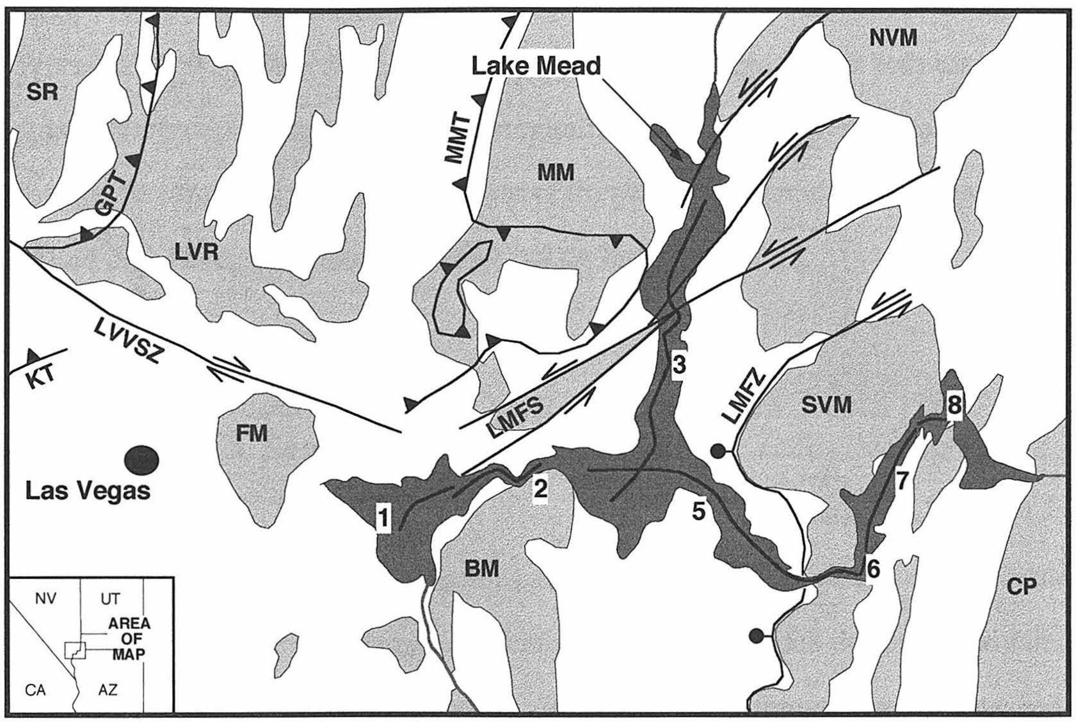
SR
GPT
LVR
Lake Mead
MMT
MM
NVM
KT
LVVSZ
FM
Las Vegas
LMFS
LMFZ
SVM
1
2
3
5
6
7
8
BM
CP
NV
UT
AREA OF MAP
CA
AZ

eastern edge of the BRP, since Miocene extension of the eastern Lake Mead region exceeded 80% (Fryxell et al., 1992; Brady et al., 1996), while the adjacent Colorado Plateau remained essentially unextended. In addition, the profiles cross over the transition from the amagmatic eastern Lake Mead region to the magmatic western Lake Mead region, both of which have experienced large magnitude Tertiary extension (Anderson, 1971; Bohannon, 1984; Duebendorfer et al., 1990; Duebendorfer and Simpson, 1994; Fitzgerald et al., 1991; Fryxell et al., 1992; Wernicke and Axen, 1988; Wernicke et al., 1988). Since the BARGE seismic lines cross over both magmatic and amagmatic extended regions in close proximity to unextended continental crust, they seem to be ideally located for evaluation of the roles of magmatism, flow, and brittle failure in the deep crust during extensional deformation.

3.2 Geologic Setting

During the Late Jurassic and Cretaceous, the Lake Mead area was part of the foreland to the thin skinned Sevier thrust belt (Burchfiel et al., 1974) which developed within the sediments of the Paleozoic miogeocline. The easternmost thrusts seem to have been localized along the hinge zone of the miogeocline, which trends roughly NE-SW, and runs just to the west of Lake Mead. Accordingly, the easternmost thrust sheet at the latitude of Lake Mead is exposed close by to the west, in the Muddy Mountains (Longwell, 1949; Longwell et al., 1965; Bohannon, 1983) (Figure 1). South of Lake Mead, the thrust belt changes to a NW-SE trend, and thrusting involves Precambrian crystalline basement rocks (Burchfiel and Davis, 1975).

Following Cretaceous thrusting, the Lake Mead region seems to have been tectonically stable until the Neogene, although Late Cretaceous arc magmatism and Paleocene volcanism affected areas approximately 100 km to the south of Lake Mead. In addition, Paleozoic and Mesozoic strata were removed from a basement high which formed immediately to the south of Lake Mead. The exact age and extent of this basement high remains unclear, due in part to an incomplete understanding of the age and pre-extensional configuration of the sub-Tertiary unconformity. However, the presence of Eocene or older deposits filling northeastward draining paleocanyons, which cut into the southwestern part of the Colorado Plateau, shows that the basement high had formed by Eocene time (Young, 1966, 1979).

The present day physiographic features of the Lake Mead area are primarily the result of Miocene extensional processes. During the Miocene, the eastern Lake Mead region became a breakaway zone, where extension initiated at the edge of what is now the Colorado Plateau (Fryxell et al., 1992). Extension in the eastern Lake Mead region was accommodated by a set of closely spaced west-dipping normal faults (Brady; unpublished mapping, 1996). This breakaway zone represents a sharp transition from stable, essentially unextended crust of the Colorado Plateau to highly extended crust of the Basin and Range (stretching factor $\beta \approx 3.5$; Wernicke et al., 1988)). West of the breakaway, large magnitude top to the west extension is accommodated by at least one and possibly two major detachments, one of which forms the western margin of the Gold Butte crystalline complex (Brady et al., 1996; Fryxell et al., 1992), the other being the Saddle Island Detachment (Duebendorfer et al., 1990). Numerous moderate to steeply dipping normal faults accommodated lesser amounts of extension across the region. The region also includes a major left lateral shear zone, the Lake Mead shear zone, which was apparently active post ~13.5 Ma (Bohannon, 1984). Extension in the eastern Lake Mead region occurred from ~20 to 9 Ma, (peak extension ~ 15 Ma; Fitzgerald et al., 1991; Fryxell et al., 1992) and progressed into the western Lake Mead region (peak extension ~ 13.5 Ma to 8.5 Ma; Duebendorfer et al., 1990).

Eastern Lake Mead extension was accompanied by minimal magmatism, represented by the post-extensional basalts of Gold Butte (9.15 to 9.46 Ma; Cole, 1989) and Grand Wash Trough (3.99 to 6.9 Ma; Feuerbach et al., 1993). Extension in the western Lake Mead Region was, however, associated with significant magmatism, including the pre- to syn-extensional mafic to felsic volcanics of the Eldorado Mountains (18.5 to 12 Ma; Anderson, 1971; Darvall et al., 1991),the Hamblin-Cleopatra volcanics (14.2 to 11.5 Ma; Anderson, 1973; Thompson, 1985), the River Mountains volcanics (13.4 to 12.1 Ma; Feuerbach et al, 1993; Anderson, 1972; Armstrong, 1966, 1970), and the post-extensional basalts of Malpais Flattop (10.6 to 9.7 Ma; Faulds and Gans, unpub. data *in* Feuerbach et al., 1993) and Fortification Hill (5.88 to 4.3 Ma; Anderson et al., 1972; Feuerbach et al., 1991).

3.3 Acquisition and Processing

For the experiment on Lake Mead, a 40' x 90' barge (trade name Flexifloat) was built on Lake Mead, using sections brought in to Lake Mead Marina on flat bed trucks. The barge was assembled from 10' wide sections which ranged in length from 10' to 40'. The completed barge carried a streamer reel, a 3 km long streamer, 2 Price A-300 compressors, their associated generators and hydraulic drives, two air gun arrays of four guns each, a van which housed the DSS-5 recording system, and a small mobile home. The barge was powered by twin diesel props located on the stern corners. Construction of the barge and installation of all the necessary equipment took about one week. The streamer, recording systems, compressors and air guns were equipment which had originally been installed on the R/V *Conrad*.

The 3 km long streamer was a Digicon 120 channel analogue system with 25 meter receiver spacing. Due to the fact that the streamer was designed to be neutrally buoyant in salt water, it was suspended from floats in order to prevent it from sinking in the fresh water of Lake Mead. The floats maintained the streamer at a constant depth of 10 meters when it was deployed.

BARGE collected eight deep reflection seismic lines on the waters of Lake Mead (Fig. 1 and Plates 5 through 11). For lines 1 through 4, acquired on Boulder Basin and the Overton Arm of western Lake Mead, the full 3 km streamer was deployed. In the narrow canyons of eastern Lake Mead, the streamer was shortened in order to negotiate the relatively tight turns. This was achieved by taking the unused part of the cable up onto the drum on deck, which resulted in the trailing portion of the streamer no longer being separated from the barge by an isolation cable. For lines 6 and 7, in Virgin Canyon and Gregg Basin to Iceberg Canyon, the streamer was shortened to ~ 2 km. For line 8 in northern Iceberg Canyon to Wheeler Ridge, it was shortened to ~ 1 km. Line 4 was shot along the same path as line 3, with the streamer shortened to 20 channels. Line 4 was not processed as part of this study, because it provided the same spatial coverage as Line 3, but with lower quality data (lower fold).

During data acquisition, the barge traveled at approximately 3 knots (~5.6 km/hr), with both 4-gun arrays being fired simultaneously every 30 seconds, resulting in a shot spacing of approximately 50 meters. This provided a maximum coverage of ~ 30 fold (for lines 1,2 and 3), with variable lesser coverage on lines 6 and 7, and a minimum coverage of ~ 10 fold (for line 8). Recording time for all shots was 15.3 seconds.

The data was processed using Western Geophysicals Omega Seismic Processing System, the same procedure was used for lines 1,2,3,5 and 7. The procedure followed was: editing for bad traces and shots, followed by wave equation multiple attenuation, common mid-point (CMP) gathering, refraction muting, normal moveout (NMO) correction, CMP stacking, spiking deconvolution, time variant band pass filtering, random noise attenuation, and application of automatic gain control. The processing procedure for lines 6 and 8 was the same, except wave equation multiple attenuation was not applied. For lines 6,7 and 8 the ten channels closest to the barge were particularly noisy, since these lines were collected with the shortened streamer and no isolation cable. This problem was easily dealt with by killing the noisy channels.

Velocities could only be determined approximately and the velocity structure used for processing was the same for all lines (Fig. 2). This velocity structure probably overestimated the velocities at depth (particularly below 8 s TWT), and was not applied when converting travel times to depths during interpretation. The velocity structure used during interpretation is also shown in Figure 2 (grey line). This velocity structure allows a reasonable estimate of depths to various reflectors by assuming an average crustal velocity of 6.3 km/s for rock below 3 s TWT, and a lower velocity for rock above 3 s TWT, which is dominantly Tertiary basin fill. Calculated depths were rounded to the nearest 0.5 km for purposes of discussion in this paper; reported depths are depths below lake level (~ 360 m a.s.l.).

The final processing step was the creation of line drawings (Figure 3). This was done by hand, with reflections being identified as any arrivals which were coherent and linear over significant distances (e.g. reflections R on Figure 4 a, 4b and 4c). In many cases, the identified reflections differed in frequency and orientation (in distance vs. time coordinates) from the surrounding noise patterns (compare reflections R on Figure 4a with low frequency noise T and diffractions D).

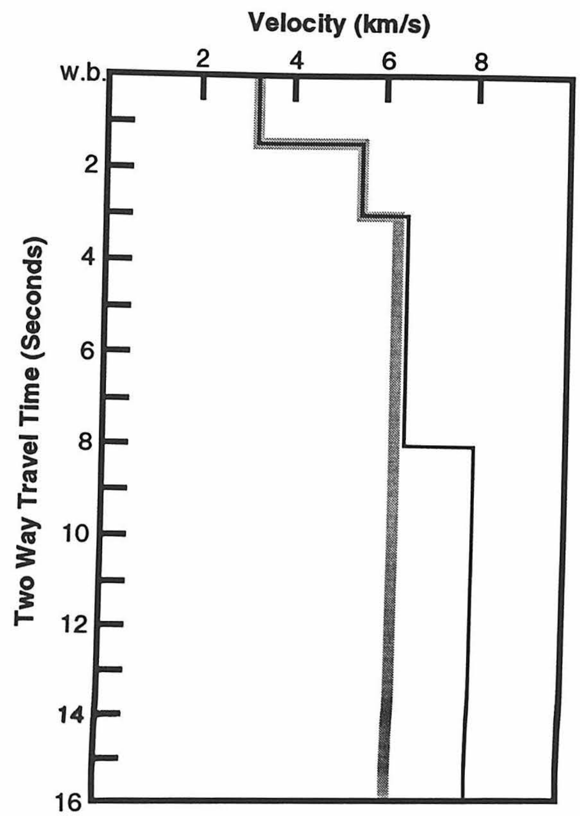

Figure 2. Black line indicates the velocity structure used during processing of all lines; w.b. indicates water bottom, a velocity of 1.48 km/s was used above the water bottom. Grey line indicates velocity structure used during conversion of travel times to depths during interpretation, the velocity of 6.3 km/s was applied down to Moho.

3.4 Results

All of the lines (Fig. 3) show strong horizontal or sub-horizontal reflectivity in the upper one to four seconds two way time (TWT); below this the sections are relatively unreflective. In the six to nine second range several strong reflections occur, these reflections stand out in the data because some of them are continuous over lengths of two to four kilometers. There are also a number of gently dipping reflections in the ~9 to 13 second range which form a band across the data (most obvious on lines 3 and 5). The deepest reflections (down to ~14 s TWT) are sub-horizontal reflections clustered near the west end of the survey on lines 1,2, and 5.

Since the survey was conducted in a relatively shallow (generally < 100 m) and narrow body of water, problems with strong water bottom multiples as well as diffractions from irregular canyon walls were expected. Surprisingly, relatively few strong diffractions were observed in the shallow part of the data. Diffractions, inferred to be from irregularities in the canyon walls, were only problematic where line 3 passed through the Overton Islands. Water bottom multiples were not particularly pronounced, and those which did appear were effectively suppressed by the wave equation multiple attenuation applied during processing.

One significant problem in the data set was the occurrence of semi-coherent noise trains, which formed bands through the entire record section. Since the noise occurred over the entire frequency range of the useful data, bandpass filtering was of limited use. These noise trains are thought to have resulted from the streamer being coupled to buoys at surface. As the buoys were towed behind the barge, they 'fluttered' or 'strummed' back and forth in the current. It is speculated that the connection between the buoys and the streamer resulted in this 'strumming' being transmitted to the

Figure 3. Line drawings of BARGE data, showing interpreted base of Tertiary basin fill (**T**), east dipping carbonates of Iceberg Ridge (**E**), Moho (**M**), and the approximate base of deep reflectivity on lines 1, 2, and 5 (**B**). Boxes labelled a), b), c) and d) show the location of the data panels displayed in Figure 4. Note that all sections are exaggerated horizontally by approximately a factor of 4X.

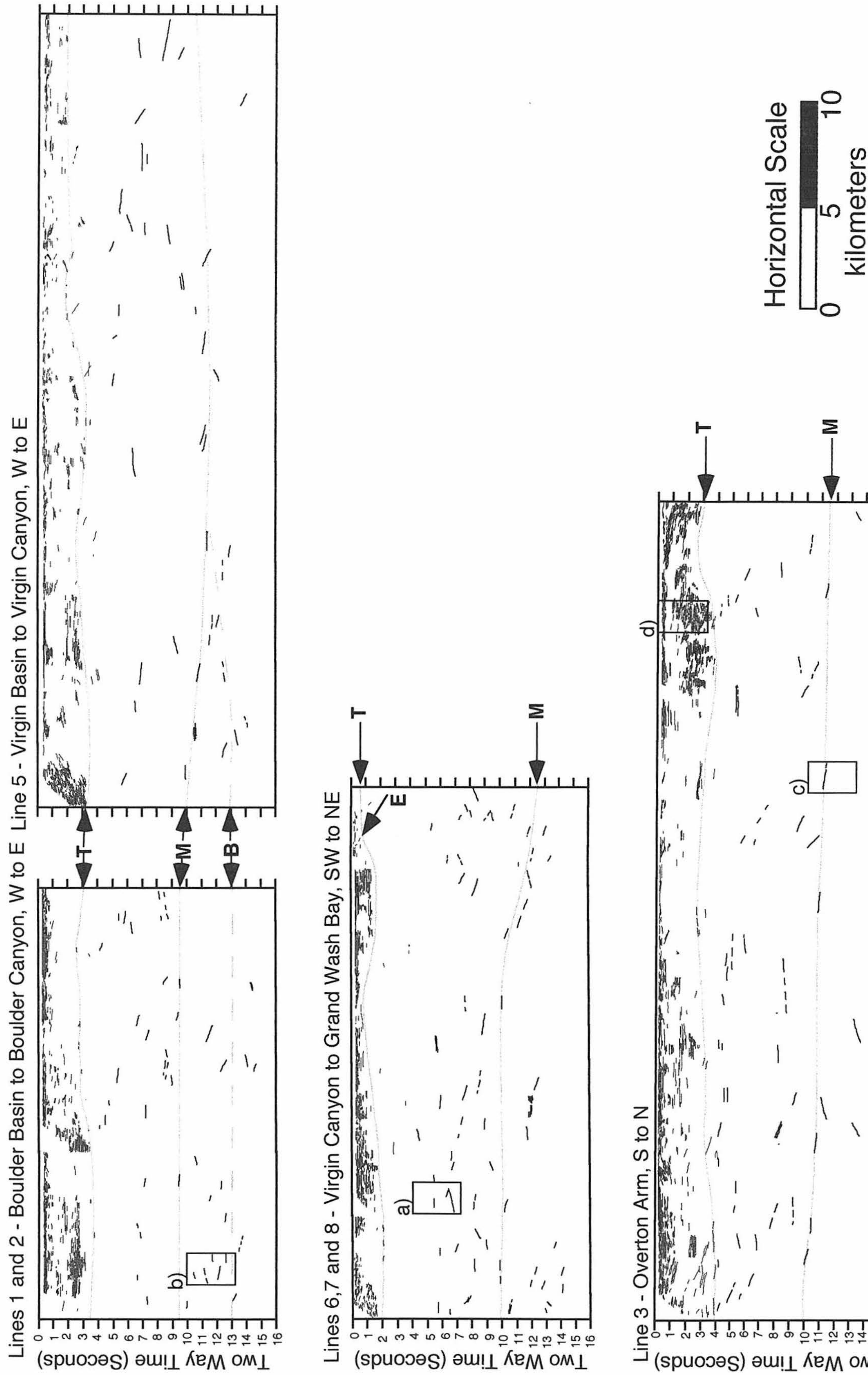
Lines 1 and 2 - Boulder Basin to Boulder Canyon, W to E
Line 5 - Virgin Basin to Virgin Canyon, W to E
Lines 6,7 and 8 - Virgin Canyon to Grand Wash Bay, SW to NE
Line 3 - Overton Arm, S to N
Two Way Time (Seconds)
T
M
B
E
a)
b)
c)
d)
Horizontal Scale
0 5 10
kilometers

streamer, moving it up and down in the water. This 'strumming', as well as surface wave noise, would have been recorded as pressure variations in the hydrophones, thus creating a semi-coherent noise pattern in the recorded data.

3.5 Interpretation

A band of gently dipping reflections which is visible across much of the data set between ~ 9.5 and 12 s TWT (~25 to 33.5 km) is interpreted to be the reflection Moho (line M on Figure 3). There is an abrupt end of reflectivity downward beneath the reflection Moho, as is commonly seen on BRP and Colorado Plateau data sets (e.g. Klemperer et al., 1986; Hauge et al., 1987; Hauser et al., 1987; Serpa et al., 1988; Hauser and Lundy, 1989; McCarthy and Parsons, 1994). The Moho under lines 3 and 5 occurs at depths of ~ 27 to 32 km (~ 10 to 11.5 s TWT). On line 3 the Moho deepens slightly from south to north. The location of the Moho becomes less clear on lines 6, 7 and 8 due in part to lower data quality, but appears to remain at ~ 27 km (~ 10 s TWT) until somewhere near the northeast end of line 7, where it begins to deepen, reaching a depth of ~ 35 km (~ 12.5 s TWT) by the east end of line 8. This deepening is not surprising, as the edge of the extended terrain lies immediately to the east of line 8 and crustal thickness must increase to reach a thickness of 40 to 50 km under the Colorado Plateau (Roller, 1965; Warren, 1969; Prodehl, 1979; Hauser and Lundy, 1989; Wolf and Cipar, 1993). Furthermore, an eastward thickening of the crust is consistent with the results of Montana et al. (1995), who reported an eastward thickening of the crust beginning in the vicinity of the Grand Wash Cliffs.

The Moho on lines 1 and 2 is interpreted to lie at a depth of ~25 km (~ 9.5 s TWT), and deepen to the east, reaching a depth of ~ 32 km (~ 11.5 s TWT) under the middle of line 5. This interpretation is based on the occurrence of a band of gently dipping reflections (line M on Figure 3) which seems to correlate with the interpreted Moho from the rest of the survey. It is possible, however, that the base of the crust is deeper than this, since there are a significant number of deeper reflections on lines 1, 2 and the western end of line 5 (see line B on Figure 3 and deep reflections R on Figure 4b). If these reflections are from the deep crust, then the Moho under lines 1, 2, and 5 could be as deep as ~ 36.5 km (~ 13 s TWT). However, these reflections are both unusually deep for BRP crustal reflections, and are some of the less clearly defined reflections from the data set (compare these deep reflections on Figure 4b with the more distinct reflections on Figures 4a and 4c), therefore it is likely that this apparent deep reflectivity is due to misinterpretation of unusually coherent noise.

Although the mid-crust is generally unreflective, it does show some of the strongest and most continuous individual reflections visible in the data (for example, the lowest reflection R on Figure 4a). These reflections are probably from contacts within the complex Precambrian crystalline basement which underlies the area and outcrops in the Gold Butte Block, or from younger sills or shear zones within the mid to lower crust (~6 to 9 s TWT, ~14.5 to 24 km). Given the available data it is difficult to distinguish between these possibilities.

The numerous sub-horizontal to horizontal reflections in the upper 1 to 4 s TWT (~1.5 to 8.5 km) of all lines are most likely due to reflectors within the Tertiary basin fill (see Figure 4d and reflections above line T on Figure 3). These reflections are interpreted to be from horizons within the little-extended Tertiary Red Sandstone and Muddy Creek Formation. The same units, only mildly faulted, are seen on seismic reflection profiles

Figure 4. Selected data panels from the processed BARGE data. See Figure 3 for locations. Interpreted reflections (R) are labelled on panels a), b), and c). Note the greater continuity, apparent higher frequency, and different orientation from the strong diffraction pattern (D) and semi-coherent sub-horizontal noise trains (T). a) Typical mid-crustal reflections, b) The apparently reflective deep crust under eastern Lake Mead, d) An example of shallow reflections from Tertiary strata.

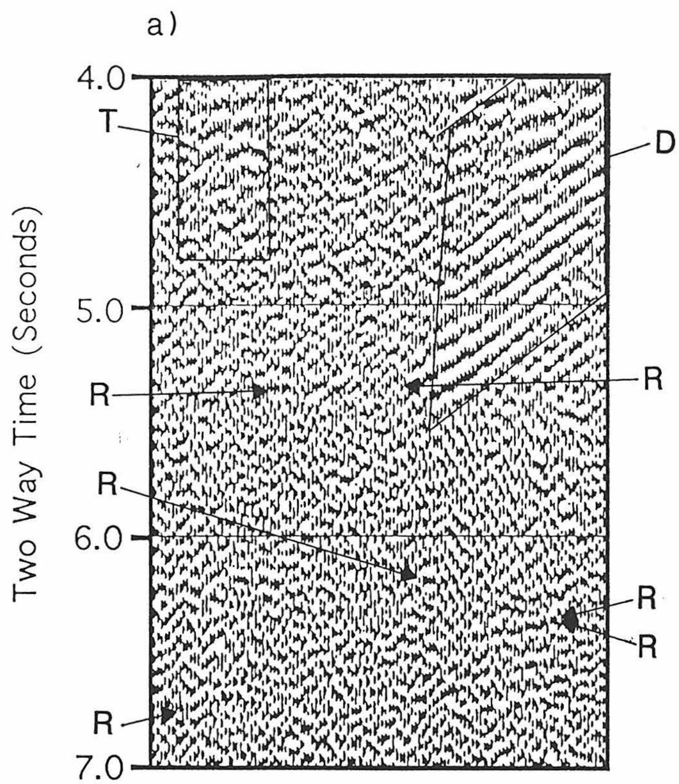
a)
4.0
T
D
5.0
R
R
R
6.0
R
R
R
7.0
Two Way Time (Seconds)

b)

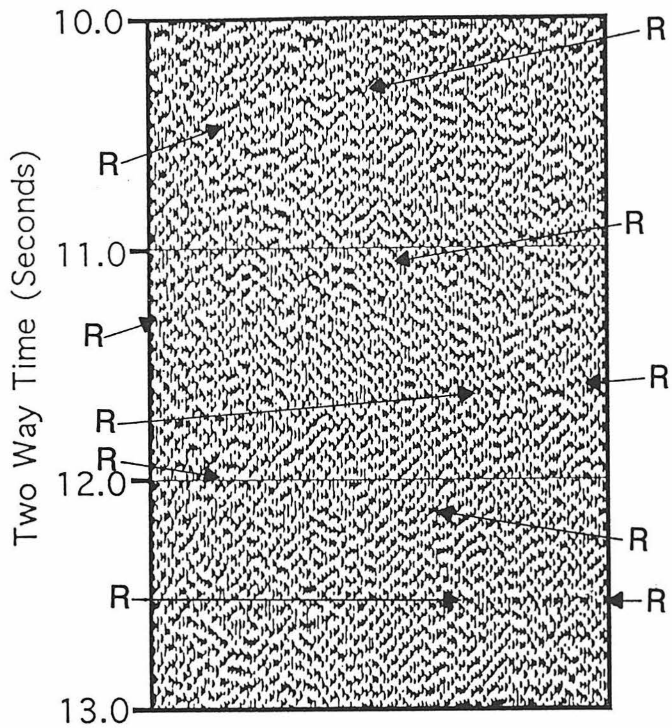

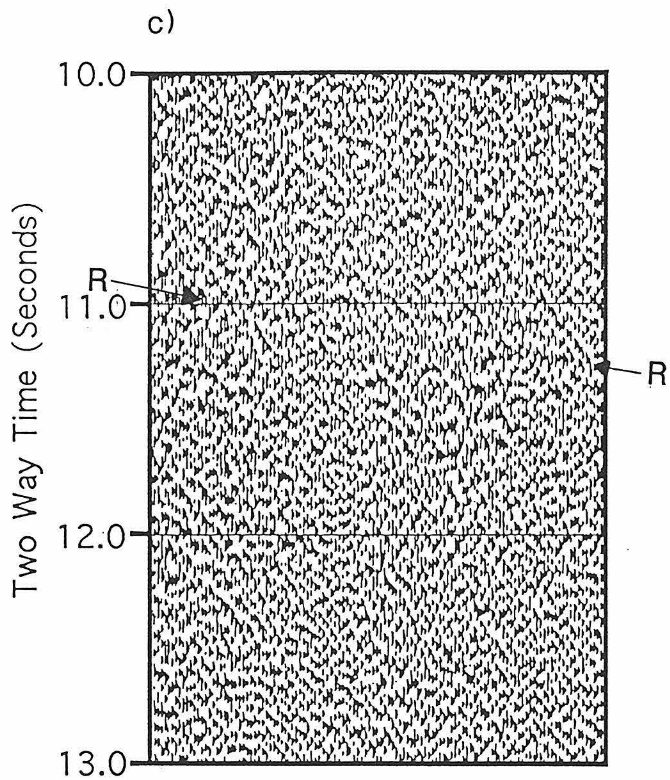
c)
10.0
11.0
12.0
13.0
Two Way Time (Seconds)
R
R

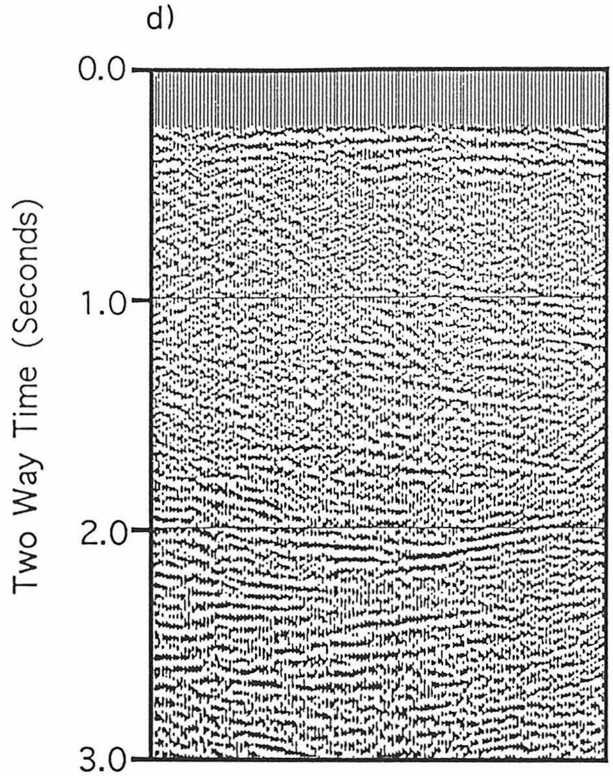
d)
0.0
1.0
2.0
3.0
Two Way Time (Seconds)

acquired just to the north of Lake Mead, in the Virgin River Valley, where they extend to depths of ~ 2.5 s (Bohannon et al., 1994). Identification of more steeply dipping reflections within the upper ~4 s of the data was generally not possible, however, one dipping reflection seen on line 8 does tie to the east dipping Paleozoic carbonates of Iceberg Ridge (E on Figure 3).

The overall character of the crust and Moho imaged by the BARGE survey is similar to that observed under the Colorado Plateau. For example, on COCORP line AZ6 (Figure 2; Hauser and Lundy, 1989) the upper 5 s of data shows abundant sub-horizontal reflectivity, the interval between ~ 5 s and ~16 s shows scattered, gently dipping to sub-horizontal reflections, and below 16 s reflections are nearly absent. The similar seismic character of the crust under the Lake Mead region and the Colorado Plateau suggests that the crust under Lake Mead has not been strongly altered by processes related to Basin and Range extension.

The fact that the Moho on the BARGE data is not well expressed is unusual when compared to other reflection seismic profiles from the highly extended BRP. By comparison, much of the COCORP 40° North transect (Klemperer et al., 1986; Hauge et al., 1987; Potter et al., 1987; Hauser et al., 1987b) and the COCORP Arizona transect (Hauser et al., 1987a), show a well expressed reflection Moho. The strong reflection Moho on these data sets is generally attributed either to magmatic underplating or the presence of a shear zone at the base of the crust. The magmatic underplating model is consistent with the high velocity of the lowermost crust, which is appropriate for a mafic restite or cumulate (e.g. Klemperer et al., 1986; Valasek et al., 1989), it is also consistent with the estimated pressure and temperature conditions at the base of the crust under the BRP, which are near the dry basalt solidus in some locations today (Lachenbruch and Sass, 1977; Klemperer et al., 1986). The shear zone model is consistent with the high amplitude, laterally discontinuous, multicyclic nature of BRP Moho reflections, which can be explained by juxtaposition of peridotitic and more felsic rocks (Valasek et al., 1989) or by creation of mylonites, which may be seismically reflective (Jones and Nur, 1984). If one or both of these models represents the correct interpretation of the BRP data, then the observed reflection character of the Moho under Lake Mead suggests that the base of the crust is not significantly magmatically underplated or sheared.

3.6 Discussion

3.6.1 Origin of the Present Crustal Structure

Interpretation of the BARGE seismic reflection data shows that the crust in the Gold Butte region is thinned but essentially unaltered Colorado Plateau type crust, whereas crust in the western Lake Mead region is similarly thinned, but is possibly altered by shearing and/or magmatism near its base. In both areas, the present crustal thickness is greater than expected if the crust had been extended without addition of material (given an original thickness of 45 km and $\beta \approx 3.5$ (Wernicke et al, 1988), the unaugmented present thickness should be ~13 km). Because of its pre-extensional position in the foreland of a thin skinned thrust belt, it is reasonable to assume that the pre-extensional thickness of the crust in the Lake Mead region was nearly the same as that of the adjoining Colorado Plateau (i.e. 40 to 50 km; Wolf and Cipar, 1993; Hauser and Lundy, 1989). This assumption is based on the observation that crustal thicknesses are known to increase only gradually toward the interior of the thrust belt in similar positions elsewhere (e.g., Price, 1981).

The present crustal structure may have resulted from an evolutionary sequence which began with localized extension in the Gold Butte region in the upper crust and more diffuse extension under the western Lake Mead region in the lower crust (note that the entire Lake Mead region would have been compressed in an east - west direction by a factor of ~ 3.5 times relative to its present width). Thinning of the lower crust under the western Lake Mead region would have resulted in uplift of isotherms and may have triggered volcanism in the region. Extension in the Gold Butte region coincides with volcanism in the western Lake Mead region: Peak extension at Gold Butte occurred at ~15 Ma (Bohannon, 1984; Fryxell et al., 1992; Fitzgerald et al., 1991), but growth faults in the base of the Rainbow Gardens Member of the Horse Spring Formation (~ 24 to 19 Ma; Beard, 1996) indicate that minor extension began earlier than that (Brady; unpublished mapping, 1996). These ages are coincident with volcanism in the western Lake Mead region (~ 18.5 to 11.5 Ma; Anderson, 1971,1973; Darvall et al., 1991).

An alternate explanation for the present crustal geology has recently been proposed by Howard and Foster (1996), who suggest that extension of the eastern Lake Mead area (the South Virgin Mountains) may be the result of passive failure of the crust toward a nearby growing low area of actively thinning hot crust. This model is also consistent with the coincident timing of extension in the eastern Lake Mead region and volcanism in the western Lake Mead region.

In either case, extension eventually leads to extreme thinning of the crust in the Gold Butte region, potentially resulting in lateral mass transfer of mid to lower crustal material from under the less extended surrounding regions (Wernicke, 1990, 1992; Kruse et al., 1993). Possible sources of mid to lower crustal material include the unextended terrain to the north, as well as the unextended Colorado Plateau and the less extended western Lake Mead region. The terrain to the south apparently extended at the same time as the Gold Butte region (Cascadden, 1991; Cascadden and Smith, 1991) and would therefore not act as a source of mid to lower crustal material. If the lower crust of the western Lake Mead region was warmer due to extension-related uplift of isotherms or active magmatism, it would have been the most mobile of the surrounding lower crustal regions, and may have provided most of the flow into the Gold Butte region (Fig. 5). This ductile flow of material, along with the magmatism, may have generated the greater lower crustal reflectivity seen in the BARGE data.

As upper crustal thinning progressed westward across the Lake Mead region, the source of mid to lower crustal material needed to compensate for the thinning presumably also migrated westward. Since the thinning is so extreme, it would have been necessary to draw mid to lower crustal material from ever increasing distances. Clearly, if this pattern progressed westward, the shear along the margins of a mid to lower crustal channel would increase to the west.

3.6.2 Constraints on the Source of Mid to Lower Crustal Material

If both pre- and post-extensional crustal geometry can be constrained, it is relatively simple to make mass balance calculations which constrain the volume and source of lower crustal flow into the central Basin and Range. In order to simplify matters, all calculations will be made for a two dimensional east - west cross-section of crust extending from the Sierra Nevada to the Colorado Plateau at the latitude of Lake Mead. This does not mean that all deformation is assumed to be east-west plane strain, since north-south constriction can be factored in as thickening of the cross-section. The current cross-sectional geometry of the central Basin and Range crust is well known. It is constrained by the results of the BARGE experiment, along with seismic reflection

Figure 5. Possible west to east cross-section of the Lake Mead region at ~ 16 Ma, showing location of Moho and pattern of mid to lower crustal mass transfer. Note that the lowermost crust under the western part of the section has been uplifted and should be warmer than crust at an equivalent depth under the Colorado Plateau. Upper crustal structure of the eastern Gold Butte region is based on a simplification of 1:12 000 scale geologic mapping conducted in association with the BARGE project.

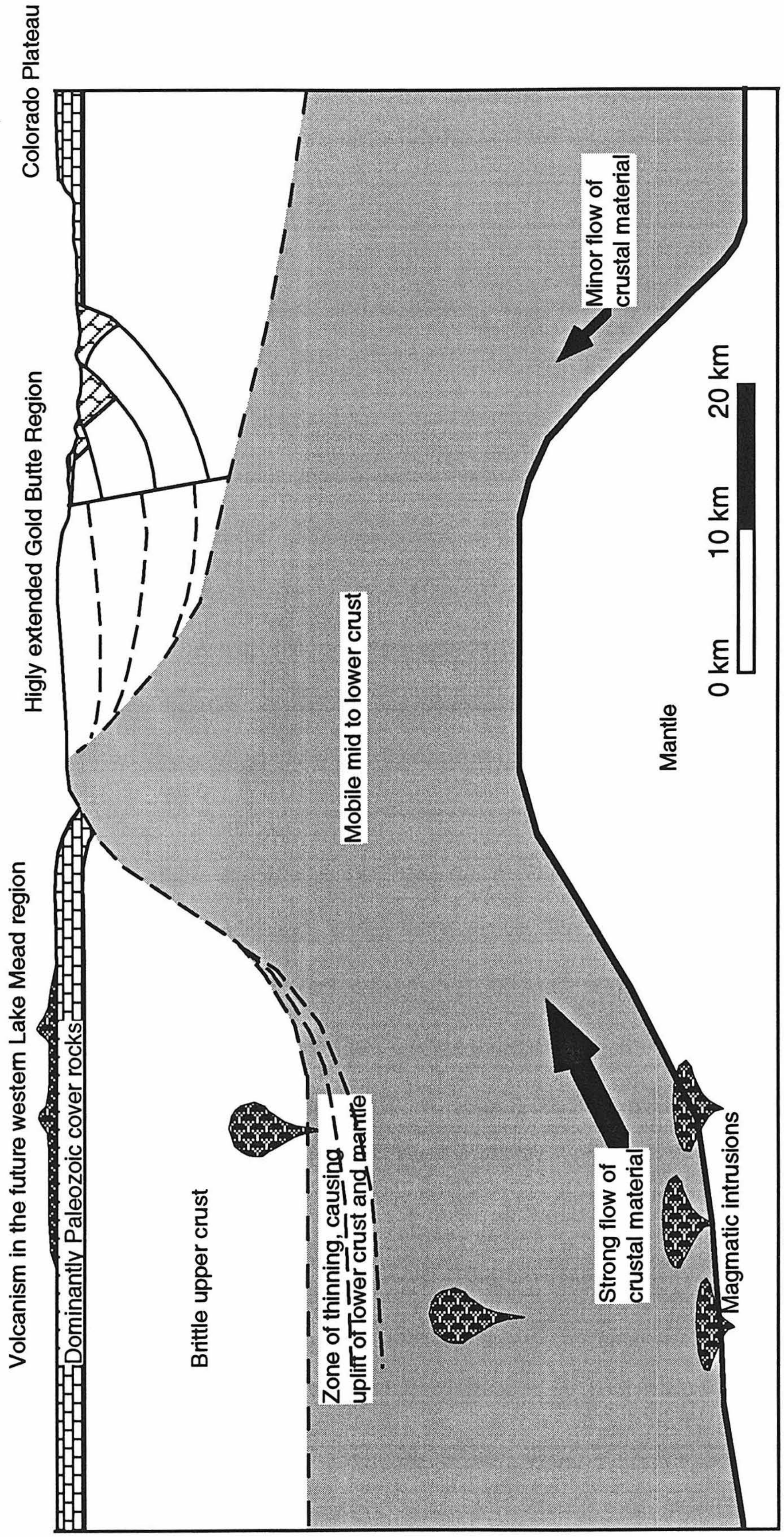
Colorado Plateau
Higly extended Gold Butte Region
Volcanism in the future western Lake Mead region
Dominantly Paleozoic cover rocks
Brittle upper crust
Zone of thinning, causing
uplift of lower crust and mantle
Mobile mid to lower crust
Mantle
Minor flow of
crustal material
Strong flow of
crustal material
Magmatic intrusions
0 km
10 km
20 km

data from the Basin and Range to Sierra Nevada transition (Wernicke et al., 1996), and refraction data from the Colorado Plateau (Wolf and Cipar, 1993). In addition, the pre-extensional geometry of the central Basin and Range can be inferred from geologic data (e.g. Burchfiel et al., 1992).

Prior to extension, the crust at this latitude was probably an Andean type orogenic belt (Burchfiel et al., 1992), and probably had an average crustal thickness of roughly 57.5 km^2. This corresponds to a crust which reached a maximum thickness of approximately 70 km under the Sierra Nevada (c.f. Ducea and Saleeby, 1996), and tapered eastward to the 45 km thickness of the stable Colorado Plateau (Wolf and Cipar, 1993). Restoration of the surface geology shows that the pre-extensional width of the central Basin and Range was approximately 100 km (Wernicke et al., 1988; Wernicke and Snow, in prep.). These values yield a cross-sectional area of 5750 km^2 for the pre-extensional central Basin and Range.

The central Basin and Range currently has a width of 350 km and an average crustal thickness of approximately 30 km (this study; Wernicke et al., 1996). Thus, it has a cross-sectional area of approximately 10 500 km^2, which is an increase in area from it's pre-extensional state of 4750 km^2. This requires that since the onset of Neogene extension, approximately 4750 km^3 of crust have been added to every kilometre of the north - south length of the central Basin and Range.

This additional crust could only come from two sources, these being magmatic addition from the mantle and influx of crustal material from the edges of the extending region. The maximum amount of magmatic addition is about a 5 km thickness of crust, this being the maximum bound suggested for the more volcanic rich southern Basin and Range (McCarthy and Parsons, 1994). This means that, at most, 1750 km^2 were added to the cross-sectional area of the central Basin and Range by magmatism, leaving 3000 km^2 still to be explained.

A recent map view reconstruction of the central Basin and Range by Wernicke and Snow (in prep.) suggests that Neogene extension was accompanied by north - south shortening of approximately ten percent. Thus, about 1050 km^2 of the current cross-sectional area is due to influx of material from the north and south. This leaves 1950 km^2 which must be due to influx from the east and west edges of the central Basin and Range. Since these edges are structurally intact at surface, it seems that this influx must have occurred by ductile flow of mid to lower crustal material, as suggested by Wernicke (1992).

The source of the mid to lower crustal material can be constrained by using the BARGE data and refraction data from the Colorado Plateau (Wolf and Cipar, 1993). The interpreted depth to Moho at the east end of BARGE line 8 is 35 km, and the depth to Moho under the Colorado Plateau 180 km to the east is 45 km. Since the east edge of the extended terrain probably had a pre-extensional thickness nearly equal to that of the Colorado Plateau, it would seem that as much as 900 km^2 of material has flowed out from under the Colorado Plateau (see Figure 6).

This leaves at least 1050 km^2 of material which had to be added to the cross-section by material flowing out from under the Sierra Nevada and regions further to the west. This would correspond to emptying a mid-crustal channel with a thickness of 10 km and a length of 105 km. This figure is probably a minimum value, since it assumes the maximum reasonable values for addition of material by magmatism and flow from under the Colorado Plateau. The amount of material required from under the Sierra Nevada and regions further to the west could easily be two to three times as large as the

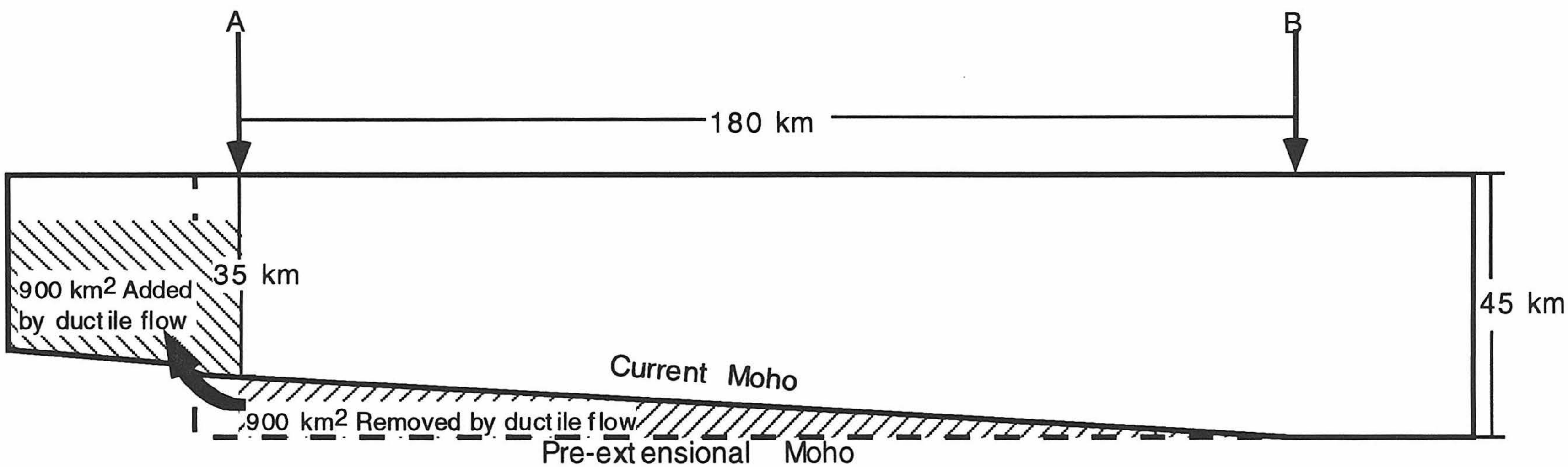

Figure 6. Simplified west to east cross section of the western Colorado Plateau crust, both before (dashed line) and after (solid line) extension. Current depth to Moho is known under point A from the BARGE data, and under point B from Wolf and Cipar (1993). The shaded area represents a maximum, since the post-extensional Moho may reach a depth of 45 km somewhere between points A and B.

value stated above . Removal of this amount of material from under the Sierra Nevada and Great Valley is certainly allowed by the results of Wernicke et al. (1996), which suggest that the crust under the Sierra Nevada may have thinned by as much as a factor of two since 20 Ma. It is also consistent with the calculations of Kruse et al. (1991) which show that pressure gradients created by Basin and Range extension are sufficient to drive flow of crustal material in such a channel.

3.6.3 The Nature of the Transition Zone Moho

One of the most interesting features of the BARGE data set is the lack of Moho reflectivity. This is a common theme in reflection profiles which cross over the transition from the Basin and Range to the Colorado Plateau. COCORP seismic reflection profiles from the eastern Basin and Range in Utah (Allmendinger et al., 1983) and across the transition from Basin and Range to Colorado Plateau in Arizona (Hauser et al., 1987a; McCarthy and Parsons, 1994) show a relatively unreflective Moho. McCarthy and Parsons (1994) note that the decreasing Moho reflectivity across the transition zone in Arizona corresponds to a decreasing amount of extension at surface. Interestingly, this is not true for the BARGE or COCORP Utah line 1 data sets. Both BARGE and COCORP Utah line 1 were collected across highly extended Basin and Range. Thus, it seems that Moho reflectivity is not directly linked to the local magnitude of extension.

It also seems that Moho reflectivity is not necessarily linked to the nature of the upper mantle. This is best demonstrated by BARGE line 3, which crosses over the geochemically defined boundary between lithospheric upper mantle of the central Basin and Range (Farmer et al., 1989; Feuerbach et al, 1993) and asthenospheric upper mantle of the Colorado River extensional corridor (Feuerbach et al, 1989). The geochemically defined change in upper mantle type is not accompanied by any change in the character of Moho reflectivity on line 3.

While Moho reflectivity under the Basin and Range, transition zone, and Colorado Plateau does not seem to be controlled by the type of upper mantle or the local magnitude of extension, it apparently is affected by extensional processes. This is evident from the fact that the Moho under most of the extended Basin and Range is highly reflective, whereas the Moho under the stable Colorado Plateau is relatively unreflective. These conditions are consistent with the reflectivity being the product of shear near the crust-mantle boundary and/or magmatic underplating, as suggested by Klemperer et al. (1986).

The shear near the crust-mantle boundary would increase away from the east edge of the Basin and Range, particularly if shearing is due to flow in a lower crustal channel and most of the inflowing material came from the west edge of the extended region. Most of the shear due to flow in such a channel would be concentrated at its lower margin for two reasons. First, the flow rate of crustal materials by power law creep increases exponentially with increasing temperature (Christie et al, 1979; Goetze, 1978; Goetze and Brace, 1972; Griggs et al., 1960), so maximum flow rates should be strongly shifted toward the bottom of a lower crustal channel (assuming an increase in temperature with depth). Second, the upper boundary of a mid to lower crustal channel would probably be a transitional one where flow rate gradually increases with increasing temperature, while the lower boundary might be more sharply defined, since it may be controlled by the rheological contrast at the crust-mantle boundary. These two factors should combine to create a narrow, highly sheared boundary at the base of the crust.

The evidence presented here does not rule out the possibility that magmatic underplating creates the highly reflective Moho in some cases. However, it does seem that underplating is a less generally applicable explanation. For example, the Moho under the transition zone in Arizona is relatively unreflective (Hauser et al., 1987a, McCarthy and Parsons, 1993) , despite significant volcanism (c.f. Reynolds, 1988), while the Moho under the Sierra Nevada to Basin and Range transition is highly reflective (Wernicke et al., 1996) despite relatively little volcanism. These observations are inconsistent with reflectivity being due to magmatic underplating, but are consistent with reflectivity being due to shearing at the base of a mid to lower crustal channel.

3.7 Conclusions

Interpretation of the BARGE data set shows that the reflection Moho under most of the Lake Mead region is at a depth of about 30 km. It begins to deepen near the edge of the Colorado Plateau, reaching approximately 35 km depth under easternmost Lake Mead. It may also deepen slightly toward the north, across the Lake Mead Fault system.

The mid to lower crust under the Lake Mead region is seismically transparent, and Moho reflections are relatively weak and discontinuous. This weakly reflective Moho seems to be characteristic of the Basin and Range to Colorado Plateau transition. Similar weak, discontinuous Moho reflections have been recorded by other seismic lines which cross over the transition north and south of Lake Mead (Allmendinger et al., 1983; Hauser et al., 1987a).

The typical highly reflective Moho of the Basin and Range province may be due to shearing at the base of a mid to lower crustal flow channel, as suggested by Klemperer et al. (1986). This is consistent with the increased reflectivity of the Moho further to the west under the highly extended Basin and Range. An alternate explanation of Moho reflectivity being due to magmatic underplating (Klemperer et al., 1986) is less satisfactory, since the transition zone Moho remains unreflective to the southeast (Hauser et al. 1987a), in a region which has experienced voluminous magmatism (e.g. Reynolds, 1988).

Mass balance calculations for the central Basin and Range, constrained by the results of seismic experiments (this study, Wernicke et al., 1996; McCarthy and Parsons, 1994; Wolf and Cipar, 1993) and geologic data (Wernicke and Snow, in prep.; Brady et al., 1996; Burchfiel et al., 1992; Wernicke et al., 1988) suggest that a significant volume of deep crustal material has flowed into the central Basin and Range during the Neogene. Furthermore, the constraints dictate that most of this material probably flowed out from under the Sierra Nevada - enough to empty a channel at least 10 km thick and 105 km wide.

3.8 References Cited

Allmendinger, R.W., J.W. Sharp, D. Von Tish, L. Serpa, L. Brown, S. Kaufman, and J. Oliver, Cenozoic and Mesozoic structure of the eastern Basin and Range province, Utah, from COCORP seismic-reflection data, *Geology, 11*, 532-536, 1983.

Allmendinger, R., K.D. Nelson, C.J. Potter, M. Barazangi, L.B. Brown, and J.E. Oliver, Deep seismic reflection characteristics of the continental crust, *Geology, 15*, 304-310, 1987.

Anderson, R.E., Thin skin distension in Tertiary rocks of southeastern Nevada, *Geol. Soc. Am. Bull., 82*, 42-58, 1971.

Anderson, R.E., Large-magnitude late Tertiary strike-slip faulting north of Lake Mead, Nevada, 18 pp., *U.S. Geol. Surv. Prof. Paper 794*, 1973.

Anderson, R.E., C.R. Longwell, R.L. Armstrong, and R.F. Marvin, Significance of K-Ar ages of Tertiary rocks from the Lake Mead region, Nevada-Arizona, *Geol. Soc. Am. Bull., 83*, 273-288, 1972.

Armstrong, R.L., K-Ar dating using neutron activation for Ar analysis, *Geochim. Cosmochim. Acta, 30,* 565-600, 1966.

Armstrong, R.L., Geochronology of Tertiary igneous rocks, eastern Basin and Range province, western Utah, eastern Nevada, and vicinity, U.S.A., *Geochim. Cosmochim. Acta, 34*, 203-232, 1970.

Beard, L.S., Paleogeography of the Horse Spring Formation in relation to the Lake Mead fault system, Virgin Mountains, Nevada and Arizona, *Spec. Pap. Geol. Soc. Am., 303*, 27-60, 1996.

Bohannon, R.G., Mesozoic and Cenozoic tectonic development of the Muddy, North Muddy, and northern Black Mountains, Clark County, Nevada, in Tectonic and stratigraphic studies in the eastern Great Basin, edited by Miller, D.M., Todd, R., and K.A. Howard, *Mem. Geol. Soc. Am., 157*, 125-148, 1983.

Bohannon, R.G., Nonmarine sedimentary rocks of Tertiary age in the Lake Mead region, 72 pp., *U.S. Geol. Surv. Prof. Pap., 1259*, 1984.

Bohannon, R.G., J.A. Grow, J.J. Miller, and R.H. Blank Jr., Seismic stratigraphy and tectonic development of Virgin River depression and associated basins, southeastern Nevada and northwestern Arizona, *Geol. Soc. Am. Bull., 105*, 501-520, 1993.

Brady, R.J., B.P. Wernicke, J.E. Fryxell, and D.R. Lux, Large magnitude Miocene extension in the Lake Mead region, *Geol. Soc. Am. Abst. Programs, 28 (7)*, 449, 1996.

Burchfiel, B.C., D.S. Cowan, and G.A. Davis, Tectonic overview of the Cordilleran orogen in the western United States, in *The Cordilleran Orogen: Conterminous U.S., The Geology of North America, G-3*, edited by Burchfiel, B.C., Lipman, P.W., and M.L. Zoback, pp. 553-582, Geol. Soc. Am., Boulder, Colorado, 1992.

Burchfiel, B.C., and G.A. Davis, Nature and controls of Cordilleran orogenesis, western United States; Extensions of an earlier synthesis, *Am. J. Sci., 275-A*, 363-396, 1975.

Burchfiel, B.C., R.J. Fleck, D.T. Secor, R.R. Vincelette, and G.A. Davis, Geology of the Spring Mountains, Nevada, *Geol. Soc. Am. Bull., 85*, 1013-1022, 1974.

Cascadden, T.E., Style of volcanism and extensional tectonics in the eastern Basin and Range Province; northern Mohave County, Arizona, M.S. thesis, 209 pp., University of Nevada, Las Vegas, 1991.

Cascadden, T.E., and E.I. Smith, The eastern boundary of the extensional allochthon in the eastern Basin and Range: volcanic and structural geology of the northern White Hills, Arizona, *Geol. Soc. Am. Abst. Programs, 23 (2),* 12, 1991.

Chamberlin, R.M., Cenozoic domino-style crustal extension in the Lemitar Mountains, New Mexico; A summary, in *Soccorro Region II: Soccorro, New Mexico Geological Society, Guidebook 34*, edited by Chapin, C.E., and J.F. Callender, pp. 111-118, New Mexico Geol. Soc., 1983.

Christie, J.M., P.S. Koch, and R.P. George, Flow law of quartzite in the alpha-quartz field, *EOS Trans. AGU, 60,* 948, 1979.

Cole, E.D., Petrogenesis of late Cenozoic alkalic basalt near the eastern boundary of the Basin-and-Range: Upper Grand Wash trough, Arizona and Gold Butte, Nevada, M.S. thesis, 68 pp., University of Nevada, Las Vegas, 1989.

Cook, F.A., J. L. Varsek, R.M. Clowes, E.R. Kanasewich, C.S. Spencer, R.R. Parrish, R.L. Brown, S.D. Carr, B.J. Johnson, and R.A. Price, Lithoprobe crustal reflection cross section of the southern Canadian Cordillera, 1, foreland thrust and fold belt to Fraser River Fault, *Tectonics, 11*, 12-35, 1992.

Darvall, P., P.B. Gans, and G.S. Lister, Normal faulting in the Eldorado Mountains, southeastern Nevada, *Geol. Soc. Am. Abst. Programs, 23(2),* 17, 1991.

Ducea, M.N., and J.B. Saleeby, Buoyancy sources for a large, unrooted mountain range, the Sierra Nevada, California: Evidence from xenolith thermobarometry, *J. Geophys. Res., 101,* 8229-8244, 1996.

Duebendorfer, E.M., A.J. Sewall, and E.I. Smith, The Saddle Island detachment; An evolving shear one in the Lake Mead area, Nevada, in Basin and Range extensional tectonics near the latitude of Las Vegas, Nevada, edited by Wernicke, B.P. , *Mem. Geol. Soc. Am., 176,* 77-98, 1990.

Duebendorfer, E.M., and D.M. Simpson, Kinematics and timing of Tertiary extension in the western Lake Mead region, Nevada, *Geol. Soc. Am. Bull., 106,* 1057-1073, 1994.

Farmer, G.L., F. Perry, S. Semken, B. Crowe, D. Curtis, and D.J. DePaolo, Isotopic evidence on the structure and origin of the subcontinental lithospheric mantle in southern Nevada., *J. Geophys. Res., 94*, 7885-7898, 1989.

Feuerbach, D.L., E.I. Smith, M. Shafiqullah, and P.E. Damon, New K-Ar dates for late-Miocene to early Pliocene mafic volcanic rocks in the Lake Mead area, Nevada and Arizona, *Isochron West, 57,* 17-20, 1991.

Feuerbach, D. L., E. I. Smith, J. D. Walker, and J. A. Tangeman, The role of the mantle during crustal extension: Constraints from geochemistry of volcanic rocks in the Lake Mead area, Nevada and Arizona, *Geol. Soc. Am. Bull., 105,* 1561-1575, 1993.

Fitzgerald, P.G., J.E. Fryxell, and B.P. Wernicke, Miocene crustal extension and uplift in southeastern Nevada: Constraints from fission track analysis, *Geology, 19*, 1013-1016, 1991.

Fryxell, J.E., G.S. Salton, J.E. Selverstone, and B. Wernicke, Gold Butte crustal section, South Virgin Mountains, Nevada, *Tectonics, 11*, 1099-1120, 1992.

Gans, P.B., G.A. Mahood, and E. Schermer, Synextensional magmatism in the Basin and Range Province; a case study from the eastern Great Basin, *Spec. Pap. Geol. Soc. Am., 233*, 53 pp., 1989.

Gans, P.B., E.L. Miller, J. McCarthy, and M.L. Ouldcott, Tertiary extensional faulting and evolving brittle-ductile transition zones in the northern Snake Range and vicinity: New insights from seismic data, *Geology, 13*, 189-193, 1985.

Goetze, C., and W.F. Brace, Laboratory observations of high-temperature rheology of rocks, *Tectonophysics, 13*, 538-600, 1972.

Goodwin, E.B., and J. McCarthy, Composition of the lower crust in west-central Arizona from three-component seismic data, *J. Geophys. Res., 95*, 20097-20109, 1990.

Goodwin, E.B., G.A. Thompson, and D.A. Okaya, Seismic identification of basement reflectors: The Bagdad reflection sequence in the Basin and Range-Colorado Plateau Transition Zone, *Tectonics, 8*, 821-831, 1989.

Griggs, D.T., F.H. Turner, and H.C. Heard, Deformation of rocks at 500 to 800°C, *Mem. Geol. Soc. Am., 79*, 39-104, 1960.

Guth, P.L., Tertiary extension north of the Las Vegas Valley shear zone, Sheep and Desert Ranges, Clark County, Nevada, *Geol. Soc. Am. Bull., 92*, 763-771, 1981.

Hauge, T.A., R.W. Allmendinger, C. Caruso, E. Hauser, S. Klemperer, S. Opdyke, C. Potter, W. Sanford, L. Brown, S. Kaufman, and J. Oliver, Crustal structure of western Nevada from COCORP deep seismic reflection data, *Geol. Soc. Am. Bull., 98*, 320-329, 1987.

Hauser, E.C., and J. Lundy, COCORP deep reflections; Moho at 50 km (16s) beneath the Colorado Plateau, *J. Geophys. Res., 94*, 7071-7081, 1989.

Hauser, E.C., J. Gephart, T. Latham, J. Oliver, S. Kaufman, L. Brown, and I. Lucchita, COCORP Arizona transect: Strong crustal reflections and offset Moho beneath the transition zone, *Geology, 15*, 1103-1106, 1987a.

Hauser, E.C., C. Potter, T. Hauge, S. Burgess, S. Burtch, J. Mutschler, R. Allmendinger, L. Brown, S. Kaufman, and J. Oliver, Crustal structure of eastern Nevada from COCORP deep seismic reflection data, *Geol. Soc. Am. Bull., 99*, 833-844, 1987b.

Howard, K.A., and D.A. Foster, Thermal and unroofing history of a thick, tilted Basin-and-Range crustal section in the Tortilla Mountains, Arizona,, *J. Geophys. Res., 101*, 511-522, 1996.

Howie, J.M., T. Parsons, and G.A. Thompson, High-resolution P- and S-wave deep crustal imaging across the edge of the Colorado Plateau, USA: Increased reflectivity caused by initiating extension, in *Continental lithosphere: Deep seismic reflections, Geodynamics Series vol. 22*, edited by Mesiner, R., Brown, L., Durbaum, H.J., Franke, W., Fuchs, K., and F. Seifert, pp. 21-29, AGU, Washington, D.C. , 1991.

Jones, T.D., and A. Nur, The nature of seismic reflections from deep crustal fault zones, *J. Geophys. Res., 89,* 3153-3171, 1984.

Klemperer, S., T.A. Hauge, E.C. Hauser, J.E. Oliver, and C.J. Potter, The Moho in the northern Basin and Range province, Nevada, along the COCORP 40°N seismic-reflection transect, *Geol. Soc. Am. Bull., 97*, 603-618, 1986.

Knuepfer, P.L.K., P.J. Lemiszki, T.A. Hauge, L.D. Brown, S. Kaufman, and J.E. Oliver, Crustal structure of the Basin and Range-Sierra Nevada transition from COCORP deep seismic reflection profiling, *Geol. Soc. Am. Bull., 98*, 488-496, 1987.

Kruse, S., M. McNutt, J. Phipps-Morgan, L. Royden, and B. Wernicke, Lithospheric extension near Lake Mead, Nevada: A model for ductile flow in the lower crust: *J. Geophys. Res., 96*, 4435-4456, 1991.

Lachenbruch, A.H., and J.H. Sass, Heat flow in the United States and the thermal regime of the crust, in The Earths Crust, edited by J.G. Heacock, *American Geophysical Union Geophysical Monograph , 20,* 626-675, 1977.

Longwell, C.R., Structure of the northern Muddy Mountains area, Nevada, *Geol. Soc. Am. Bull., 60*, 923-967, 1949.

Longwell, C.R., E.H. Pampeyan, B. Bowyer, and R.J. Roberts, Geology and mineral deposits of Clark County, Nevada, *Nev. Bur. Mines Bull., 62*, 218 pp., 1965.

McCarthy, J., and T. Parsons, Insights into the kinematic Cenozoic evolution of the Basin and Range-Colorado Plateau transition from coincident seismic refraction and reflection data, *Geol. Soc. Am. Bull., 106*, 747-759, 1994.

Miller, E.L., P.B. Gans, and J. Garing, The Snake Range decollement; An exhumed mid-Tertiary ductile-brittle transition, *Tectonics, 2*, 239-263, 1983.

Montana, C.J., G.R. Keller, and K.C. Miller, Lithospheric structure in the Basin and Range - Colorado Plateau from the delta force seismic experiment, *EOS Trans. AGU, 76*, 552, 1995.

Parsons, T., J.M. Howie, and G.A. Thompson, Seismic constraints on the nature of lower crustal reflectors beneath the extending southern Transition Zone of the Colorado Plateau, Arizona, *J. Geophys. Res., 97*, 12391-12407, 1992.

Potter, C.J., C.S. Liu, J. Huang, L. Zheng, T.A. Hauge, E.C. Hauser, R.W. Allmendinger, J.E. Oliver, S. Kaufman, and L. Brown, Crustal structure of north-central Nevada: Results from COCORP deep seismic profiling, *Geol. Soc. Am. Bull., 98*, 330-337, 1987.

Price, R.A., The Cordilleran foreland thrust and fold belt in the southern Canadian Rocky Mountains, in *Thrust and Nappe Tectonics*, edited by McClay, K., and N.J. Price, pp. 427-448, Geological Society of London, 1981.

Prodehl, C., Crustal structure of the western United States, *U.S. Geol. Surv. Prof. Pap., 1034*, pp. 1-74, 1979.

Proffett, J.M., Jr., Cenozoic geology of the Yerington district, Nevada, and implications for the nature and origin of Basin and Range faulting, *Geol. Soc. Am. Bull., 88*, 247-266, 1977.

Reynolds, S.J., Geologic map of Arizona, Arizona Geological Survey, Map 26, 1988.

Roller, J.C., Crustal structure in the eastern Colorado Plateaus province from seismic refraction measurements, *Bull. Seismol. Soc. Am., 55*, 107-119, 1965.

Serpa, L., B. de Voogd, L. Wright, J. Willemin, J. Oliver, E. Hauser, and B. Troxel, Structure of the central Death Valley pull-apart basin and vicinity from COCORP profiles in the southern Great Basin, Geol. Soc. Am. Bull., 100, 1437-1450, 1988.

Sonder, L.J., P.C. England, B.P. Wernicke, and R.L. Christiansen, A physical model for Cenozoic extension of western North America, in Continental extensional tectonics, edited by Coward, M.P., Dewey, J.F., and P.L. Hancock, *Spec. Publ. Geol. Soc. London, 28*, 187-202, 1987.

Thompson, K.G., Stratigraphy and petrology of the Hamblin-Cleopatra volcano, Clark County, Nevada, M.S. thesis, 306 pp., University of Texas, Austin, 1985.

Valasek, P.A., A.W. Snoke, C.A. Hurich, and S.B. Smithson, Nature and origin of seismic reflection fabric, Ruby-East Humboldt metamorphic core complex, Nevada, *Tectonics, 8*, 391-415, 1989.

Warren, D.H., A seismic-refraction survey of crustal structure in central Arizona, *Geol. Soc. Am. Bull., 80,* 257-282, 1969.

Wernicke, B., The fluid crustal layer and its implications for continental dynamics, in *Exposed Cross Sections of the Continental Crust*, edited by M. Salisbury, NATO Advanced Studies Institute, Kluwer Academic Publishers, D. Riedel, Dordrecht, Holland, 509-544, 1990.

Wernicke, B., Cenozoic extensional tectonics of the U.S. Cordillera, in *The Cordilleran Orogen: Conterminous U.S., The Geology of North America, G-3*, edited by Burchfiel, B.C., Lipman, P.W., and M.L. Zoback, pp. 553-582, Geol. Soc. Am., Boulder, Colorado, 1992.

Wernicke, B., and G.J. Axen, On the role of isostasy in the evolution of normal fault systems, *Geology, 16*, 848-851, 1988.

Wernicke, B., G.J. Axen, and J.K. Snow, Basin and Range extensional tectonics at the latitude of Las Vegas, Nevada, *Geol. Soc. Am. Bull., 100,* 1738-1757, 1988.

Wernicke, B., R.L. Christiansen, P.C. England, and L.J. Sonder, Tectonomagmatic evolution of Cenozoic extension in the North American Cordillera, Continental extensional tectonics, edited by Coward, M.P., Dewey, J.F., and P.L. Hancock, *Spec. Publ. Geol. Soc. London, 28*, 203-221, 1987.

Wernicke, B., R. Clayton, M. Ducea, C.H. Jones, S. Park, S. Ruppert, J. Saleeby, J.K. Snow, L. Squires, M. Fliedner, G. Jiracek, R. Keller, S. Klemperer, J. Luetgert, P. Malin, K. Miller, W. Mooney, H. Oliver, and R. Phinney, Origin of high mountains in the continents: the southern Sierra Nevada, *Science, 271*, 190-193, 1996.

Wolf, L.W., and J.J. Cipar, Through thick and thin: A new model for the Colorado Plateau from seismic refraction data from Pacific to Arizona Crustal Experiment, *J. Geophys. Res., 98*, 19881-19894, 1993.

Wright, L.A., and B.W. Troxel, Shallow-fault interpretation of Basin and Range structure, southwestern Great Basin, in *Gravity and tectonics*, edited by DeJong, R., and R. Scholten, pp. 397-407, Amsterdam, Elsevier, 1973.

Young, R.A., Cenozoic geology along the edge of the Colorado Plateau in northwestern Arizona, Ph.D. thesis, 155 pp., Washington University, St. Louis, Missouri, 1966.

Young, R.A., Laramide deformation, erosion and plutonism along the southwestern margin of the Colorado Plateau, *Tectonophysics, 61*, 25-47, 1979.

Chapter 4

The Effects of Isostatically Driven Lower Crustal Flow on Normal Fault Longevity and Orientation

Robert Brady

(This chapter was re-formatted from a manuscript submitted to *Journal of Geophysical Research* on January 15, 1998

Abstract. In recent years much work has focused on documenting and explaining the pattern of normal faulting within highly extended continental regions and the occurrence of normal faults which have slipped at relatively low dips. Both the initiation of such structures and the accumulation of large amounts of offset on them seems to violate the commonly accepted Andersonian view of faulting (Anderson, 1942). This paper presents a model invoking isostatically induced flexural stresses as a mechanism for shutting down active normal faults. Flexural stresses are generated as isostatically driven flow of fluid lower crust inflates and upflexes the region of brittlely extending upper crust. The stress state which results from isostatic upflexing of the thinning region shuts down the active normal fault system and may favor formation of a new normal fault which flattens at shallow depths in the upper crust. Comparisons of model predictions with field observations from a variety of Basin and Range detachment faults suggest that the model is viable, and may be a step forward in explaining many of the features seen in regions of large magnitude continental extension.

4.1 Introduction

Explaining the spatial and temporal evolution of continental extension requires an understanding of the factors which shut down an active normal fault system, and thereby allow the locus of extension to migrate. It is widely accepted that the shutdown of many normal faults occurs by domino style rotation of fault planes to lower angles, until the resolved shear stress on the fault plane becomes too low and it is easier to break a new fault than it is to continue slip on the existing fault (e.g. Agnon and Reches, 1995; Nur et al., 1986; Sibson, 1985; Miller et al., 1983). While this explanation for the shutdown of normal faults in actively extending regions may be valid in many cases, it is inconsistent with the existence of major extensional detachment systems which slipped at very low angles (cf. John and Foster, 1993; Wernicke et al., 1985).

The model presented in this paper predicts the observed lifespans of major normal fault systems; it also predicts a state of stress in extending regions which should favor formation of shallowly dipping normal faults. It is based on consideration of the effects of isostatic restoring forces on a region of elastic upper crust which is thinning uniformly above a master detachment fault. Thinning of the elastic upper crust creates an isostatic imbalance which drives lower crustal flow from unextended to extended regions (c.f. Kruse et al., 1991, Block and Royden, 1990). Since the lower crust is assumed to have a finite viscosity, there will be a lag between thinning of the upper crust and full isostatic compensation by influx of lower crust. Therefore a depressed region of thinned crust develops, which is gradually upwarped as flow of the lower crust inflates the thinning region. Upwarping of the extending, thinning region generates compressional fiber stresses in the lower part of the elastic upper crust. These fiber stresses eventually shut down active normal faults within the extending region (Figure 1). In addition, the fiber stresses and basal shear stresses due to flow of the lower crust may create a stress state which favors the formation of shallow-flattening normal faults.

The magnitude of uplift of the thinned crust depends on the magnitude of isostatic disequilibrium. This, in turn, depends on the rates of tectonic thinning, sedimentation, and restoring lower crustal flow (which is non-linearly dependent on the rate of development of isostatic disequilibrium). This system, while complex, can be simplified and solved analytically.

Calculations have been made using reasonable estimates of the rate of tectonic thinning, sedimentation rate, effective elastic thickness of the upper crust, and lower crustal rheology for a 'typical' continental detachment fault. These calculations show that the model predicts lifespans for major detachment fault systems which are in reasonable agreement with those observed in the Basin and Range Province.

4.2 Model Description

The lithosphere was modeled as three distinct rheological layers; a strong elastic upper crust, a weak viscous lower crust, and a strong viscous upper mantle (Brace and Kohlstedt, 1980). For this model lithosphere, isostatic compensation of loads on the upper crust should occur first by flow in the lower crust, since its viscosity is significantly lower than that of the mantle and the upper crust is effectively decoupled from the mantle. For all lower crustal flow calculations, the thickness of the flow channel was set equal to the entire thickness of the ductile lower crust (Figure 1).

Figure 1. a) Assumed cross-section of the upper crust prior to extension. Strength profiles were calculated assuming a crust composed of quartz diorite and a mantle composed of olivine (see Table 2 for flow law parameters). b) Model crust during thinning and increasing isostatic disequilibrium. Note that thinning is modeled as being symmetrically distributed. c) Thinned crust at time of shut-down of normal faulting by isostatically generated flexural stresses; paired arrows in upflexed region indicate sense of σ_{xxflex}.

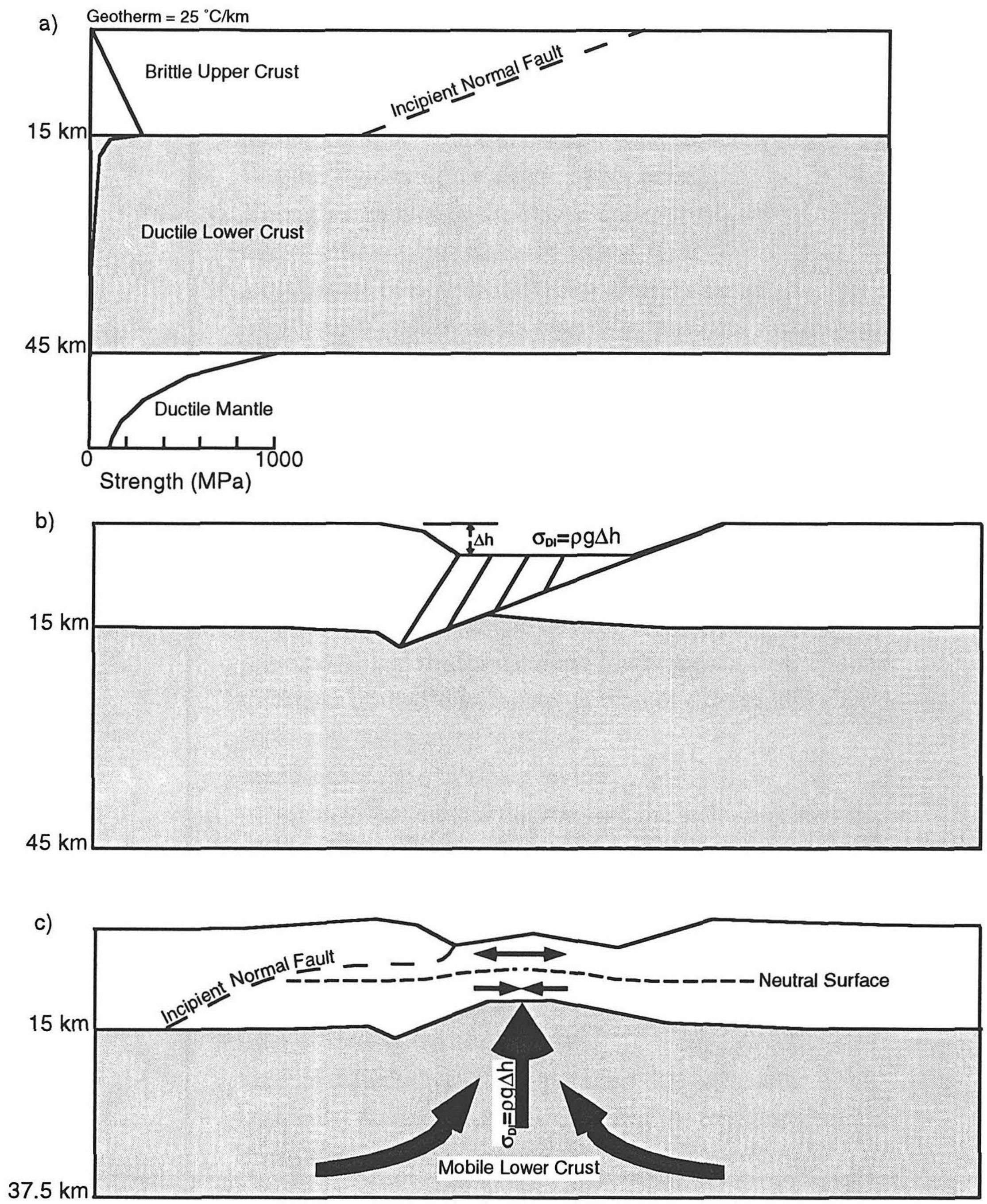
a)
Geotherm = 25 °C/km
Brittle Upper Crust
Incipient Normal Fault
15 km
Ductile Lower Crust
45 km
Ductile Mantle
0
1000
Strength (MPa)
b)
Δh
σDI=ρgΔh
15 km
45 km
c)
Incipient Normal Fault
Neutral Surface
15 km
σDI=ρgΔh
Mobile Lower Crust
37.5 km

σ_D	strength of the upper crust
σ_{DI}	vertical stress due to isostatic disequilibrium
σ_{xxflex}	horizontally directed fiber stress due to flexure
σ_1	maximum principal stress
σ_3	minimum principal stress
ε	strain rate
μ_{eff}	effective viscosity of the lower crust
v	Poisson's ratio of the elastic upper crust
ρ	crustal density
A	pre-exponential factor in lower crustal flow law (Table 2)
D	flexural rigidity of the elastic upper crust
E	Young's modulus of the elastic upper crust
F	rate of inflation due to lower crustal flow
L	length scale of flow in the lower crustal channel
L_f	length scale of flow at the time of extensional shut-down
Q	activation energy (see Table 2)
R	gas constant (8.31441 J $K^{-1mol-1}$)
S	rate of sedimentation
T	temperature in Kelvins
T_e	effective elastic thickness of the upper crust
Z	rate of tectonic thinning
c	ratio of strength of faulted crust to strength of unfaulted crust
d	thickness of the lower crustal flow channel
d_o	pre-extensional thickness of the lower crustal flow channel
d_f	thickness of the flow channel at time of extensional shut-down
g	acceleration due to gravity
h	thickness of the extending region
h_o	pre-extensional crustal thickness of the extending region
l	width of the extending region
l_o	pre-extensional width of the extending region
n	lower crustal flow law exponent (Table 2)
t	time since initiation of extension
t_o	time of onset of extension
t_f	time of shut-down of extension
w	vertical deflection of the upper crust due to isostatic uplift
x	horizontal distance from the center of the extending region
z	depth below Earth's surface

Table 1. List of Variables

Material	$\log_{10}A$ (Gpa^{-n} s^{-1})	n	Q (kJ mol^{-1})
Quartz Diorite	4.3	2.4	219
Westerly Granite	1.6	3.4	139
Olivine	4.8	3.5	533

Table 2. Flow law constants at $10^{-15}s^{-1}$ strain rate (data from Kruse et al., 1991)

The pre-extensional thickness of the upper and lower crust, as well as the strength profiles of the lithosphere are shown in Figure 1. The strength of the elastic upper crust increases linearly with depth, as suggested by Byerlee (1978). Following Buck (1993), the equation used to calculate strength as a function of depth was:

$$\sigma_D = (18\ MPa/km)z \qquad \text{(i)}$$

All variables are defined in Table 1. The strength of the lower crust and mantle were calculated using:

$$\sigma_D = \left(\frac{\varepsilon}{Ae^{Q/RT}}\right)^{1/n} \qquad \text{(ii)}$$

This equation assumes deformation by power law creep, and is based on extrapolation of experimental results (e.g. Christie et al., 1979; Goetze, 1978; Goetze and Brace, 1972; Griggs et al., 1960).

The development of isostatic disequilibrium (σ_{DI}) can be expressed as a function of time by:

$$\sigma_{DI}(t) = \rho g \int_{to}^{t} Z - S - F dt \qquad \text{(iii)}$$

where Z and S will be assigned positive constant rates and t_o will equal zero. S is the rate of sedimentation of material with an average density equal to that of the crust and Z is the rate of tectonic thinning of the upper crust. Kruse et al. (1991) show that the rate of flow in a lower crustal channel can be calculated if it is approximated as two-dimensional linear viscous flow; dividing their analytical solution by the width (l) of the extended region yields the inflation rate (F) due to lower crustal flow:

$$F = \frac{A \sigma_{DI}{}^n d^3}{6 l e^{Q/RT} L} \qquad \text{(iv)}$$

Note that the temperature (T) refers to the temperature at the depth of average flow rate, which is near the bottom of the lower crustal channel if temperature increases linearly with depth, since the flow rate increases in proportion to e^T. T can therefore be approximated by the Moho temperature.

If the thickness of the elastic upper crust prior to extension is h_o, and the original width of the extending region is l_o, then l from equation (iv) is given by:

$$l = \frac{h_o l_o}{h_o - Zt} \qquad \text{(v)}$$

Both d and L from equation (iv) can be approximated as linear functions:

$$d = d_o + \frac{(d_f - d_o)t}{(t_f - t_o)} \qquad \text{(vi)}$$

$$L = \frac{(L_f)t}{(t_f - t_o)} \qquad \text{(vii)}$$

Substituting equations (iv) through (vii) and the condition $t_o = 0$ into (iii), yields the result:

$$\sigma_{DI}(t) = \rho g \left(Zt - St - \frac{A}{6e^{Q/RT}} \int_0^t \frac{\sigma_{DI}^{\,n} \left(\frac{(d_f - d_o)t}{(t_f)} \right)^3}{\frac{h_o l_o L_f t}{(h_o - Zt)t_f}} dt \right) \qquad \text{(viii)}$$

This equation can be solved iteratively for σ_{DI} (Figure 2). Since the isostatic restoring force as a function of time can be calculated, it will now be relatively simple to calculate the duration of activity for a given normal fault system; all that is needed is one statement which describes the magnitude of flexural fiber stresses required to inhibit slip on a normal fault and another relating isostatic disequilibrium to flexural fiber stresses.

The required statement describing the magnitude of flexural fiber stresses required to inhibit slip on a normal fault is:

$$c\sigma_D \geq \sigma_1 - \sigma_3 - \sigma_{xxflex} \qquad \text{(ix)}$$

where c is the ratio of the strength of faulted crust to the strength of unfaulted crust and σ_D is defined by equation (i). Since the crust is undergoing extension by brittle failure, σ_3 is assumed to be the horizontally directed regional stress and $\sigma_1 = \rho g z$, which is the vertically directed overburden stress. The value of $\sigma_1 - \sigma_3$ can constrained by assuming it remains constant, and therefore meets the condition for initial brittle failure of the upper crust, which is:

$$\sigma_D = \sigma_1 - \sigma_3 \qquad \text{(x)}$$

The horizontally directed stress σ_{xxflex} is the compressive fiber stress generated at the base of the elastic crust by flexure. It works against σ_3 to reduce the differential stress, if σ_{xxflex} becomes large enough, the differential stress becomes too small to allow slip on

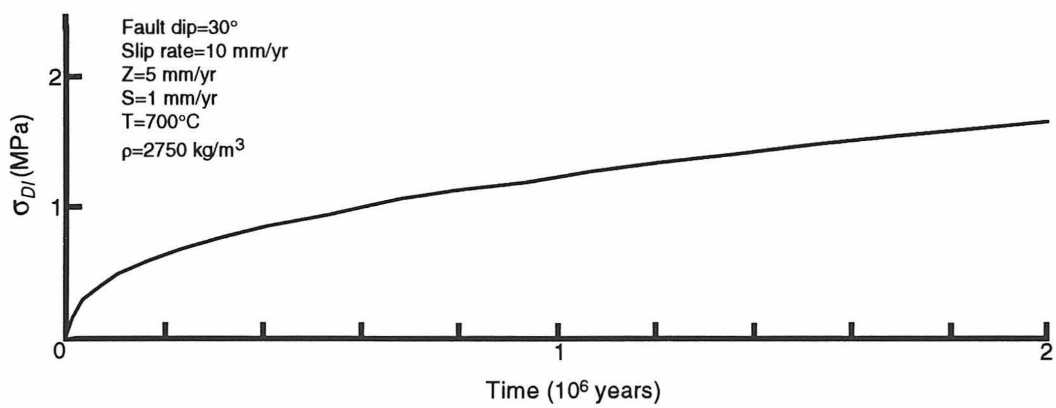

Figure 2. Plot of the magnitude of isostatic disequilibrium (σ_{DI}) as function of time for a region thinning uniformly above a hypothetical Basin and Range detachment fault.

a normal fault. In order to calculate the duration of activity for a given fault system, it is simply necessary to calculate the time at which expression (ix) is first satisfied (i.e. the time at which $c\sigma_D = \sigma_1 - \sigma_3 - \sigma_{xxflex}$).

The only parameters in (ix) which remain undefined are c and σ_{xxflex}. The value of c is poorly constrained, but probably ranges from ~0.1 to 1, since the relative strengths of active faults in the Basin and Range seem to fall in this range (Wesnousky and Jones, 1994). This range for c is also consistent with the results of experimental work which suggest that the strength of saw cut rock is ~0.5 to ~0.8 times that of intact rock (Stesky et al., 1974; Handin, 1969). In the absence of better control, it seems reasonable to assign a value of 0.5 to c, since this is an intermediate value in the probable range. Fortunately, the predicted time for shutdown of a fault system is relatively insensitive to the precise value of c, since the value of the right hand side of (ix) decreases exponentially with time (Figure 3).

The final undefined parameter, σ_{xxflex}, can be defined using equations derived by Turcotte and Schubert (1982). Since the isostatic restoring stress (σ_{DI}) is analagous to the upward load created by injection of a laccolith, the deflection it produces can be calculated using equation (3-98) from Turcotte and Schubert (1982), with modified nomenclature:

$$w = \frac{\sigma_{DI}}{24D}(x^4 - l^2x^2 + l^4/16) \qquad \text{(xi)}$$

Slight modification of the nomenclature in equations (3-64), (3-70) and (3-72) from Turcotte and Schubert (1982) then shows that σ_{xxflex} is given by:

$$\sigma_{xxflex} = -\frac{E(z-h/2)}{(1-v^2)}\frac{d^2w}{dx^2} \tag{xii}$$

where:

$$D = \frac{Eh^3}{12(1-v^2)} \tag{xiii}$$

Examination of equation (xii) shows that it will attain its maximum negative value, or maximum compressional stress value, when z and d^2w/dx^2 reach their maximum positive values. By definition, z reaches a positive maximum at the base of the brittle upper crust (i.e. at $z = h$), and the point of maximum value for d^2w/dx^2 can be established by examination of:

$$\frac{d^2w}{dx^2} = \frac{\sigma_{DI}}{12D}\left(6x^2 - l^2\right) \tag{xiv}$$

Since σ_{DI} is negative, and all other variables in (xiv) are positive, d^2w/dx^2 reaches a positive maximum at x=0.

Substituting x=0 and z=h, as well as equations (xi) through (xiii) into equation (ix), then equating the left and right hand sides, yields the following equation:

$$c\sigma_D = \sigma_D - \frac{h\sigma_{DI}l^2}{2T_e^3} \tag{xv}$$

where all variables except c are functions of time. Solution of this equation yields the time at which a given normal fault system should shut down (Figure 3).

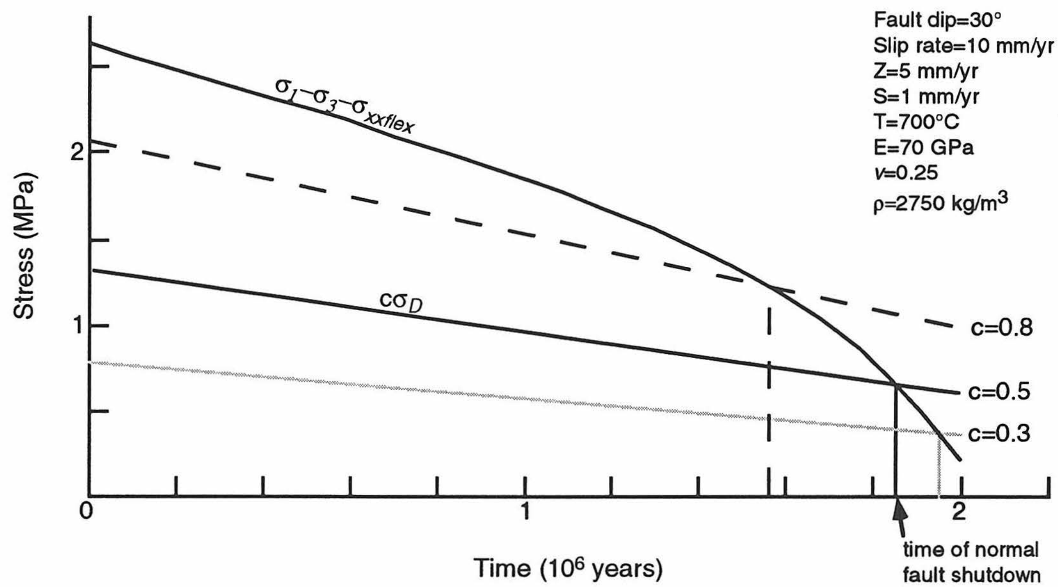

Figure 3. Graph showing duration of activity on a hypothetical Basin and Range fault. Note that time of normal fault shut-down for preferred value of c=0.5 is approximately 1.86 million years. Varying c from 0.3 to 0.8 causes the predicted duration of activity to vary by a relatively small amount; from approximately 1.56 to 1.95 million years.

4.3 Results

The model was tested by calculating the expected lifespan of a hypothetical normal fault system, using parameters appropriate for the core complex belt of the Basin and Range (Figure 3). The lower crust was assumed to have a rheology appropriate to quartz diorite (Table 2) (changing the lower crustal rheology to Westerly Granite increases the predicted lifespan by less than 15%). The temperature at the depth of average flow was assumed to be 700°C, consistent with a suggested Basin and Range Moho temperature of ~700°C (Lachenbruch and Sass, 1978). Both upper and lower crust were assumed to have densities of 2750 kg/m^3.

Reasonable approximations for both d and L were taken from geologic observations. For the case of the breakaway fault system in the central Basin and Range (the Gold Butte region) , the lower crustal channel thickness probably varied from an initial thickness d_o of ~30 km to a final thickness d_f of ~22.5 km. The initial channel thickness was calculated by assuming that the crust initially had the same 45 km thickness as the adjacent Colorado Plateau (Wolf and Cipar, 1993) and the top of the channel was defined by the brittle-ductile transition, a geothermal gradient of 25°C/km was assumed. The final channel thickness assumes thinning of the upper crust by ~50%, and present crustal thickness of ~30 km, as indicated by BARGE seismic data (Brady et al., in prep.). Fission track data suggests that most of this thinning occurred over a relatively short time period (Fitzgerald et al., 1991), probably of order one million years. During the same time period, the length scale l_o of lower crustal flow started at zero and increased to, at most, the approximate width of the unextended future Basin and Range plus Sierra Nevada and Great Valley (~300 km). Since the actual length scale of flow is unknown, a more conservative estimate of the length scale of flow (150 km) was used for model calculations. Thus, the linear approximations to d and L become:

$$d = 30km - \frac{(30km - 22.5km)t}{1m.y.}$$

$$L = 0km + \frac{(150km)t}{1m.y.}$$

If a value of c=0.5 is assumed, the calculated duration of activity for the hypothetical normal fault system is ~1.86 million years (Figure 3), allowing a cumulative slip of ~18.6 km. Figure 3 shows solutions for c equal to 0.3, 0.5 and 0.8 to illustrate the relatively small effect of varying c, particularly for values below 0.5. The predicted values for duration of activity and cumulative slip are in reasonable agreement with the slip history of major detachment faults in the southeastern Basin and Range, which were apparently active at dips of less than 30°, slipped at rates of 3-9 mm/yr, and apparently slipped for ten to a few tens of kilometers (e.g. Foster et al., 1993; John and Foster, 1993). As will be discussed later, decreasing the fault dip would increase the predicted cumulative slip to values in excess of 30 km, making model predictions consistent with even greater cumulative displacements. Thus, it seems that the model is successful in predicting the observed lifespans and cumulative offsets of major normal faults.

4.4 Sensitivity Analysis

Calculations were made to evaluate the sensitivity of the predicted duration of activity to variations in net thinning rate (F), temperature at depth of average flow (T), and flexural rigidity (D). The effect of varying fault dip is also investigated along with varying thinning rate.

4.4.1 Thinning Rate Variations

Figure 4a shows the calculated duration of activity for normal faults dipping at 10, 30, and 60 degrees with net thinning rates varying from 1 mm/yr to 10 mm/yr and all other parameters fixed as for the hypothetical Basin and Range fault of Figures 2 and 3. Figure 4a shows a strong, nonlinear dependence of duration of activity on the net thinning rate for all three faults. Duration of activity decreases with increasing slip rate and with decreasing fault dip. However, cumulative offset does not behave in the same way.

In order to achieve the same thinning rate on a 10° dipping fault as on a 60° dipping fault, the 10° dipping fault must slip nearly five times faster than the 60° dipping fault. For this reason, it is important to consider the relationship between fault dip, slip rate, and cumulative offset. Decreasing fault dip has two main effects; it decreases the thinning rate Z achieved for a given slip rate and it increases the length L of the uniformly thinning region, since it creates a longer section of deforming hanging wall. Examination of equation (xv) shows that both of these factors will affect the predicted lifespan and cumulative slip values. Figure 4b shows the predicted cumulative slip as a function of slip rate for the same three differently dipping faults. It is interesting that

Figure 4. a) Duration of activity vs. net thinning rate for hypothetical Basin and Range normal faults with different dips. Net thinning rate is equal to tectonic thinning minus sedimentation, sedimentation rate was fixed at 1 mm/yr for all calculations (all other parameters as in Figure 3). b) Total slip accumulated prior to shut-down of the fault vs. slip rate for the same three hypothetical faults. Note that higher angle faults are predicted to accumulate less total slip despite remaining active for a longer period of time.

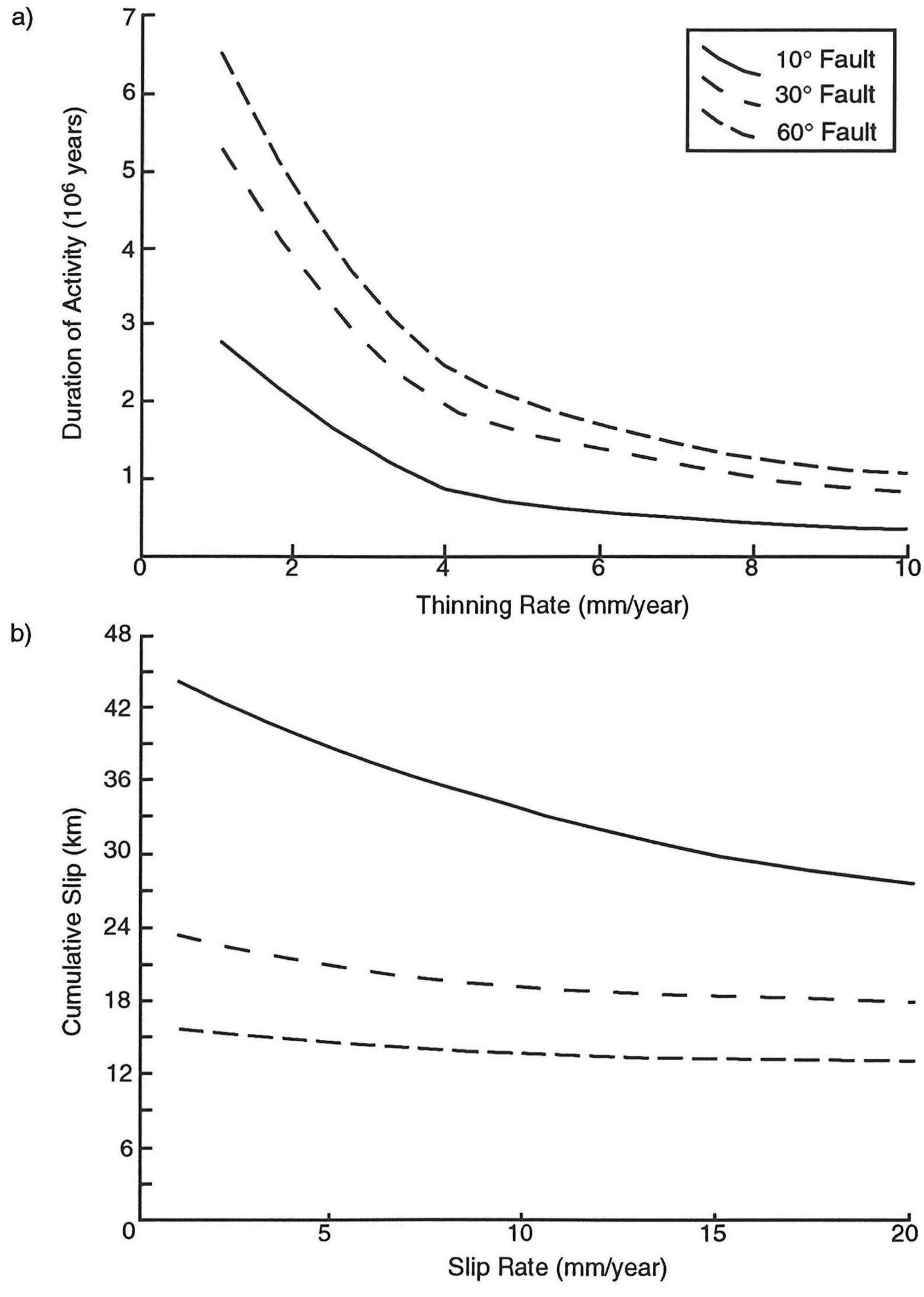
a)
7
6
5
4
3
2
1
0
2
4
6
8
10
Duration of Activity (10^6 years)
Thinning Rate (mm/year)
10° Fault
30° Fault
60° Fault
b)
48
42
36
30
24
18
12
6
0
5
10
15
20
Cumulative Slip (km)
Slip Rate (mm/year)

although more steeply dipping faults are predicted to remain active for longer periods of time, they accumulate much less total slip than lower angle structures. Note that in all cases the cumulative slip decreases with increasing slip rate (and thinning rate), but eventually flattens out near some constant value. In addition, the cumulative slip varies relatively little as a function of slip rate. This is true for all fault dips, although the variation does increase with decreasing fault dip.

4.4.2 Temperature Variations

Figure 5 shows the calculated duration of activity for the hypothetical 30° dipping fault, with the net thinning rate fixed at 4 mm/yr and the temperature at the depth of average flow varying from 400°C to 800°C. It is important to note that the predictions regarding duration of activity for the lower part of this temperature range may be invalid, because the assumption of non-involvement of mantle flow becomes weaker at low crustal temperatures. Nevertheless, it is apparent that duration of activity is very strongly dependent on temperature in the lower crustal channel, since a 400°C temperature range causes the predicted duration of activity to vary by roughly a factor of four. Furthermore, the calculations suggest that long lived normal faults with large cumulative displacements are only possible in regions with a relatively high Moho temperature, with temperatures of greater than 500°C necessary for faults to slip for $\sim 10^6$ years.

4.4.3 Effective Elastic Thickness Variations

Figure 6 shows the duration of activity predicted for the hypothetical 30° dipping Basin and Range normal fault for a range of effective elastic thicknesses at time of shutdown, with F=4 mm/yr and T=700°C. T_e at time of shutdown was allowed to range from

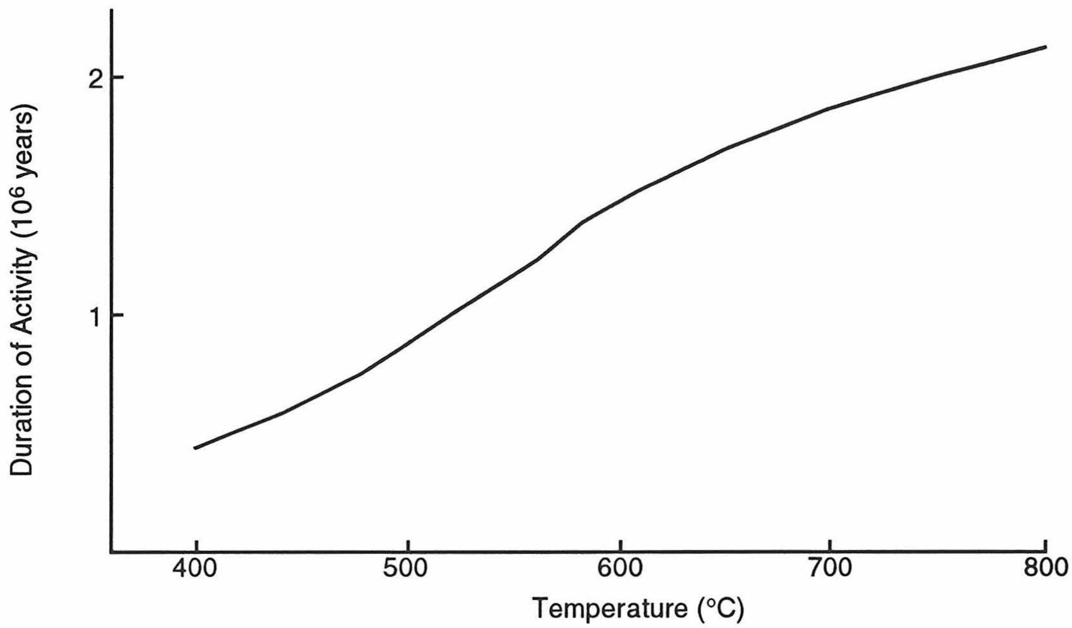

Figure 5. Duration of activity for the hypothetical 30° dipping Basin and Range detachment fault as a function of temperature at depth of average flow (all other parameters as in Figure 3).

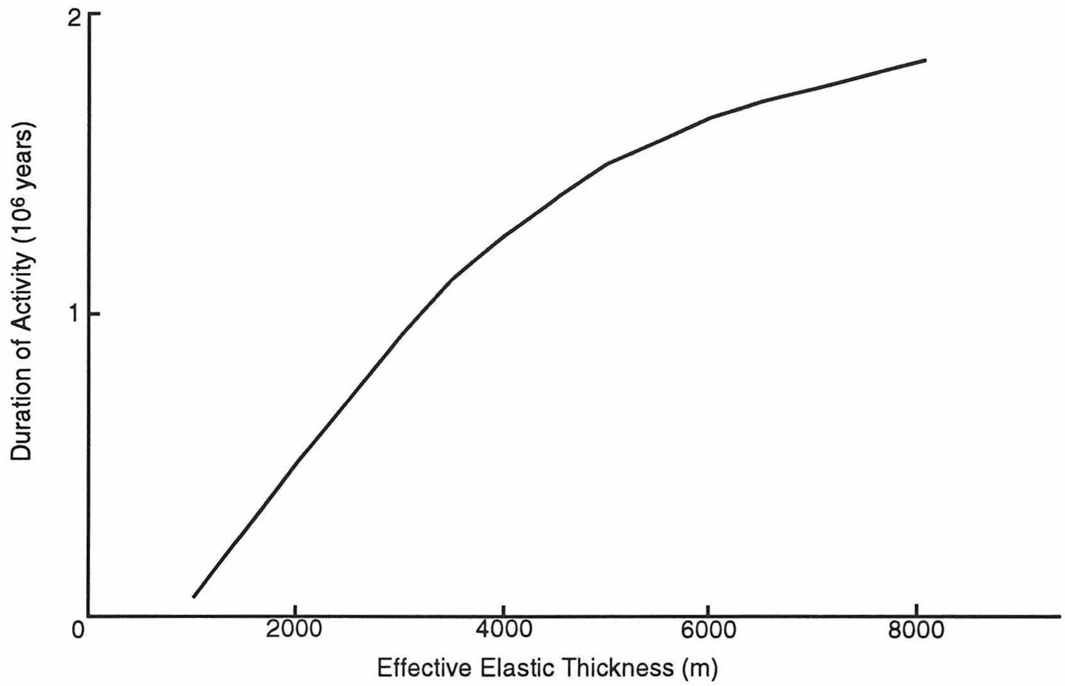

Figure 6. Duration of activity for the hypothetical 30° dipping Basin and Range normal fault as a function of effective elastic thickness of the upper crust (all other parameters as in Figure 3).

1000 m to 8000 m. This resulted in calculated durations of activity which range from roughly 65 thousand years to 1.9 million years. The largest value of effective elastic thickness, 8000 m, roughly corresponds to the true thickness of the upper crust at the time of shutdown if it had an initial thickness of 15 000 m. The lowest value of effective elastic thickness, 1000 m, is only about 1/15 of the thickness of the upper crust at the time of shutdown, since the normal fault system is too short-lived to thin the upper crust significantly.

The lower values of effective elastic thickness may not be reasonable, particularly if they are interpreted as being that part of the upper crust in which flexural stresses are below the failure strength of the crust (c.f. Buck, 1988). In fact, if T_e is interpreted this way, it may be invalid to let the effective elastic thickness deviate at all from the true thickness of the brittle upper crust, given the model scenario. The curvature created by isostatically driven upwarp of the extending region is at all times fairly small (e.g. using the parameters from Figure 3, $\left|d^2w/dx^2\right| \leq 2\times10^{-9}$), so the thickness of the brittle upper crust which exhibits elastic behavior should remain essentially equal to the total thickness of the brittle upper crust (c.f. Fig. 9(c); Buck, 1988).

Effective elastic thicknesses as low as 1 km to 5 km have been reported from the Basin and Range (e.g. Block and Royden, 1990; Bechtel et al., 1990). It is possible that these low effective elastic thickness values are due mainly to footwall flexure (e.g. Buck, 1988), and it may therefore be unreasonable to expect low values within an extending region in the hanging wall of a detachment fault (i.e. within the area under consideration in this paper). On the other hand, some authors have suggested that low values of effective elastic thickness may be due to thermal weakening (e.g. Block and Royden, 1990; Bechtel et al., 1990). If this is true, then values of effective elastic thickness lower than the brittle crustal layer thickness may be reasonable. It is for this reason that the effect of varying T_e on model predictions was examined.

4.5 Discussion

One of the ongoing debates regarding large offset low angle normal faults has centered on the question of their dip at initiation. There is strong field evidence that some of these structures initiated at low angles (e.g. Axen et al., 1990; Wernicke et al., 1985), however some models have suggested that most or all low angle structures must be due to later rotation of inactive segments of originally steeply dipping structures (e.g. Buck, 1993, 1988). The model presented in this paper suggests that active low angle structures are necessary in order to achieve cumulative offsets of greater than approximately 20 kilometers (Figure 4 b). Therefore, this model is consistent with the observation of active low angle structures.

The model predicts the cumulative offsets of several tens of kilometers which are observed on low angle detachment faults such as those in the Harcuvar Mts., Buckskin and Rawhide Mts., and Mormon Mts. (Ketcham, 1996; Foster et al., 1993; John and Foster, 1993; Axen et al., 1990; Wernicke et al., 1985). Model predictions are also consistent with the cumulative slip of approximately 10 km to 15 km which is interpreted to have occurred on the initially steeply dipping faults of the Gold Butte breakaway system (Wernicke and Axen, 1988; Brady, unpublished mapping). This consistency between model results and interpretation of field data bolsters both the validity of the model and the geologic interpretations.

Overall, the relationship between cumulative slip, slip rate, and fault dip suggests that low angle faults should be favored for accomplishing large magnitude extension, as they accommodate large extension for a given slip rate (or thinning rate) before shutting off. This result is similar to that obtained by Forsyth (1992), but for different reasons. Essentially, he calculated the additional stress required to drive uplift and flexure of the hanging wall and footwall of an active normal fault where the faulted plate was treated as if it were continually being flexed to achieve local isostatic equilibrium. The model presented here differs in so far as the hanging wall is not considered to be a rigid block; rather it is assumed to collapse into numerous smaller fault blocks above the footwall and the resulting scenario is one of essentially symmetrically distributed thinning (Figure 1b). Furthermore, the finite viscosity assumed for the lower crust means that isostatic equilibrium lags behind extensional strain, so faulting does not require that the same flexural stresses due to bending of the broken plate be continually overcome. Flexural stresses act differently on this system because both hangingwall and footwall are being upwarped during late stages of extension, rather than the hanging wall being continually downwarped while the footwall is upwarped. Despite these differences, the models are similar insofar as they both call on flexural stresses due to isostatic adjustment as a mechanism for impeding slip on a normal fault; therefore both suggest that low angle faults are more stable than high angle faults because they produce lower thinning rates and thus generate flexural stresses more slowly.

The sensitivity of this model to temperature in the lower crustal layer means that major detachment faults and core complexes should only develop in regions of high heat flow and high Moho temperatures. This is consistent with geologic observations of high heat flow, high geothermal gradients (Lachenbruch and Sass, 1978) and regional magmatism synchronous with or preceding extension (Gans et al., 1989; Wernicke et al., 1987) near major detachment faults.

As discussed earlier, this model predicts that shallowly dipping normal faults should accommodate larger cumulative offsets than steeply dipping faults; in addition, it may offer some insight into how these faults can initiate. The model makes predictions regarding the state of stress in the upper crust at the time of shutdown of normal faulting. Specifically, it predicts that at the time of shutdown, there should be a region of compressional stress at the base of the thinned upper crust and a region of high extensional stress near the top of the thinned crust. In addition, there should be some horizontal shear stress at the base of the upper crust due to flow of lower crustal material toward the thinning region. This stress state should influence the position and orientation at which the next normal fault breaks. Although detailed calculation of the stress field and the orientation of the next fault are beyond the scope of this paper, some suggestions can be made based on the results of other modeling (e.g. Spencer and Chase, 1989; Yin, 1989).

The shear stress on the base of the upper crust due to flow of lower crustal material toward the thinned region should rotate the principal stresses so that lower angle faults which dip away from the thinned region are favored (Yin, 1989). In addition, the region of extensional fiber stresses in the upper part of the thinned region will make it easier to break a fault up into that region, but that fault must root outside of the thinned region in order to avoid the compressionally stressed lower crust within the thinned region. All of these factors seem to favor breaking a new fault which daylights within or near the thinned region, flattens at a shallow depth, and roots outside of the thinned region (e.g. the schematic incipient fault of Figure 1c). This suggests that while early faults should be steeply dipping, later faults may dip shallowly over much of their length, and therefore should accommodate larger cumulative offsets.

The suggestion that a combination of flexural stresses and basal shear stresses may alter the regional stress state and thus control the location and orientation of normal faults is certainly not a new one (c.f. Yin, 1989; Spencer and Chase, 1989; Hafner, 1951). However, at least two recent papers (Wills and Buck, 1997; Buck, 1989) have noted problems with existing models, such as the models of Yin (1989) and Spencer and Chase (1989). In particular, Wills and Buck (1997) have correctly pointed out that these earlier models may predict low angle failure surface trajectories, but do not predict large enough shear stresses to make these surfaces slip, or they predict stress states which should make high angle structures slip and thus lower the regional deviatoric stress before shear stresses in the region of the potential low angle failure surfaces become high enough to cause slip.

It is not clear that the model presented in this paper solves the problems pointed out by Wills and Buck (1997), since it predicts a stress state which is at least qualitatively similar to conditions dealt with by Yin (1989) and Spencer and Chase (1989). The model presented here may, however offer a partial solution to the problem, since it predicts a stress state which will not allow steeply dipping structures to break through the compressionally stressed lower crust, thus possibly forcing the fault trajectories to flatten at shallow depths for some distance and root outside of the flexurally stressed region. In addition, this model points out a mechanism for generation of flexural stresses and horizontal shear tractions that has not been considered in earlier literature. This mechanism would seem to be an inevitable product of active normal faulting and therefore an appeal to special circumstances may not be necessary to explain the occurrence of active low angle faults.

4.6 Conclusions

The model predicts that normal fault systems should be shut down by the generation of compressional flexural stresses in the lower part of the elastic upper crust. These flexural stresses are due to upwarping caused by the influx of lower crustal material, which is driven by pressure gradients resulting from isostatic disequilibrium.

The duration of active faulting on a given normal fault system is largely controlled by the rate of upper crustal thinning and the temperature of the lower crust. A low thinning rate and hot, inviscid lower crust favor longevity of a normal fault system. Conversely, rapid thinning and a relatively cold, viscous lower crust should result in short-lived normal fault systems.

Since low-angle normal faults generate very low thinning rates for a given slip rate, or very high slip rates for a given thinning rate, they should accumulate large total offsets prior to shutdown (even if they are generally active for short periods of time). For this reason, low angle faults may become the dominant structures in highly extended regions, even if they initiate less often than high angle faults.

This model may offer an explanation for the initiation of active low angle structures. As mentioned above, isostatic restoring flow is expected to generate flexural stresses which shut down the active fault system. The restoring flow will also create shear stresses at the base of the elastic upper crust. The combined effect of flexural stresses and shear stresses due to flow in the lower crust should favor the formation of shallow flattening normal faults which dip away from the thinned region.

Acknowledgements I would like to thank Brian Wernicke, Slawomir Tulaczyk, Nathan Niemi, and Martha House for helpful comments and discussion during the preparation of this paper. This research was supported by National Science Foundation grants EAR 92-19939 and EAR 96-28262.

4.7 References Cited

Agnon, A., and Z. Reches, Frictional rheology: hardening by rotation of active normal faults, *Tectonophysics, 247,* 239-254, 1995.

Anderson, E.M., *The Dynamics of Faulting and Dyke Formation with Application to Britain,* 191 pp. Oliver and Boyd, Edinburgh, Scotland, 1942.

Axen, G.J., B.P. Wernicke, M.F. Skelly, and W.J. Taylor, Mesozoic and Cenozoic tectonics of the Sevier thrust belt in the Virgin River Valley area, southern Nevada, in *Basin and Range Extensional Tectonics at the Latitude of Las Vegas, Nevada,* edited by B.P. Wernicke, *Mem. Geol. Soc. Am., 176,* 123-153, 1990.

Bechtel, T.D., D.W. Forsyth, V.L. Sharpton, and R.A.F. Grieve, Variations in effective elastic thickness of the North American lithosphere, *Nature, 343,* 636-638, 1990.

Block, L., and L.H. Royden, Core complex geometries and regional scale flow in the lower crust, *Tectonics, 9,* 557-567, 1990.

Brace, W.F., and D.L. Kohlstedt, Limits on lithospheric stress imposed by laboratory experiments, *J. Geophys. Res., 85,* 6248-6252, 1980.

Brady, R.J., B.P. Wernicke, J.E. Fryxell, and D.R. Lux, Large magnitude Miocene extension in the Lake Mead region, *Geol. Soc. Am. Abst. Programs, 28* , *449*, 1996.

Buck, W.R., Flexural rotation of normal faults, *Tectonics, 5,* 959-973, 1988.

Buck, W.R., Comment on "Origin of regional rooted low-angle normal faults: A mechanical model and its tectonic implications" by An Yin, *Tectonics, 9*, 545-546, 1990.

Buck, W.R., Effect of lithospheric thickness on the formation of high- and low-angle normal faults, *Geology, 21,* 933-936, 1993.

Byerlee, J.D., Friction of rocks, *Pure Appl. Geophys., 116,* 615-626, 1978.

Christie, J.M., P.S. Koch, and R.P. George, Flow law of quartzite in the alpha-quartz field, *EOS Trans. AGU, 60,* 948, 1979.

Fitzgerald, P.G., J.E. Fryxell, and B.P. Wernicke, Miocene crustal extension and uplift in southeastern Nevada: Constraints from fission track analysis, *Geology, 19,* 1013-1016, 1991.

Forsyth, D.W., Finite extension and low-angle normal faulting, *Geology, 20,* 27-30, 1992.

Foster, D.A., A.J.W. Gleadow, S.J. Reynolds, and P.G. Fitzgerald, The denudation of metamorphic core complexes and the reconstruction of the Transition Zone, west-central Arizona: Thermochronologic constraints, *J. Geophys. Res., 98,* 2167-2186, 1993.

Fryxell, J.E., G.S. Salton, J.E. Selverstone, and B. Wernicke, Gold Butte crustal section, South Virgin Mountains, Nevada, *Tectonics, 11, 1099-1120*, 1992.

Gans, P.B., An open system, two-layer crustal stretching model for the eastern Great Basin, *Tectonics, 6,* 1-12, 1987.

Gans, P.B., G.A. Mahood, and E. Schermer, Synextensional magmatism in the Basin and Range Province; a case study from the eastern Great Basin, *Geol. Soc. Am. Spec. Paper, 233,* 53 pp. 1989.

Goetze, C., The mechanisms of creep in olivine, *Phil. Trans. R. Soc. Lond. A., 288,* 99-119, 1978.

Goetze, C., and W.F. Brace, Laboratory observations of high-temperature rheology of rocks, *Tectonophysics, 13,* 583-600, 1972.

Griggs, D.T., F.H. Turner, and H.C. Heard, Deformation of rocks at 500 to 800°C, *Geol. Soc. Am. Mem., 79,* 39-104, 1960.

Hafner, W., Stress distributions and faulting, *Bull. Geol. Soc. Am., 62,* 373-398, 1951.

Handin, J., On the Coulomb-Mohr failure criterion, *J. Geophys. Res., 74,* 5343-5348, 1969.

Howard, K.A., and D.A. Foster, Thermal and unroofing history of a thick, tilted Basin-and-Range crustal section in the Tortilla Mountains, Arizona, *J. Geophys. Res., 101,* 511-522, 1996.

John, B.E., and D.A. Foster, Structural and thermal constraints on the initiation of angle of detachment faulting in the southern Basin and Range: The Chemehuevi Mountains case study, *Geol. Soc. Am. Bull., 105,* 1091-1108, 1993.

Ketcham, R.A., Thermal models of core-complex evolution in Arizona and New Guinea: Implications for ancient cooling paths and present-day heat flow, *Tectonics, 15,* 933-951, 1996.

Kruse, S., M. McNutt, J. Phipps-Morgan, and L. Royden, Lithospheric extension near Lake Mead, Nevada: A model for ductile flow in the lower crust, *J. Geophys. Res., 96,* 4435-4456, 1991.

Lachenbruch, A.H., and J.H. Sass, Models of an extending lithosphere and heat flow in the Basin and Range province, in *Cenozoic Tectonics and Regional Geophysics of the Western Cordillera,* edited by R.B. Smith and G. Eaton, *Mem. Geol. Soc. Am., 152,* 209-250, 1978.

Miller, E., P.B. Gans, and J. Garing, The Snake Range decollement: an exhumed mid-Tertiary ductile-brittle transition, *Tectonics, 2,* 239-263, 1983.

Nur, A., H. Ron, and O. Scotti, Fault mechanics and the kinematics of block rotations, *Geology, 14,* 746-749, 1986.

Sibson, R.H., A note on fault reactivation, *J. Struct. Geol., 7,* 751-754, 1985.

Spencer, J.E., and C.G. Chase, Role of crustal flexure in initiation of low-angle normal faults and implications for structural evolution of the Basin and Range Province, *J. Geophys. Res., 94,* 1765-1775, 1989.

Stesky, R.M., W.F. Brace, D.K. Riley and P.Y.F. Robin., Friction in faulted rock at high temperature and pressure, *Tectonophysics, 23,* 177-203, 1974.

Turcotte, D.L., and G. Schubert, *Geodynamics: Applications of Continuum Physics to Geological Problems,* 450 pp., John Wiley, New York, 1982.

Wernicke, B., and G.J. Axen, On the role of isostasy in the evolution of normal fault systems, *Geology, 16,* 848-851, 1988.

Wernicke, B., J.D. Walker, and M.S. Beaufait, Structural discordance between Neogene detachments and frontal Sevier thrusts, central Mormon Mountains, southern Nevada, *Tectonics, 4,* 213-246, 1985.

Wernicke, B., R.L. Christiansen, P.C. England, and L.J. Sonder, Tectonomagmatic evolution of Cenozoic extension in the North American Cordillera, *Geol. Soc. Spec. Pub., 28,* 203-221, 1987.

Wesnousky, S.G., and C.H. Jones, Oblique slip, slip partitioning, spatial and temporal changes in the regional stress field, and the relative strength of active faults in the Basin and Range, western United States, *Geology, 22,* 1031-1034, 1994.

Wills, S., and W.R. Buck, Stress-field rotation and rooted detachment faults: A Coulomb failure analysis, *J. Geophys. Res., 102*, 20503-20514, 1997.

Wolf, L.W., and J.J. Cipar, Through thick and thin: A new model for the Colorado Plateau from seismic refraction data from the Pacific to Arizona Crustal Experiment, *J. Geophys. Res., 98,* 19881-19894, 1993.

Yin, A., Origin of regional, rooted low-angle normal faults: A mechanical model and its tectonic implications, *Tectonics, 8,* 469-482, 1989.

Chapter 5

Summary

The South Virgin Mountains of southeastern Nevada and northwestern Arizona contain one of the best exposed large offset continental normal fault systems in the world. This normal fault system, the Gold Butte breakaway zone, was studied using detailed structural mapping, geochronology, and a seismic reflection experiment (BARGE). These investigations have resulted in a relatively good understanding of the kinematic evolution of this normal fault system, which may aid in understanding the kinematic evolution of other normal fault systems. In addition, these studies have helped reveal the behavior of the mid to lower crust during and after large magnitude extension. Together with the published results of other studies, this work on the Gold Butte breakaway zone provides constraints for testing a new model of stress state evolution in extending continental regions.

New detailed mapping and thermochronology from the South Virgin Mountains, combined with previous work (Fitzgerald, 1991; Fryxell, 1992), has allowed a well constrained reconstruction of this highly extended region. This reconstruction shows that extension in the Gold Butte breakaway zone was directed roughly N60W, and began on a set of steeply west dipping, gently listric, normal faults. Extension in the Gold Butte breakaway zone may have initiated synchronously with the deposition of the lower part of the Rainbow Gardens Member of the Horse Spring Formation (~19 - 24 Ma; Beard, 1996), but apparently most of the extension occurred rapidly at about 15 Ma. After a small amount of slip and accompanying rotation of the early west dipping normal faults, a later set of steeply to moderately west dipping normal faults developed. This later set of faults soled into, rather than cross-cutting the earlier faults, thus requiring the rotated earlier faults to continue slipping. The earlier set of faults

apparently continued slipping to dips at least as low as 20°. One of the early normal faults, the Lakeside Mine Fault Zone, seems to have 'taken off' as the major extensional structure in the region, unroofing the Gold Butte crystalline block, a slice of upper crust which extended to paleodepths of ~15 km (Fryxell et al., 1992), total extension across the South Virgin Mountains is at least ~21 km. As it was unroofed, the Gold Butte crystalline block had to rebound isostatically. This rebound resulted in formation of the current domal shape of the crystalline block, as well as upwarping and folding of the adjacent fault blocks and formation of late stage, steeply dipping faults which accommodated some of the uplift. The folding of the adjacent fault blocks further reduced the dip of the normal fault surfaces within them, resulting in some of the gently west dipping surfaces being rotated to gentle east dips.

It is commonly inferred that initially steeply dipping faults continue to slip only until they have rotated to moderate dips, at which time they become unfavorably oriented for slip due to increasing normal stresses across the fault plane, and a new set of faults must break which cuts across the old, inactive faults (e.g. Proffett, 1977; Miller et al., 1983). The scenario of normal fault evolution seen in the Gold Butte breakaway zone, in which initially steeply dipping faults rotate and act as extensional decollements for later faults, is contrary to the popular paradigm of how normal fault systems evolve. This contradiction begs the question: is the pattern of kinematic evolution seen in the Gold Butte breakaway zone a widespread occurrence, in which case it should be adopted as a model to aid in the interpretation of other regions, or is it unusual, in which case the existing paradigm or some other alternative should be used? To test the applicability of the 'Gold Butte' scenario to other regions, two well studied extended regions from the southwestern U.S. were re-examined, these being the Lemitar Mountains (Chamberlin, 1982, 1983) and the Yerington District (Proffett, 1977; Proffett and Dilles, 1984). This re-examination showed that the pattern of normal faulting exposed in both of these regions fit very well into a 'Gold Butte' model of normal fault system evolution.

The BARGE (Basin and Range Geoscientific Experiment) seismic reflection data reveals a considerable amount about the structure of the crust under the highly extended Lake Mead region. As is seen under other parts of the Basin and Range (e.g. Klemperer et al., 1986; Hauser et al., 1987b), the crustal thickness is approximately 30 to 35 km (10 - 11 s two way travel time to the Moho). However, the character of the crust imaged on the BARGE data set is otherwise somewhat different from other Basin and Range seismic profiles. Most reflection profiles from the Basin and Range Province show gently dipping discontinuous reflectivity through the mid-crust , and a highly reflective deep crust and Moho (e.g. Klemperer et al., 1986; Hauser et al., 1987a; Hauge et al., 1987; McCarthy and Parsons, 1994). The mid-crust under the Lake Mead region is apparently nearly seismically transparent, and the Moho is relatively unreflective and is defined by a discontinuous band of weak reflections, with virtually no reflectivity beneath it. This reflection character is similar to that seen under the Colorado Plateau (Hauser et al., 1987a; Hauser and Lundy, 1989).

Overall, the BARGE data suggests that the crust under the highly extended Lake Mead region is similar to that under the Colorado Plateau. Together with the high elevation of the denuded Gold Butte crystalline block, this is consistent with the idea that plateau-type continental crust moved into the Lake Mead region at depth in response to extension of the upper crust.

The idea that during extension, the upper crust fails brittley while the lower crust responds by ductile flow has been discussed in many studies (e.g. Block and Royden, 1990; Wernicke, 1990, 1992; Kruse et al., 1991), and is consistent with experimental evidence (Brace and Kohlstedt, 1980). This rheological scenario is also consistent with the surficial geology of the South Virgin Mountains and the smooth Moho and plateau-type crust which underlies the region. It was, therefore, the starting point for a model which examines the evolution of fiber stresses in the elastic upper crust during extension. This model may explain several aspects of the kinematic evolution of the Gold Butte breakaway zone, as well as other major normal fault systems.

The model calculations predict that, for a region of thinning elastic upper crust which is being isostatically compensated by restoring flow in the ductile lower crust, horizontally directed fiber stresses near the base of the elastic upper crust may eventually shut down normal faulting. This is due to the fact that restoring flow of the lower crust results in the thinning region being continually upwarped. As the upwarping force (isostatic disequilibrium) increases in a rapidly thinning region, the compressional fiber stresses near the base of the upwarping region will increase. Eventually, these fiber stresses may become large enough to locally reduce the deviatoric stress below the strength of the faulted crust, and thereby shut down active normal faulting and force extension to be accommodated on faults which root outside of the affected area.

The predicted duration of a given normal fault system is a function of many parameters, including but not limited to: the upper crustal thinning rate, the strength of the faulted upper crust, the Poisson's ratio of the upper crust, and the viscosity of the lower crust. All of these factors are, in turn, functions of other parameters, most notably composition and temperature. Fortunately, most of these parameters can be estimated for a hypothetical 'typical' Basin and Range detachment fault system. Calculations based on such estimates allow the model to be tested against real world observations.

Model predictions of cumulative offset and duration of activity for a number of hypothetical detachments fit reasonably well with observed values from the Basin and Range and other extended regions (see Chapter 4 for examples).

Appendix A

$^{40}Ar/^{39}Ar$ Geochronology

52-1-89M Muscovite
Furnace Data

T (°C)	$^{40}Ar/^{39}Ar$	$^{37}Ar/^{39}Ar$	$^{36}Ar/^{39}Ar$	^{39}Ar moles	^{39}Ar %	$^{40}Ar_{rad}$ %	K/Ca	Age (Ma)
730	296.46	0.0273	0.3551	7.8	1.3	64.6	17.92	1320.5 ±36.2
840	218.27	0.0041	0.0578	46.8	7.6	92.2	118.78	1367.1 ±10.3
935	206.08	0.0027	0.0094	59.8	9.7	98.6	184.21	1377.1 ±10.7
1015	204.61	0.0033	0.0060	109.2	17.8	99.1	150.43	1374.9 ±10.4
1090	203.20	0.0030	0.0040	145.6	23.7	99.4	161.88	1371.1 ±13.9
1160	196.35	0.0417	0.0014	44.2	7.2	99.8	11.76	1341.9 ±10.2
1220	192.15	0.0625	0.0016	33.8	5.5	99.7	7.84	1321.2 ±10.5
1280	204.35	0.0086	0.0028	85.8	14.0	99.6	57.13	1378.1 ±11.1
FUSE	204.56	0.0069	0.0034	81.9	13.3	99.5	71.17	1378.4 ±11.0

Total Gas Age: 1368.5 ±11.7 J: 0.005635
Plateau Age: 1374.4 ±13.0

47-5-89M Muscovite
Furnace Data

T (°C)	$^{40}Ar/^{39}Ar$	$^{37}Ar/^{39}Ar$	$^{36}Ar/^{39}Ar$	^{39}Ar moles	^{39}Ar %	$^{40}Ar_{rad}$ %	K/Ca	Age (Ma)
730	402.75	0.0990	0.9307	3.9	0.4	31.7	4.95	954.0 ±15.7
840	179.22	0.0221	0.1585	15.6	1.7	73.9	22.20	980.7 ±11.9
935	143.44	0.0091	0.0299	39.0	4.2	93.8	53.90	993.3 ±8.2
1015	143.29	0.0040	0.0110	85.8	9.3	97.7	123.54	1023.8 ±8.0
1090	141.34	0.0013	0.0069	172.9	18.7	98.5	385.80	1019.7 ±9.8
1160	136.55	0.0009	0.0052	158.6	17.1	98.8	561.83	995.5 ±7.9
1220	136.45	0.0028	0.0037	166.4	18.0	99.2	174.48	997.5 ±7.9
1280	135.09	0.0006	0.0028	166.4	18.0	99.4	779.11	991.3 ±7.8
FUSE	133.19	0.0021	0.0029	117.0	12.6	99.3	229.70	980.3 ±7.8

Total Gas Age: 999.8 ±8.8 J: 0.005456
Plateau Age: 994.8 ±11.4

5-10-88M Muscovite
Furnace Data

T (°C)	$^{40}Ar/^{39}Ar$	$^{37}Ar/^{39}Ar$	$^{36}Ar/^{39}Ar$	^{39}Ar moles	^{39}Ar %	$^{40}Ar_{rad}$ %	K/Ca	Age (Ma)
730	37.814	0.0240	0.1003	49.4	1.7	21.6	20.40	80.41 ±2.32
840	15.308	0.0125	0.0235	210.6	7.3	54.3	39.15	82.01 ±1.72
935	9.673	0.0047	0.0036	393.9	13.7	88.6	103.39	84.39 ±1.13
1015	9.536	0.0058	0.0022	404.3	14.1	92.7	85.20	87.00 ±0.92
1090	9.600	0.0060	0.0023	461.5	16.0	92.6	81.98	87.53 ±0.96
1160	9.494	0.0072	0.0016	531.7	18.5	94.6	68.37	88.37 ±1.25
1220	9.911	0.0090	0.0012	461.5	16.0	96.0	54.50	93.50 ±1.10
1280	9.928	0.0121	0.0011	243.1	8.5	96.3	40.66	93.92 ±1.17
FUSE	10.285	0.0185	0.0017	119.6	4.2	94.9	26.54	95.80 ±1.05

Total Gas Age:	88.50 ±1.16	J:	0.00559
Plateau Age:	none		

16-1-88M Muscovite
Furnace Data

T (°C)	$^{40}Ar/^{39}Ar$	$^{37}Ar/^{39}Ar$	$^{36}Ar/^{39}Ar$	^{39}Ar moles	^{39}Ar %	$^{40}Ar_{rad}$ %	K/Ca	Age (Ma)
730	79.669	0.0241	0.2259	13.0	0.4	16.2	20.36	123.20 ±17.67
840	21.600	0.0251	0.0436	65.0	1.8	40.1	19.52	83.90 ±2.54
935	13.102	0.0039	0.0087	221.0	6.2	80.2	125.16	101.23 ±1.19
1015	12.122	0.0013	0.0048	421.2	11.8	88.0	365.78	102.69 ±1.07
1090	10.833	0.0009	0.0039	582.4	16.3	89.1	528.81	93.14 ±0.97
1160	10.349	0.0014	0.0035	608.4	17.1	89.8	343.62	89.79 ±0.91
1220	10.331	0.0009	0.0032	677.3	19.0	90.4	538.96	90.26 ±0.92
1280	10.139	0.0008	0.0028	562.9	15.8	91.6	633.98	89.69 ±0.90
FUSE	9.975	0.0019	0.0023	414.7	11.6	92.9	256.77	89.51 ±0.99

Total Gas Age:	92.63 ±1.05	J:	0.005491
Plateau Age:	89.81 ±1.09		

1-10-88M Muscovite
Furnace Data

T (°C)	$^{40}Ar/^{39}Ar$	$^{37}Ar/^{39}Ar$	$^{36}Ar/^{39}Ar$	^{39}Ar moles	^{39}Ar %	$^{40}Ar_{rad}$ %	K/Ca	Age (Ma)
730	129.773	0.0381	0.4215	29.9	0.9	4.0	12.86	55.29 ±9.47
840	39.329	0.0243	0.1110	84.5	2.4	16.5	20.19	69.12 ±3.58
935	12.784	0.0093	0.0184	202.8	5.8	57.3	52.68	77.81 ±1.45
1015	9.022	0.0052	0.0038	364.0	10.4	87.2	94.73	83.43 ±0.92
1090	8.768	0.0058	0.0017	500.5	14.2	94.0	83.78	87.30 ±0.90
1160	9.021	0.0059	0.0012	685.1	19.5	95.8	82.91	91.39 ±0.98
1220	9.521	0.0078	0.0010	741.0	21.1	96.4	63.18	96.98 ±0.97
1280	9.946	0.0097	0.0010	575.9	16.4	96.7	50.68	101.46 ±1.07
FUSE	10.547	0.0134	0.0011	330.2	9.4	96.7	36.56	107.41 ±1.23

Total Gas Age:	92.69 ±1.16	J:	0.006015
Plateau Age:	none		

Appendix B

Monazite U/Pb Geochronology

		Concentration					Error 2-sigma (%)						Age (Ma)		
SAMPLE	Weight	U	Pb	206 Pb*	208 Pb†	206 Pb††		207 Pb††		207 Pb††		206 Pb	207 Pb	207 Pb	corr.
Fractions	(mg)	(ppm)	(ppm)	204 Pb	206 Pb	238 U	% err	235 U	% err	206 Pb	% err	238 U	235 U	206 Pb	coef.
GB-2mg															
m4	0.0570	147.45	17.79	106.89	11.541	0.01042	(.29)	0.06639	(1.22)	0.04623	(1.13)	**66.8**	**65.3**	**9.7**	0.40
m3	0.0718	142.70	25.75	69.25	17.531	0.01042	(.27)	0.06618	(1.23)	0.04607	(1.15)	**66.8**	**65.1**	**1.3**	0.40
m2	0.0487	111.81	19.78	72.17	17.689	0.01019	(.37)	0.06404	(1.44)	0.04558	(1.34)	**65.4**	**63.0**	**-24.3**	0.38
m1	0.0767	108.99	23.33	51.61	20.276	0.01050	(.25)	0.06336	(2.11)	0.04377	(2.01)	**67.3**	**62.4**	**-123.9**	0.46
m5	0.0536	91.22	14.86	63.79	16.726	0.00973	(.46)	0.06021	(3.20)	0.04486	(3.01)	**62.4**	**59.4**	**-63.2**	0.48
m6	0.0527	125.77	19.84	51.48	18.878	0.00825	(.50)	0.05271	(5.76)	0.04635	(5.45)	**53.0**	**52.2**	**15.6**	0.64

* Radiogenic Pb. † Measured ratio corrected for spike and fractionation only. Mass fractionation correction of 0.15%/amu ± 0.04%/amu was applied to all analyses.
†† Corrected for fractionation, spike, blank, and initial common Pb. Blank isotopic composition: 206Pb/204Pb = 19.10 ± 0.1, 207Pb/204Pb = 15.71 ± 0.1, 208Pb/204Pb = 38.65 ± 0.1. All errors are reported as 2-sigma. Each fraction represents a single cystal. Sample weights are estimated using a video monitor with gridded screen and are known to within 40%. Common Pb corrections were calculated using the model of Stacy and Kramers (1975) and the interpreted age of the sample.

References Cited

Agnon, A., and Z. Reches, Frictional rheology: hardening by rotation of active normal faults, *Tectonophysics, 247,* 239-254, 1995.

Anderson, E.M., *The Dynamics of Faulting and Dyke Formation with Application to Britain,* 191 pp. Oliver and Boyd, Edinburgh, Scotland, 1942.

Anderson, R.E., Thin skin distension in Tertiary rocks of southeastern Nevada, *Geol. Soc. Am. Bull., 82*, 42-58, 1971.

Armstrong, R.L., Low-angle (denudation) faults, hinterland of the Sevier orogenic belt, eastern Nevada and western Utah, *Geol. Soc. Am. Bull., 83*, 1729-1754, 1972.

Axen, G.J., Pore pressure, stress increase, and fault weakening in low-angle normal faulting, *J. Geophys. Res., 97*, 8979-8991, 1992.

Beard, L.S., Paleogeography of the Horse Spring Formation in relation to the Lake Mead fault system, Virgin Mountains, Nevada and Arizona, *Geol. Soc. Am. Spec. Paper 303*, 27-60, 1996.

Block, L., and L.H. Royden, Core complex geometries and regional scale flow in the lower crust, *Tectonics, 9*, 557-567, 1990.

Brace, W.F., and D.L. Kohlstedt, Limits on lithospheric stress imposed by laboratory experiments, *J. Geophys. Res., 85,* 6248-6252, 1980.

Buck, W.R., Flexural rotation of normal faults, *Tectonics, 5,* 959-973, 1988.

Byerlee, J.D., Friction of rocks, *Pure Appl. Geophys., 116,* 615-626, 1978.

Chamberlin, R.M., Geologic map, cross-sections, and map units of the Lemitar Mountains, Socorro County, New Mexico, *New Mexico Bur. Mines and Min. Res. Open-file Report No. 169*, 3 plates, scale 1:12,000, 1982.

Chamberlin, R.M., Cenozoic domino-style crustal extension in the Lemitar Mountains, New Mexico; A summary, in *New Mexico Geological Society Guidebook, 34th Field Conference, Soccorro Region II*, edited by Chapin, C.E., and Callender, J.F., Soccorro, New Mexico Geological Society, pp. 111-118. 1983

Coney, P.J., Structural analysis of the Snake Range 'decollement,' east-central Nevada, *Geol. Soc. Am. Bull., 85*, 973-978, 1974.

Davis, W.M., The Basin-Range problem, *Proc. Nat. Acad. Sci., 11*, 387-392, 1925.

Davis, G.H., Mid-Tertiary gravity-glide folding near Tucson, Arizona, *Geol. Soc. Am. Abst. Programs, 5*, 592, 1973.

Fitzgerald, P.G., J.E. Fryxell, and B.P. Wernicke, Miocene crustal extension and uplift in southeastern Nevada: Constraints from fission track analysis, *Geology, 19,* 1013-1016, 1991.

Forsyth, D.W., Finite extension and low-angle normal faulting, *Geology, 20,* 27-30, 1992.

Fryxell, J.E., G.S. Salton, J.E. Selverstone, and B. Wernicke, Gold Butte crustal section, South Virgin Mountains, Nevada, *Tectonics, 11, 1099-1120*, 1992.

Gilbert, G.K., Report on the geology of portions of Nevada, Utah, California, and Arizona, etc., *U.S. Geog. Geol. Surveys W. of 100th Mer. Rep., 3*, 1875.

Hauge, T.A., R.W. Allmendinger, C. Caruso, E. Hauser, S. Klemperer, S. Opdyke, C. Potter, W. Sanford, L. Brown, S. Kaufman, and J. Oliver, Crustal structure of western Nevada from COCORP deep seismic reflection data, *Geol. Soc. Am. Bull., 98*, 320-329, 1987.

Hauser, E.C., and J. Lundy, COCORP deep reflections; Moho at 50 km (16s) beneath the Colorado Plateau, *J. Geophys. Res., 94*, 7071-7081, 1989.

Hauser, E.C., J. Gephart, T. Latham, J. Oliver, S. Kaufman, L. Brown, and I. Lucchita, COCORP Arizona transect: Strong crustal reflections and offset Moho beneath the transition zone, *Geology, 15*, 1103-1106, 1987a.

Hauser, E.C., C. Potter, T. Hauge, S. Burgess, S. Burtch, J. Mutschler, R. Allmendinger, L. Brown, S. Kaufman, and J. Oliver, Crustal structure of eastern Nevada from COCORP deep seismic reflection data, *Geol. Soc. Am. Bull., 99*, 833-844, 1987b.

Klemperer, S., T.A. Hauge, E.C. Hauser, J.E. Oliver, and C.J. Potter, The Moho in the northern Basin and Range province, Nevada, along the COCORP 40°N seismic-reflection transect, *Geol. Soc. Am. Bull., 97*, 603-618, 1986.

Kruse, S., M. McNutt, J. Phipps-Morgan, and L. Royden, Lithospheric extension near Lake Mead, Nevada: A model for ductile flow in the lower crust, *J. Geophys. Res., 96,* 4435-4456, 1991.

McCarthy, J., and T. Parsons, Insights into the kinematic Cenozoic evolution of the Basin and Range-Colorado Plateau transition from coincident seismic refraction and reflection data, *Geol. Soc. Am. Bull., 106*, 747-759, 1994.

Miller, E., P.B. Gans, and J. Garing, The Snake Range decollement: an exhumed mid-Tertiary ductile-brittle transition, *Tectonics, 2,* 239-263, 1983.

Nur, A., H. Ron, and O. Scotti, Fault mechanics and the kinematics of block rotations, *Geology, 14,* 746-749, 1986.

Proffett, J.M., Jr., Cenozoic geology of the Yerington district, Nevada, and implications for the nature and origin of Basin and Range faulting, *Geol. Soc. Am. Bull., 88*, 247-266, 1977.

Proffett, J.M., Jr., and Dilles, J.H., Geologic map of the Yerington District, Nevada, *Nev. Bur. Mines and Geol., Map 77*, scale 1:24,000, 1984.

Sibson, R.H., A note on fault reactivation, *J. Struct. Geol., 7,* 751-754, 1985.

Spencer, J.E., Role of tectonic denudation in warping and uplift of low-angle normal faults, *Geology, 12*, 95-98, 1984.

Spencer, J.E., and C.G. Chase, Role of crustal flexure in initiation of low-angle normal faults and implications for structural evolution of the Basin and Range Province, *J. Geophys. Res., 94,* 1765-1775, 1989.

Thompson, G.A., and D.B. Burke, Regional geophysics of the Basin and Range province, *Ann. Rev. Earth Plan. Sci., 2*, 213-238, 1974.

Wernicke, B., The fluid crustal layer and its implications for continental dynamics, in *Exposed cross sections of the continental crust, NATO Advanced Studies Institute*, edited by Salisbury, M., and D.M. Fountain, pp. 509-544, Kluwer Academic Publishers, Dordrecht, Holland, 1990.

Wernicke, B., Low-angle normal faults in the Basin and Range Province: nappe tectonics in an extending orogen, *Nature, 291*, 645-648, 1981.

Wernicke, B., Cenozoic extensional tectonics of the U.S. Cordillera, in *The Cordilleran Orogen: Conterminous U.S., The Geology of North America, G-3*, edited by Burchfiel, B.C., Lipman, P.W., and M.L. Zoback, pp. 553-582, Geol. Soc. Am., Boulder, Colorado, 1992.

Wills, S., and W.R. Buck, Stress-field rotation and rooted detachment faults: A Coulomb failure analysis, *J. Geophys. Res., 102*, 20503-20514, 1997.

Wright, L.A., and B.W. Troxel, Shallow-fault interpretation of Basin and Range structure, southwestern Great Basin, in *Gravity and tectonics*, edited by R. DeJong and R. Scholten, pp. 397-407, Amsterdam, Elsevier, 1973.

Yin, A., Origin of regional, rooted low-angle normal faults: A mechanical model and its tectonic implications, *Tectonics, 8,* 469-482, 1989.